DTU Library

Modeling nitrogen chemistry in combustion

Glarborg, Peter; Miller, James A.; Ruscic, Branko; Klippenstein, Stephen J.

Modeling Nitrogen Chemistry in Combustion

Peter Glarborg[1], James A. Miller[2], Branko Ruscic[2], and Stephen J. Klippenstein[2]

[1] *Department of Chemical and Biochemical Engineering, Technical University of Denmark, DK-2800 Kgs. Lyngby, Denmark*
[2] *Chemical Sciences and Engineering Division, Argonne National Laboratory, Argonne, IL, 60439, USA*

Understanding of the chemical processes that govern formation and destruction of nitrogen oxides (NO_x) in combustion processes continues to be a challenge. Even though this area has been the subject of extensive research over the last four decades, there are still unresolved issues that may limit the accuracy of engineering calculations and thereby the potential of primary measures for NO_x control. In this review our current understanding of the mechanisms that are responsible for combustion-generated nitrogen-containing air pollutants is discussed. The thermochemistry of the relevant nitrogen compounds is updated, using the Active Thermochemical Tables (ATcT) approach. Rate parameters for the key gas-phase reactions of the nitrogen species are surveyed, based on available information from experiments and high-level theory. The mechanisms for thermal and prompt-NO, for fuel-NO, and NO formation via NNH or N_2O are discussed, along with the chemistry of NO removal processes such as reburning and Selective Non-Catalytic Reduction of NO. Each subset of the mechanism is evaluated against experimental data and the accuracy of modeling predictions

1

is discussed.

1 Introduction

Emission of oxides of nitrogen from combustion and high temperature industrial processes continues to be an environmental concern. Nitrogen oxides, collectively termed NO_x, are formed in essentially all combustion processes, mostly as nitric oxide (NO) with smaller amounts of nitrogen dioxide (NO_2) and nitrous oxide (N_2O). Nitric oxide is subsequently oxidized to NO_2 in the atmosphere. Nitric oxide and nitrogen dioxide are acid rain precursors and participate in the generation of photochemical smog, while nitrous oxide is a greenhouse gas.

Several separate mechanisms have been identified that can lead to formation of nitrogen oxides in significant quantities. These mechanisms involve either fixation of the molecular nitrogen contained in the combustion air or oxidation of organic nitrogen chemically bound in the fuel. Figure 1 provides an overview of the most important sources of NO in combustion.

For gaseous fuels with no or negligible amounts of fuel–bound nitrogen (e.g., natural gas), as well as for fuels with a low nitrogen content (oil, woody biomass, plastic waste), formation of NO arises from fixation of N_2 in the combustion air. Homogeneous mechanisms for fixation of N_2 involve the attack of reactive radicals (O, CH_n, H) on the triple bond in molecular nitrogen [1–4]. These reactions form either NO or a reactive nitrogen intermediate (N_2O, cyanides, NNH) that may subsequently be oxidized to NO. For fuels with a considerable content of organically bound nitrogen, i.e., most solid fuels, oxidation of fuel-bound nitrogen constitutes the dominant source of nitrogen oxides. Here, formation of NO will depend on the partitioning of fuel-N between volatiles and char. The chemistry of the volatile nitrogen is complicated, since it may involve oxidation of tar-N, soot-N, cyclic compounds, and light species such as HCN and NH_3.

Volatile-N from coal is mostly released with tar, emerging subsequently mainly as HCN, while for biomass and low rank coals, significant amounts of NH_3 may be released directly from the solid matrix during devolatilization [3].
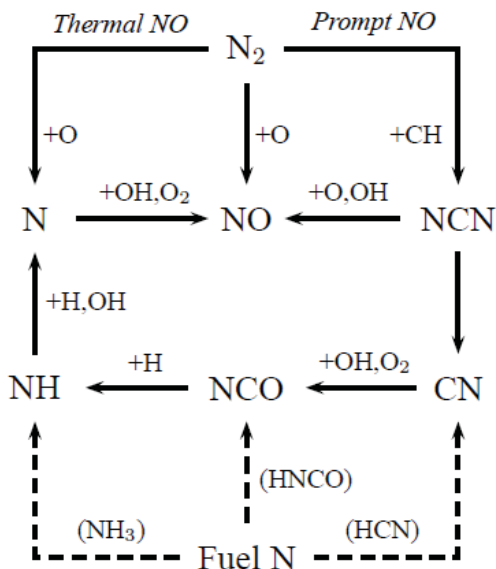

Figure 1: Simplified reaction path diagram illustrating the major steps in the formation of thermal NO, prompt NO, and fuel NO. Recycling of NO to N_2 through reaction with atomic nitrogen or to cyanides through reaction with hydrocarbon radicals is not shown.

A large amount of work has been devoted to improve the understanding of NO_x formation mechanisms in combustion and to develop control strategies to reduce emissions [1–3, 5, 6]. Restrictions on NO_x emissions that used to apply only to large combustion systems such as power plants are now implemented on ever smaller scales: they continue to be a driving force for research and development in many industrial high temperature processes. In large power plants and for certain engines, emissions are typically controlled by catalytic flue gas cleaning. However, this technology can be challenging to use for fuels such as biomass and waste due to poisoning issues or undesirable due to comparatively high costs. For this reason there is still an incentive to control NO_x emissions by primary means

or by in-situ techniques such as Selective Non-Catalytic Reduction (SNCR) or reburning. To achieve this aim, it is important to have access to reliable and versatile chemical kinetic models for formation and consumption of NO in high temperature processes. The use of detailed reaction mechanisms together with engineering models such as Computational Fluid Dynamics (CFD) has, with the strongly enhanced computational power now available, become an important tool in designing low-NO_x combustion systems.

The objective of the present work is to establish and evaluate a state-of-the-art, non-optimized chemical kinetic model for homogeneous nitrogen chemistry in combustion. It is based on the work on nitrogen chemistry reported over the last decades, drawing also on recent advances in the knowledge of thermochemistry and reaction rates from theoretical work. The different mechanisms for formation and consumption of NO are discussed and the key reaction steps are evaluated. Different subsets of the model are validated against experimental data and the predictive capability of the mechanism is assessed.

To limit the scope of the review, we emphasize nitrogen chemistry in combustion of light hydrocarbons, mostly CH_4, and/or light fuel-nitrogen species (HCN, NH_3, HNCO) at atmospheric or sub-atmospheric pressure. Oxidation of heterocyclic nitrogen compounds, which may be formed in combustion of more complex fuels, or of energetic materials such as nitroalkanes are not addressed in the current work. Furthermore, we focus on experimental conditions that are sufficiently well-defined for kinetic interpretation and refrain from modeling practical combustion systems, partly due to the fact that turbulent flow characteristics and turbulence/chemistry interactions may play a significant role, and partly due to the need for simplified chemistry when used in computational fluid dynamics calculations.

In this review, a wide range of experimental data has been selected for model validation, including results from laminar premixed flames at low and atmospheric pressure, from shock tube experiments, and from jet-stirred reactors.

4

Modeling predictions have also been compared extensively to data obtained in laminar flow reactors. However, data from flow reactors are prone to uncertainties in initial conditions, either due to conditioning (mixing, preheating) or interference from reactions on the reactor surface, even for fairly inert materials such as quartz and alumina. For this reason, care must be taken when interpreting the results [7]. In App. A, it is discussed how quartz surfaces may interact with the gas phase chemistry in flow and batch reactors. In reality, all experimental approaches suffer from complications that must be kept in mind when used for model development and evaluation.

2   Detailed Chemical Kinetic Model

A chemical kinetic model consists of a reaction mechanism along with thermodynamic properties and transport coefficients for the involved species. A reaction mechanism for nitrogen chemistry in combustion will have to include submechanisms for hydrocarbon oxidation, oxidation of reactive nitrogen species (amines, cyanides, etc.), and interactions between the hydrocarbon and nitrogen chemistry (e.g., prompt NO, reburning). The model established in this review is based on work on nitrogen chemistry published over the last 40 years. However, the thermochemistry and the rate constants for reactions important for formation and consumption of NO are re-evaluated based on recent high-level theory work. The full model in Chemkin input format is available as Supplementary Material. Specific aspects of the model are discussed in detail in the following.

2.1   Thermodynamic properties

Table 1 lists thermodynamic properties for selected species in the model. The data for these species were reevaluated in the present work using the Active Thermochemical Tables (ATcT) approach [8,9]. Particular emphasis was on the

thermochemistry of selected hydrocarbon radicals and reactive nitrogen species. Where relevant, these are discussed in more detail in the sections below. Heats of formation for the CH_n hydrocarbon radicals are entirely consistent with the recent evaluation of Ruscic [10], which was based on ver. 1.122 of the ATcT Thermochemical Network (TN) [11]. The listed values are based on the updated progeny ATcT TN ver. 1.122b, which was augmented with new determinations during a subsequent effort to extract the best currently available energy difference between HCN and HNC, as well as the enthalpies of formation of these two species and their positive and negative ions [12]. ATcT TN ver. 1.122b was also used to develop and benchmark new high-level composite electronic structure methods known as ANLn [13]. In order to obtain the requisite NASA thermodynamic polynomials for the species listed in Table 1, JANAF-style tabular ATcT outputs based on the results from TN ver. 1.122b (containing temperatures, isobaric heat capacities, entropies, enthalpy increments, and enthalpies of formation, using 50 K increments) were fitted using the gold-standard NASA PAC program of McBride and Gordon [14].

The thermodynamic properties for other species were mostly adopted from the Ideal Gas Thermochemical Database by Goos, Burcat and Ruscic [15] (which is periodically updated with available ATcT enthalpies of formation).

2.2 Reaction mechanism

The core of the reaction mechanism is based on recent work by the authors on the chemistry of C_1-C_2 hydrocarbons [16–18], amines [19], cyanides [20], and hydrocarbon/nitrogen interactions [21–23]. However, many features of the model date back to work in the 1980's [1, 24]. The nitrogen chemistry subsets of the mechanism will be discussed in the following sections. In this section we discuss briefly the reactions in the fuel oxidation subset that are of particular importance for the nitrogen chemistry.

6

| Species	H_{298}	S_{298}	$C_{p,300}$	$C_{p,400}$	$C_{p,500}$	$C_{p,600}$	$C_{p,800}$	$C_{p,1000}$	$C_{p,1500}$
NH_3	-10.89	46.07	8.53	9.24	10.04	10.81	12.22	13.44	15.76
NH_2	44.46	46.57	8.05	8.24	8.51	8.81	9.50	10.19	11.64
NH	85.75	43.32	6.97	6.97	6.99	7.04	7.22	7.47	8.07
N	112.92	36.64	4.97	4.97	4.97	4.97	4.97	4.97	4.97
NNH	59.70	53.65	8.22	8.62	9.11	9.61	10.52	11.26	12.36
NO	21.78	50.37	7.14	7.16	7.29	7.47	7.83	8.12	8.55
NO_2	8.14	57.40	8.90	9.68	10.44	11.09	12.05	12.67	13.49
NO_3	17.72	61.76	12.28	13.73	14.94	15.91	17.23	18.04	19.13
N_2O	19.73	52.58	9.25	10.21	10.96	11.59	12.54	13.20	14.15
HCN	30.90	48.24	8.59	9.38	9.98	10.47	11.31	12.01	13.23
HNC	45.98	49.13	9.64	10.20	10.60	10.94	11.56	12.10	13.11
CN	105.17	48.43	6.97	7.03	7.16	7.33	7.69	8.00	8.52
NCN	107.74	53.92	9.88	10.77	11.52	12.12	12.96	13.45	14.00
HNO	25.56	52.79	8.09	8.45	8.96	9.51	10.52	11.36	13.17
HON	51.28	55.21	8.44	9.07	9.66	10.16	10.91	11.48	12.46
HONO	-18.80	60.70	11.08	12.42	13.51	14.39	15.67	16.56	17.90
HNO_2	-10.55	57.02	9.28	10.58	11.85	12.98	14.72	15.95	17.69
$HONO_2$	-32.07	63.78	12.98	15.33	17.22	18.69	20.71	21.93	23.41
CH_4	-17.81	44.54	8.55	9.71	11.14	12.61	15.32	17.63	21.72
CH_3	34.98	46.37	9.11	9.76	10.38	10.97	12.08	13.07	14.76
$^3CH_2$	93.57	46.58	8.53	9.01	9.46	9.90	10.82	11.79	14.05
$^1CH_2$	102.54	45.25	8.11	8.37	8.71	9.10	9.93	10.73	12.28
CH	142.48	43.75	6.97	6.99	7.03	7.11	7.37	7.68	8.46
C	171.34	37.79	4.98	4.97	4.97	4.97	4.97	4.97	4.97

Table 1: Thermodynamic properties of selected species in the reaction mechanism from ATcT TN ver. 1.122b (see text). Units are kcal mol^{-1} for H, and cal mol^{-1} K^{-1} for S and C_p. Temperatures are in K.

Formation and consumption of nitric oxide in combustion are strongly dependent on the radical pool. Formation of NO through the thermal NO mechanism, or through N_2O or NNH, is dependent on the O/H radical pool, which is typically controlled by the fuel oxidation chemistry. To the extent the kinetic model is able to provide a satisfactory description of the fuel oxidation chemistry, it would be expected to predict the O/H radical pool fairly accurately. However, under some conditions trace species chemistry has an impact on the radical pool. For instance, the presence of nitrogen oxides may serve to promote or inhibit fuel oxidation, depending on the conditions [4].

A more direct interaction between the nitrogen chemistry and the fuel oxidation chemistry involves reactions of hydrocarbon radicals with N_2 (forming prompt NO), with NO (reburn type reactions), or with other reactive nitrogen species (for instance, converting amines to cyanides). Almost any fuel derived radical,

e.g., CH_3, $^3CH_2$, $^1CH_2$, CH, and C among the C_1-radicals and C_2H, C_2, HCCO, and C_2O from the C_2-radical pool, may be involved in this interaction. Among these radicals, methylidyne (CH) is of special interest since it is sufficiently reactive to attack even molecular nitrogen and initiate prompt NO formation.

In the present review, we limit our scope to nitrogen chemistry in combustion of small hydrocarbons, mostly methane. In oxidation of methane, the CH and C radicals are largely formed from the sequence

$$CH_3 \xrightarrow{+H,OH} {}^3CH_2 \xrightarrow{+H,OH} CH \xrightarrow{+H,OH} C$$
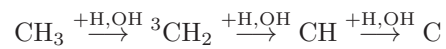
In App. B, we take a look at the reactions that determine the levels of the small hydrocarbon radicals and evaluate this part of the reaction mechanism. Compared to previous modeling efforts, an important feature in the present mechanism is the use of a more accurate rate constant for $CH + H_2O$.

3 Formation mechanisms for NO

3.1 Thermal NO

The thermal NO or Zeldovich mechanism [25] is the most important source of NO in high-temperature gas combustion. The mechanism of thermal NO formation is well established. The initiating step is attack of an oxygen atom on the triple bond in N_2,

$$O + N_2 \rightleftarrows NO + N \qquad \text{(R1b)}$$

This reaction has a high activation energy, about 75 kcal mol^{-1} [26], and it is the rate limiting step in thermal NO formation. Once formed, the nitrogen atom is rapidly oxidized to NO by reaction with OH or O_2,

$$N + OH \rightleftarrows NO + H \qquad \text{(R2)}$$

$$N + O_2 \rightleftarrows NO + O \qquad \text{(R3)}$$

The remaining issues in modeling thermal NO formation involve mainly the accuracy of the rate constant for reaction R1, discussed below.

3.1.1 Reaction subset for thermal NO

Table 2 lists the rate constants for the reactions in thermal NO formation. The rate constant for the rate limiting step (R1b) has been measured directly in shock tube studies [27, 28] and inferred from a number of flame studies [29–36]. In addition, the reverse reaction,

$$N + NO \rightleftarrows O + N_2 \qquad \text{(R1)}$$

has been characterized experimentally over a wide range of temperature [26,37–46]. The N + NO reaction is expected to have little if any pressure dependence because the minimum energy path on the ground electronic surface is purely attractive with no minimum [47].

Figure 2 shows an Arrhenius plot for reaction R1. Data for the $O + N_2$ reaction (R1b) are converted through the equilibrium constant. Baulch et al. [26] estimated the uncertainty in the rate constant to be a factor of two, providing a recommendation for k_{1b} that is 50-70% larger than their value for k_1 divided by the equilibrium constant.

		A	β	E	Source
1.	$N + NO \rightleftarrows O + N_2$	9.4E12	0.140	0	[46]
2.	$N + OH \rightleftarrows NO + H$	3.8E13	0.000	0	[48]
3.	$N + O_2 \rightleftarrows NO + O$	5.9E09	1.000	6280	[49]

Table 2: Reactions involved in thermal NO formation. Parameters for use in the modified Arrhenius expression $k = AT^{\beta} \exp(-E/[RT])$. Units are mol, cm, s, cal.

We have adopted the rate constant for reaction R1 from the recent study of Abian et al. [46]. They determined k_1 from flow reactor experiments, measuring NO formation from N_2/O_2 mixtures at 1700-1800 K, and extrapolated the rate constant to a wider temperature range taking literature data into account. Their resulting value is 25% above the recommendation of Baulch et al. for k_1, while it corresponds to a value k_{1b} 25% below the Baulch et al. evaluation, reconciling the data for the forward and reverse rate constant (Fig. 2).
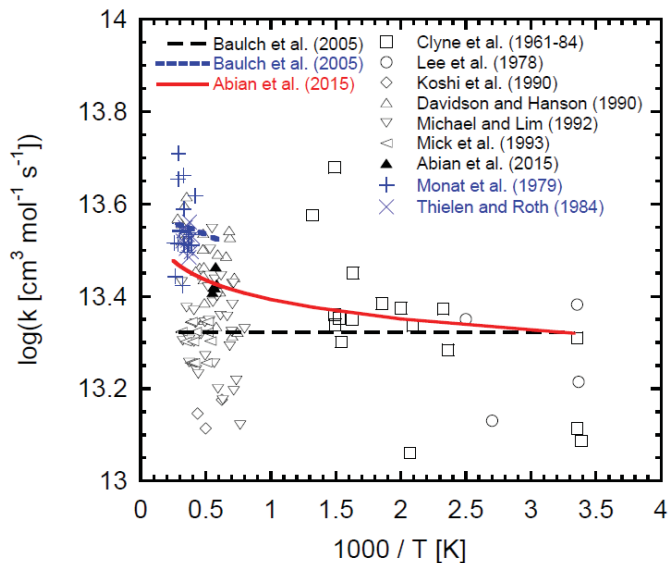
Figure 2: Arrhenius plot for the reaction $N + NO \rightleftarrows O + N_2$ (R1). The black symbols denote measurements of the forward reaction while the blue symbols denote data obtained from measurements of the reverse step, converted using the thermodynamic properties. Data for k_1: Clyne et al. [37–40], Lee et al. [41], Koshi et al. [42], Davidson and Hanson [43], Michael and Lim [44], Mick et al. [45], and Abian et al. [46]. Data derived from measurements of k_{1b}: Monat et al. [27] and Thielen and Roth [28]. The long-dashed line shows the recommendations of Baulch et al. [26] for k_1, while the short-dashed line is the value of k_1 derived from their recommendation of k_{1b}. The solid line is the rate constant recommended by Abian et al., adopted in the present work.

3.1.2   Modeling thermal NO formation

Comparatively little experimental work, reviewed in [46, 50, 51], has been conducted to characterize thermal NO formation under well-controlled conditions. Following Abian et al. [46], we have selected the flow reactor data of Arai et al. [52] and the flame data from Homer and Sutton [53] for comparison with modeling predictions.

Arai et al. [52] conducted an experimental study of the O_2/N_2 system in an isothermal laminar flow reactor, investigating the effect of the O_2 mole fraction (0.05-0.95) and the temperature (1550-1750 K) on the formation of NO. Figure 3

11

compares the measured NO concentrations reported by Arai et al. with modeling predictions. Interference of the quartz reactor surface with the NO formation in these experiments is expected to be negligible. Loss of atomic oxygen at the reactor wall, which could be a concern (App. A), can be disregarded since O is rapidly equilibrated with O_2 under these conditions [46].
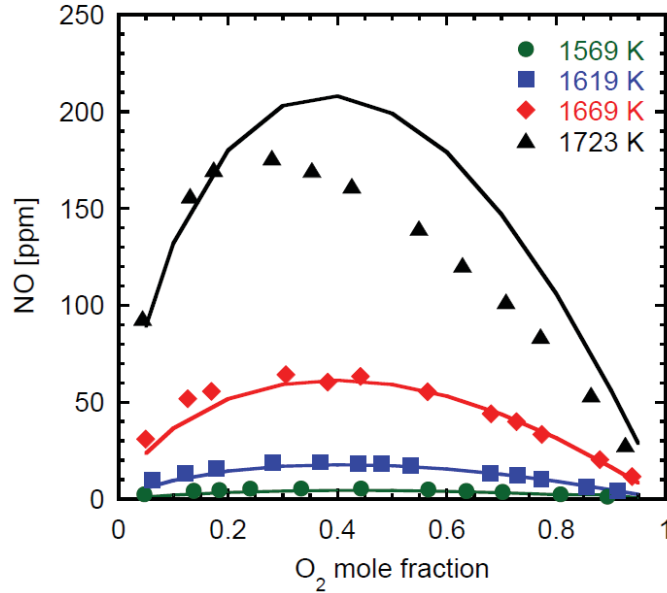

Figure 3: Comparison between experimental data [52] and modeling predictions for formation of NO from N_2 and O_2 in a flow reactor as a function of temperature and mole fraction of O_2 in the O_2/N_2 reactant gas mixture. Experimental data are shown as symbols, while modeling predictions are shown as lines.

The agreement is within 20% or better. The differences are most pronounced for the highest temperature at O_2 levels above 30%, where the predicted NO levels exceed the measurements. As pointed out by Abian et al. [46], the observed NO profile at this temperature has a different shape from those measured at other temperatures, with NO peaking at a lower O_2 concentration, and the difference may be partly attributed to an experimental artifact.

Homer and Sutton [53] reported measurements of NO concentration profiles in atmospheric-pressure premixed hydrogen-oxygen-nitrogen flames over a range of

stoichiometries and temperatures. Figure 4 compares their experimental data with modeling predictions. The flames of Homer and Sutton were heavily stabilized on the burner and conceivably the burner surface affected the flames by removing heat and radicals from the flame zone. Most of the NO formation reported by Homer and Sutton occurs very early in the flame, i.e. in a region where the flame may interact with the burner surface. Following Abian et al. [46], we choose in the calculations to fix the NO level at the measured value at about 0.25 cm above the burner and model the NO formation only in the post-flame region to minimize the uncertainty.
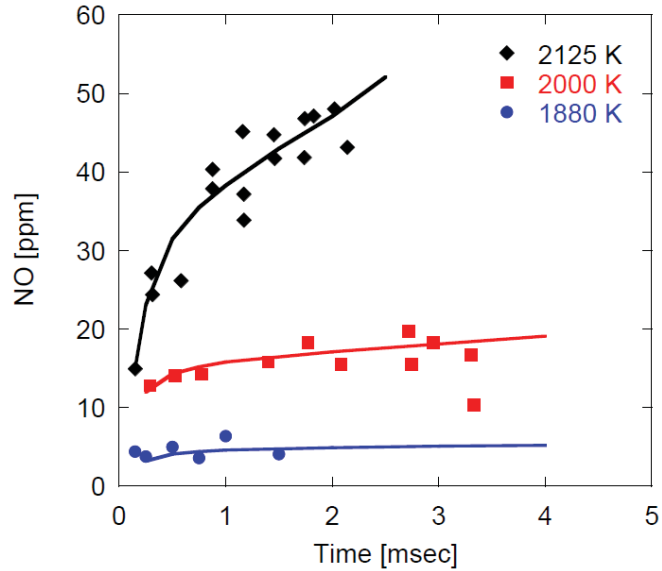

Figure 4: Comparison of measured and predicted mole fractions of NO in the post-flame zone of an atmospheric pressure $H_2/O_2/N_2$ premixed laminar flame. The symbols denote experimental data from Homer and Sutton [53], while the lines denote calculated values. Flame 1: T = 2125 K, inlet composition 25% H_2, 17.5% O_2, 57.5% N_2. Flame 2: T = 2000 K, inlet composition 23% H_2, 16.1% O_2, 60.9% N_2. Flame 3: T = 1880 K, inlet composition 21.1% H_2, 14.7% O_2, 64.2% N_2.

The flame data are scattered and there is some uncertainty in the measured flame temperatures. However, the agreement between observed and calculated NO concentrations in the post-flame region is good.

Even though the thermal NO subset can only be validated to a limited extent due to the scarcity of suitable experimental data, the uncertainty of calculations for this NO formation mechanism would be expected to be small. The accuracy in the rate constant for the rate limiting step (R1) is probably of the order of 25% at high temperatures and modeling predictions for thermal NO formation under well-controlled conditions are likely to have a similar accuracy. In practical systems, the accuracy of the calculations would be limited to a greater extent by uncertainties in temperature and/or in turbulence-chemistry interactions.

3.2 Prompt-NO

The mechanism initiated by attack of CH_n-radicals on N_2 is termed prompt NO [29, 54]. Prompt NO is an important, perhaps dominating, source of NO in turbulent hydrocarbon/air diffusion flames [55], which is the most common practical flame configuration. Early modeling studies [1, 24] identified the reaction of CH with N_2 as the most important initiation step. For a long time, this reaction was believed to form HCN + N, but it is now known to proceed via insertion of CH into the N_2 triple bond, yielding NCN + H [56, 57]:

$$CH + N_2 \rightleftarrows NCN + H \qquad (R4)$$
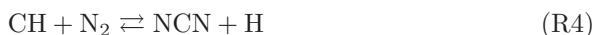
Other hydrocarbon radicals have also been proposed to attack molecular nitrogen. The reactions of both triplet and singlet methylene ($^3CH_2$, $^1CH_2$) with N_2 have been shown to have too high barriers to contribute to prompt NO formation [1, 24, 58]. Also, the $C_2O + N_2$ reaction, discussed in several publications [59–62], has a prohibitively high barrier [63]. The $C_2 + N_2$ reaction (R6) could be a candidate [64, 65], but the low C_2 concentration, typically two orders of magnitude below the CH concentration in premixed flames [66], prevents this step from being significant. Only the $C + N_2$ reaction to form CN + N (R5b) or NCN (R7b) is sufficiently fast to compete with $CH + N_2$ (R4). The direct step to form CN + N (R5b) has a higher activation energy than reaction R4 and becomes more competitive as the combustion temperature increases, but also the sequence $C + N_2$ (+M) $\rightarrow$ NCN (+M) (R7b), followed by reaction of NCN, may contribute to NO formation. The $C + N_2$ (+M) $\rightarrow$ NCN (+M) reaction (R7b) is exothermic (by 63.6 kcal mol^{-1} at 298 K) and is exergonic up to 2100 K, becoming endergonic at higher temperatures, while $C + N_2 \rightarrow$ CN + N (R5b) is both endothermic (by 17.4 kcal mol^{-1} at 298 K) and endergonic, with its endergonicity gradually growing as the temperature rises.

The NCN radical formed by CH + N_2 (R4) or C + N_2 (R7b) feeds into the

cyanide pool and is eventually oxidized to NO or N_2. Recent modeling studies [60–62,67–72] have successfully included and refined the NCN chemistry in the reaction mechanism for prompt NO formation. However, there are still unresolved issues, as discussed below.

3.2.1 Heat of formation of NCN

The thermodynamic properties for NCN are important in modeling prompt-NO formation since they affect the branching fraction of the NCN + H reaction towards CH + N_2 (R4b) and HCN/HNC + N (R8, R9). Values for the heat of formation of NCN used in modeling studies [61,62,67,71,72] vary more than three kcal mol^{-1}; differences that have a significant impact on modeling predictions.

Table 3 lists reported values of the heat of formation of NCN. Clifford et al. [73] estimated $\Delta_f H^0_{298}$(NCN) to 107.9±4.0 kcal mol^{-1} from electron affinity measurements measurements on NCN and a computed (CBS-4, CBS-Q, and CBS-APNO) gas-phase acidity of HNCN. Bise et al. [74, 75] studied the photodissociation dynamics of NCN using beam photofragment spectroscopy leading to $\Delta_f H^0_{298}$ = 111.1±0.7 kcal mol^{-1}. Canneaux et al. [76] computed a value of $\Delta_f H^0_{298}$ = 107.2±0.8 kcal mol^{-1} using CBS-QB3, CBS-APNO, G3B3, G3, and G4 calculated atomization energies.

ΔH^0_{f298}(NCN) kcal mol^{-1}	Method	Ref.
107.9±4.0	Experimental	Clifford et al. [73]
111.1±0.7	Experimental	Bise et al. [74, 75]
109.4±2.0	Theory	Harding et al. [77]
107.2±0.8	Theory	Canneaux et al. [76]
109.4±0.5	ATcT (localized TN ver. 1.112 bis)	Goos et al. [71]
107.5$^{+1.4}$	Experimental, indirect	Fassheber et al. [78]
107.7±0.2	Theory, ATcT (TN ver. 1.122b)	See text

Table 3: Reported values for the heat of formation of NCN.

Recently, Goos et al. [71] re-examined the heat of formation of NCN based on a detailed analysis of available experimental and theoretical thermochemical data combined with two Active Thermochemical Tables analyses. As discussed at length by these authors, the initial ATcT analysis using TN ver. 1.112, which included the experimental and theoretical data available at the time, suggested a tentative value of 106.5 ± 0.4 kcal mol^{-1} [79]. The value was reflecting an irreconcilable discord between available experimental data and was thus significantly influenced by several mid-level electronic structure results, such as those of Canneaux et al. [76] (CBS-QB3, CBS-APNO, G3B3, G3, G4), which appeared to be mutually consistent. Upon repetition and further scrutiny of these (and other) single-reference computations, Goos et al. [71] established that these theoretical results for NCN (which is a $^3\Sigma^-$ biradical in the ground state) suffer from significant spin contamination, a problem that escaped notice by both Canneaux et al. [76] and Clifford et al. [73]. The value proposed by Goos et al., 109.4 ± 0.5 kcal mol^{-1}, was obtained by solving a small (localized) TN (ver. 1.112 bis) that included the conflicting experimental data from Clifford et al. [73] and Bise et al. [74, 75], together with a couple of multi-reference results of Harding et al. [77], but excluded all spin-contaminated single-reference theoretical results. As discussed by Goos et al., the data available at the time produced a rather sparse TN, which subtended very few thermochemical cycles involving NCN that would normally be exploited by ATcT to check the individual determinations for consistency. As a consequence, the ATcT statistical analysis of the TN could not find clear fault with either of the two experimental studies and thus produced a result that was more-or-less mid-way between the two discordant experiments, which turned out to be in reasonable accord with the value implied by the (included) multi-reference results of Harding et al. [77]. (Parenthetically, when the content of the localized TN is conjoined with the full TN, such as in ver. 1.118 [80], the NCN-related local sparsity of the TN largely remains unchanged, and thus the result changes rather insignificantly, to 109.1 kcal mol^{-1}.) Since the proposed result deviates significantly from previous values used in modeling studies, Goos et al. [71] tested its im-

17

pact on prompt NO formation, and concluded that the value obtained from the localized TN did appear to somewhat improve the modeling of NCN and NO mole fraction profiles in a fuel-rich methane flame when compared to the high value of Bise et al. In addition, by separately examining which range of values could be accommodated in their modeling efforts, Goos et al. concluded that a feasible enthalpy of formation of NCN should fall between 106.4 and 108.3 kcal mol^{-1} - somewhat lower than the ATcT result from the localized TN - but also indirectly suggesting that the experimental value of Clifford at al. appears more acceptable than the high value of Bise et al.

Other previous modeling studies of prompt-NO have also employed values for $\Delta_f H^0_{298}$(NCN) that were varying by 3 or more kcal mol^{-1}. Konnov [61] preferred the high value of 111 kcal mol^{-1} from Bise and coworkers [74,75]. Desgroux and coworkers [62,67] initially adopted the value of 107.9 kcal mol^{-1} from Clifford et al. [73], but in their most recent work [72] they find that the best agreement with flame measurements is obtained with an even lower $\Delta_f H^0_{298}$(NCN) = 106.1 kcal mol^{-1}.

In the present work, we use the current ATcT value of $\Delta_f H^0_{298}$(NCN) = 107.7±0.2 kcal mol^{-1} (see section 2.1). The value is partially based on new experimental and theoretical information. The relevant new theoretical information emanates from recent high-accuracy computational results at the ANL1 level of theory [13], and was added to the TN as appropriate isodesmic reactions; the new experimental information is based on the 2nd and 3rd law interpretation of the studies of Fassheber et al. [78]. The recent shock tube study by Fassheber et al. on the NCN + H reaction supports a value of $\Delta_f H^0_{298}$(NCN) of approximately 107.5 kcal mol^{-1}, with an upper limit of 108.9 kcal mol^{-1}. The provenance of the current ATcT enthalpy of formation (based on species-specific variance decomposition analysis [81]) indicates that it indeed relies heavily on the new ANL1 results (which cumulatively contribute 76.5% to the provenance), followed by the experimental study of Fassheber et al. (the 2nd and 3rd law contributing

together 5.6%). Of note is also that the individual enthalpies of formation implied on one hand by the ANL1 computational results alone and on the other by the experimental study of Fassheber et al. agree rather closely, and thus it is perhaps no surprise that the current ATcT value is in excellent agreement both with the latter experimental result and with ANL1 computations. The current ATcT value is also in admirable agreement with the earlier result of Clifford et al. [73], but is outside the error bounds of the determination of Bise et al. [74,75], reinforcing the conclusion that the latter is too high. The current ATcT result is lower than the previous ATcT result from a small localized TN reported by Goos et al., but it falls comfortably in the middle of their deduced 'feasible range' for the enthalpy of formation. Perhaps somewhat surprising is that the current ATcT value also agrees well with the results obtained from mid-level computations of Canneaux et al., given that these veritably suffer from spin contamination in nearly every computational step of their composite sequences.

3.2.2   Reaction subset for prompt NO formation

Selected reactions in the prompt NO subset are listed in Table 4. Other important steps are formation and consumption of hydrocarbon radicals, discussed in App. B, and reactions in the cyanide and amine subsets, discussed in the following sections.

The rate constant for the key reaction in prompt NO formation,

$$CH + N_2 \rightleftarrows NCN + H \qquad \qquad (R4)$$

has been derived both experimentally [87, 88] and theoretically [77, 82, 89, 90]. Figure 5 shows an Arrhenius plot for the reaction. Dean et al. [87] and Vasudevan et al. [88] used the perturbation in the CH profile upon adding N_2 to the initial reaction mixture to infer the rate coefficients of the CH + N_2 reaction in the 2500-3800 K temperature range. Their results are in good agreement,

	A	β	E	Source
4. $CH + N_2 \rightleftarrows NCN + H$	5.3E09	0.790	16770	[82], a
5. $CN + N \rightleftarrows C + N_2$	5.9E14	-0.400	0	[26]
6. $C_2 + N_2 \rightleftarrows CN + CN$	1.5E13	0.000	41730	[64]
7. $NCN + M \rightleftarrows C + N_2 + M$	8.9E14	0.000	62100	[83]
8. $NCN + H \rightleftarrows HCN + N$	2.2E11	0.710	5321	[82], a
9. $NCN + H \rightleftarrows HNC + N$	4.3E-4	4.690	2434	[82], a
10. $NCN + O \rightleftarrows CN + NO$	2.5E13	0.170	-34	[84]
11. $NCN + OH \rightleftarrows HCN + NO$	2.6E08	1.220	3593	[82], a
12. $NCN + OH \rightleftarrows NCO + NH$	1.7E18	-1.830	4143	[82], a
13. $NCN + O_2 \rightleftarrows NO + NCO$	1.3E12	0.000	23167	[85]
14. $NCN + NO \rightleftarrows CN + N_2O$	1.9E12	0.000	6280	[86]

a: 1 atm (for pressure dependence, see Supplementary Material)

Table 4: Selected reactions important for prompt NO formation. Parameters for use in the modified Arrhenius expression k = $AT^\beta \exp(-E/[RT])$. Units are mol, cm, s, cal.

but the data from Vasudevan et al. show less scatter. Lindackers et al. [91] also reported measurements for the CH + N_2 reaction from shock tube experiments. However, they monitored formation of atomic N, which is now known to be a product of secondary reactions, and their results were disregarded in the present evaluation.

Harding et al. [77] reported a high level theoretical study of the CH + N_2 reaction. They determined a value for k_4 with an uncertainty of a factor of two, owing mostly to the uncertainty in the heat of formation for NCN. Recently, Klippenstein et al. [82] reanalyzed the reactions on the HNCN potential energy surface. They obtained a value for k_4, adopted in the present work, that is slightly higher than the rate constant from Harding et al. and the measurements of Vasudevan et al. (Fig. 5).

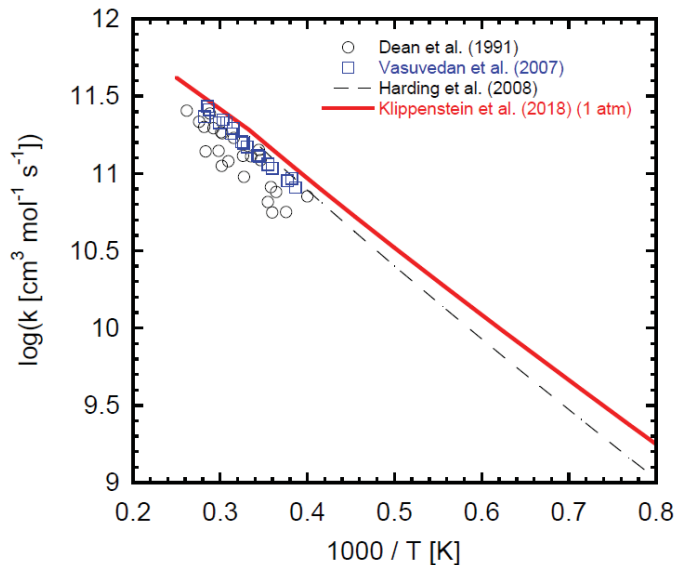Knowledge of the subsequent reactions of the NCN radical has improved con-

Figure 5: Arrhenius plot for the reaction $CH + N_2 \rightleftarrows NCN + H$ (R4). The symbols denote measurements of the rate constant while lines denote calculated values. Data are obtained from Dean et al. [87], Vasudevan et al. [88], Harding et al. [77], and Klippenstein et al. [82].

siderably in recent years, owing to a large degree to the shock tube work of Friedrichs and coworkers who determined rate constants for several of the NCN reactions, i.e., $NCN + M$ (R7) [83], $NCN + H$ [78], $NCN + O$ (R9) [83], $NCN + O_2$ (R13) [85], and $NCN + NO$ (R14) [86]. In addition, Lin and coworkers have studied theoretically a number of reactions, including $NCN + H$ [92], $NCN + O$ [84], $NCN + OH$ [93] and $NCN + O_2$ [94]. Very recently, Klippenstein et al. [82] reported a theoretical study of $NCN + H$ and $NCN + OH$. The present subset for NCN relies mostly on the experimental results of Friedrichs and coworkers and the theoretical work of Klippenstein et al.

Prompt NO formation is most important under slightly reducing conditions and the reaction with atomic hydrogen is a key step in the NCN subset. In addition to recombination to form HNCN, this reaction has three product channels,

$$NCN + H \rightleftarrows CH + N_2 \qquad \text{(R4b)}$$

$$NCN + H \rightleftarrows HCN + N \qquad\qquad (R8)$$

$$NCN + H \rightleftarrows HNC + N \qquad\qquad (R9)$$

Fassheber et al. [78] measured the overall rate constant for NCN + H in a shock tube in the temperature range 962-2425 K, while Vasudevan et al. [88] derived a rate constant for the sum of the channel to HCN + N (R8) and HNC + N (R9) at 2300-2500 K from measured time histories of the NCN radical concentration. In addition, the NCN + H reaction has been studied theoretically by Teng et al. [92] and by Klippenstein et al. [82].

In Fig. 6 the measurements of Fassheber et al. and Vasudevan et al. for NCN + H are compared with the high-level calculations of Klippenstein et al. [82] for k_{4b}, $k_8 + k_9$, and $k_{NCN+H,total}$. The NCN + H reaction is dominated by the channel to CH + N_2 (R4b) at low to medium temperatures, while HCN + N (R8) becomes competitive at high temperatures. Since k_{4b} has a negative temperature dependence while k_8 increases with temperature, the overall rate constant for NCN + H has an inflection point, which occurs at temperatures between 1000 and 1500 K.

Teng et al. calculated a rate constant for reaction R8 in good agreement with the measurements of Vasudevan et al., finding formation of HNC + N (R9) to be of little importance due to a high barrier. The analysis of Klippenstein et al. confirms that the channel to HNC + N (R9) is minor, even though there may be a contribution from inter-system crossing from ^{2}HNCN to ^{4}HNCN.

The value of k_8 ($+k_9$) inferred by Fassheber et al. from their experiments is about a factor of two higher than indicated by the data from Vasudevan et al. and the theoretical studies. However, their overall rate constant for NCN + H is in good agreement with the prediction of Klippenstein et al., in particular at high temperatures.

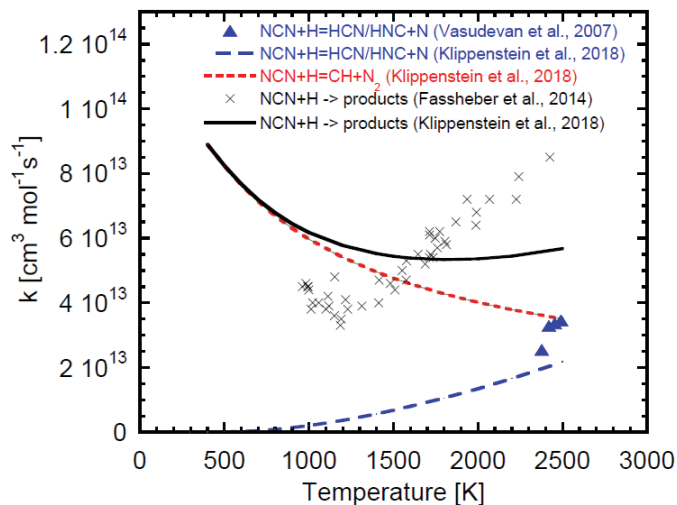In the present work, we have adopted the rate constants for the reactions on the

Figure 6: Arrhenius plot for the NCN + H reaction. The symbols denote measurements of the overall rate constant from Fassheber et al. [78] and for reaction R8 from Vasudevan et al. [88]. Lines denote values of rate constants calculated by Klippenstein et al. [82].

HNCN potential energy surface from Klippenstein et al. [82]. Their calculated values of $k_8 + k_9$ are below those derived by Fassheber et al. [78] by more than a factor of two at 2000 K. This difference has implications for modeling predictions of prompt NO formation and more work is required to resolve this issue. The accuracy of the theoretical values is affected by uncertainty in the prediction of the inter-system crossing probability for NCN + H and in the thermodynamic properties for NCN and CH when extrapolated to high temperatures [82].

Both experiment [83] and theory [84] support that the reaction of NCN with O (R10) is fast and it is important for prompt NO formation. The NCN + OH reaction (R11, R12) has only been studied theoretically [82, 93]; this step is slower and thus less important for NO formation.

3.2.3 Modeling prompt NO formation

The model for prompt-NO formation is evaluated by comparison to data from low-pressure premixed flames [62, 72, 95–99] and from jet-stirred reactors [100]. The most comprehensive experimental work on prompt NO formation in flames has been conducted by Desgroux and coworkers in a series of publications [62,72, 96–99]. Data from laminar, premixed flames are often very reliable, in particular if obtained by non-intrusive methods. Concerns include the accuracy of the measured temperature profile and possible interactions with the burner surface. The well–stirred reactor device is characterized by intense turbulent mixing, high concentrations of free radicals and short residence times. These conditions favor prompt–NO formation and make it the dominant source of NO at equivalence ratios ranging from stoichiometric to fuel–rich. However, data from jet-stirred reactors are prone to be mixing influenced, in particular at high temperatures where the chemistry is fast.

Following Glarborg et al. [24] and Miller and Bowman [1], we compare modeling predictions with the measurements of Bartok et al. [100] on NO formation in combustion of CH_4 in a jet-stirred reactor (Fig. 7). In the calculations we have used the measured temperatures, which peak at about 2000 K at slightly fuel-rich conditions. Due to the concerns about mixing influence, the uncertainty in the experimental results is presumably considerable. With this in mind, the agreement between the experimental data and the modeling predictions is good, except at very fuel-rich conditions where the NO concentration is underpredicted.

Analysis of the calculations for Fig. 7 provides information on how the dominating NO formation mechanism is controlled by the stoichiometry and the temperature. It is seen from the figure that if the prompt–NO initiation reactions are deleted from the reaction mechanism (dashed line), NO is still predicted well under lean conditions, but under stoichiometric and reducing conditions
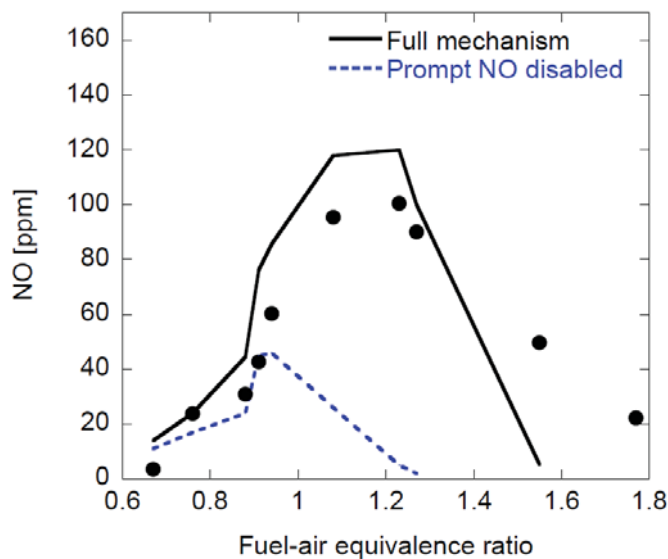
Figure 7: Comparison of measured [100] and predicted mole fractions of NO as a function of the fuel-air equivalence ratio ϕ in methane/air combustion in a jet–stirred reactor. The symbols denote experimental data, while the solid lines denote calculated values. Predictions with the full model are shown as a solid line, while the dashed line denotes calculations with prompt NO initiating reactions disabled. The nominal residence time and the pressure in the reactor were 3.0 ms and 1.0 atm, respectively.

it is severely underpredicted. Thermal NO dominates under slightly lean conditions, while NO formation through the nitrous oxide mechanism, discussed in section 3.3, becomes more important as the amount of excess air increases and the temperature decreases. Under stoichiometric conditions thermal NO and prompt NO contribute with similar amounts of nitric oxide, but prompt NO rapidly becomes the dominating source of NO for fuel-air equivalence ratios larger than 1.0.

Figure 8 shows a reaction path diagram for prompt NO formation under slightly fuel-rich conditions. Prompt-NO formation involves three overall steps [1, 24]:

- formation of CH_n–radicals, in particular CH
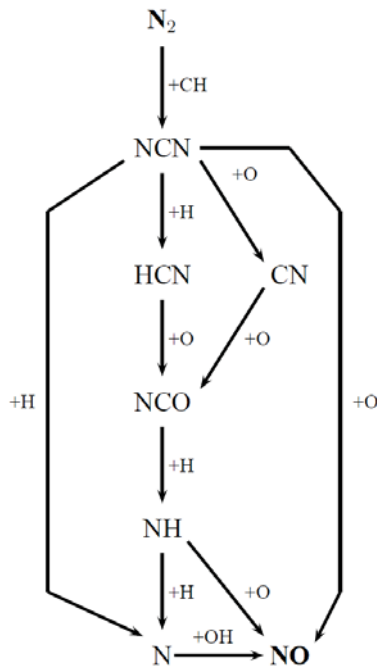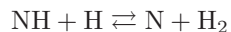
- molecular nitrogen fixation

25

Figure 8: Reaction path diagram for prompt NO formation under slightly fuel-rich conditions under the conditions of the jet-stirred reactor experiments of Bartok et al. [100] . Not shown is a sequence leading from NCN through HNC to the amine pool.

- interconversion between fixed nitrogen species

The fixation of N_2 occurs mainly through the CH + N_2 reaction (R4), even though recombination of C and N_2 (R7b) also contributes. Up to a fuel-air equivalence ratio of approximately 1.2 the NCN and N formed in these reactions are oxidized rapidly to NO, principally by the sequence:

$$NCN + H \rightleftarrows HCN + N \tag{R8}$$

$$HCN + O \rightleftarrows NCO + H \tag{R26}$$

$$NCO + H \rightleftarrows NH + CO \tag{R31}$$

26

$$NH + H \rightleftarrows N + H_2$$

$$N + OH \rightleftarrows NO + H \tag{R2}$$

A minor alternative pathway involves the sequence NCN $\xrightarrow{+H}$ HNC $\xrightarrow{+OH}$ HNCO $\xrightarrow{+H}$ NH$_2$.

At conditions richer than $\phi = 1.2$ the concentration of HCN increases rapidly, while NO decreases. The shift in fixed nitrogen partition from NO to HCN is caused by the combination of several factors. The conversion of HCN to NO by reaction (R26) is no longer rapid due to the decrease in O-atom concentration. Furthermore, recycling of amine radicals and NO back to HCN through reaction with hydrocarbon radicals becomes dominant. At richer conditions the reactions of CH$_3$ leading to CH$_n$–radicals are favored compared to the oxidation pathways leading to formaldehyde. Reactions between the CH$_n$–radicals and NO then efficiently convert NO to cyanides and isocyanides. These steps are discussed in more detail in section 4.2 on reburning. Recycling of amine radicals into the cyanide pool occurs mainly through the fast reactions,

$$CH_3 + N \rightleftarrows H_2CN + H$$

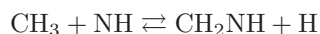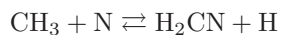$$CH_3 + NH \rightleftarrows CH_2NH + H$$

Figure 9 shows a sensitivity analysis for NO for the conditions of the experiments of Bartok et al. (Fig. 7). Results for three selected fuel-air equivalence ratio are shown. Under slightly lean conditions ($\phi = 0.91$), thermal NO contributes to formation of NO and the prediction is sensitive to the O + N$_2$ reaction (R1). Under slightly fuel-rich conditions ($\phi = 1.08$), the importance of this step is diminished and under even more reducing conditions ($\phi = 1.27$), it proceeds in the reverse direction (N + NO $\rightarrow$ N$_2$ + O) and shows a negative coefficient.

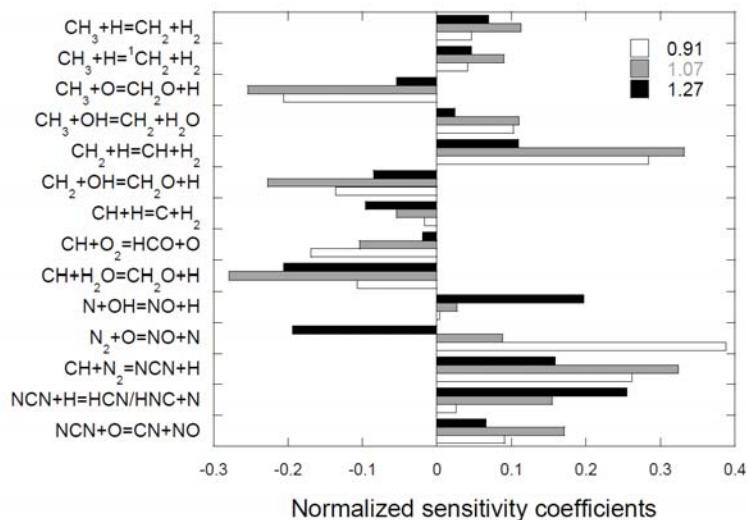Prompt NO is an important source of NO under all three conditions. The

Figure 9: Sensitivity coefficients for prediction of NO under the conditions of the jet-stirred reactor experiments of Bartok et al. [100] at three fuel-air equivalence ratios.

key reactions in the prompt NO mechanism, $CH + N_2$ (R4), $NCN + H$ (R8, R9) and $NCN + O$ (R10) exhibit positive sensitivity coefficients. Reactions that promotes formation of CH through the sequence $CH_3 \rightarrow {}^3CH_2 \rightarrow CH$, i.e., $CH_3 + H$ (R99, R100b), $CH_3 + OH$ (R103) and ${}^3CH_2 + H$ (R106), also show positive sensitivity coefficients, while steps breaking this sequence (mainly $CH_3 + O$ (R101) and ${}^3CH_2 + OH$ (R107)) and steps competing with $CH + N_2$ (R4) (primarily $CH + O_2$ (R113) and $CH + H_2O$ (R115)) inhibit NO formation. Under reducing conditions, the reaction $N + OH$ (R3) also becomes important for NO formation.

Modeling predictions were compared to concentration profiles for NO and relevant precursors from a series of low-pressure, laminar premixed methane-air flames. The experimental data were obtained by Berg et al. [95] who detected CH and NO, and by Desgroux and coworkers [62, 72, 96–99], who in addition to CH and NO reported concentration profiles for HCN, NCN, CN, and NCO. In both flame studies methane was used as fuel, at pressures of 25-30 and 40 torr,

28

respectively, and over a range of equivalence ratios.

Figure 10 compares measured NO concentration profiles with modeling predictions for six flames from Lamoureux et al. and Berg et al. Despite differences between the two sets of flames, some common trends are seen. The measured NO increases with fuel-air equivalence ratio in these flames, ranging from about 5 ppm in the lean flames ($\phi = 0.80$) to 25-40 ppm in the fuel-rich flames ($\phi = 1.25$-1.28). This is expected, since prompt NO is the controlling NO formation mechanism in these flames, with temperatures in the range 1750-1980 K. The model predicts the NO profile quite accurately under slightly lean conditions, but underpredicts NO under stoichiometric and reducing conditions. In the fuel-rich flames where we see the largest discrepancy, the calculated NO is about a factor of two below measurements.

Figure 11 compares the measured and calculated CH-profiles from the two sets of flames. Even though the equivalence ratios investigated in the studies of Lamoureux et al. and Berg et al. are similar, differences in pressure and temperature mean that the flames are not directly comparable. Modeling predictions are generally in satisfactory agreement with measurements. The only important difference is observed for the fuel-rich flame of Berg et al., where CH is underpredicted by a factor of two. However, in the similar flame from Lamoureux et al., CH is predicted quite accurately.

Figure 12 shows results for the key nitrogen intermediates in prompt NO formation for the flames of Lamoureux et al. The concentrations of HCN, NCN, and CN are all captured well by the model. The largest discrepancy is seen for NCO, which is underpredicted in the stoichiometric and the fuel-rich flame.

To bring the present modeling predictions in agreement with the measured NO profile in the rich flame, the rate constant for the reaction NCN + H → HCN + N (R8) needs to be increased by more than a factor of four, bringing it roughly in agreement with the determination from Fassheber et al. [78] and the
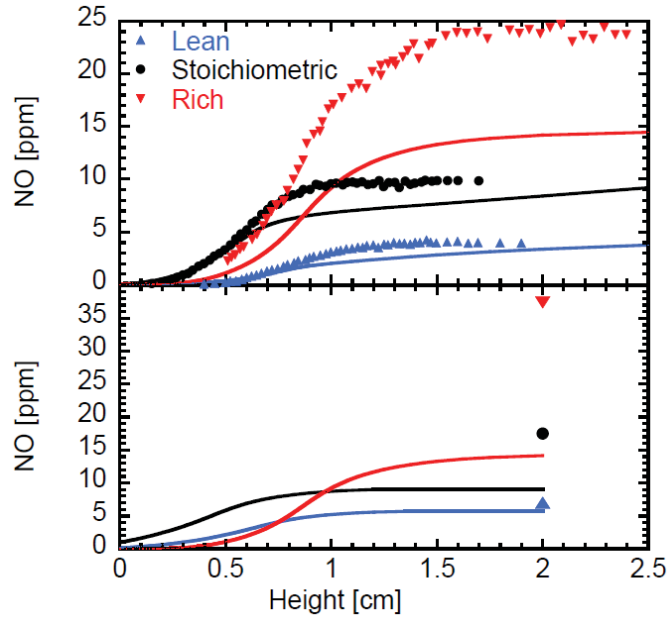
29

Figure 10: Comparison of measured [62, 72, 95, 97] and predicted mole fractions of NO low-pressure premixed methane/oxygen/nitrogen flames as a function of fuel-air equivalence ratio. The symbols denote experimental data, while the solid lines denote calculated values. Conditions for the flames of Lamoureux et al. [62, 72, 97]: fuel-air equivalence ratios of 0.80 (lean, T_{max} = 1825 K), 1.0 (stoichiometric, T_{max} = 1875 K) and 1.25 (rich, T_{max} = 1845 K); pressure 40 torr. Conditions for the flames of Berg et al. [95]: fuel-air equivalence ratios of 0.81 (lean, 25 torr, T_{max} = 1750 K), 1.07 (stoichiometric, 25 torr, T_{max} = 1920 K) and 1.28 (rich, 30 torr, T_{max} = 1980 K).

optimized rate constant used by Lamoureux et al. [72]. Such a change would be outside the estimated 2σ uncertainty of a factor of 1.5 for the theoretical rate constant [82]. While a high value for k_8 is not supported by theory, it is evident that the predictions of the present model deteriorates under reducing conditions and more work is desirable to resolve the differences.

Prediction of prompt NO formation requires an accurate rate constant for the CH + N_2 reaction (R4), as well as the ability to predict both the CH concentration and the selectivity in the oxidation of NCN to form NO or N_2. The value of k_4 is known better than a factor of two, but the rate constants for important
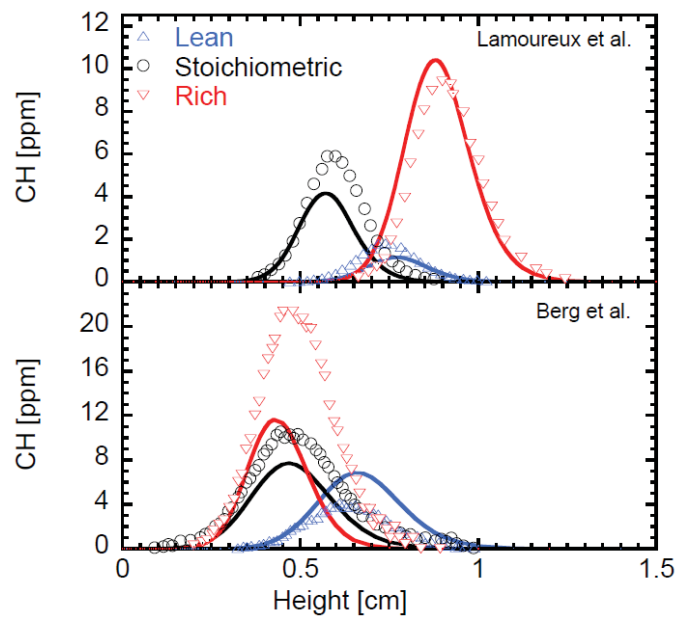
Figure 11: Comparison of measured [72, 95] and predicted mole fractions of CH in low-pressure premixed methane/oxygen/nitrogen flame as a function of fuel-air equivalence ratio. The symbols denote experimental data, while the solid lines denote calculated values. Conditions for the flames of Lamoureux et al. [72]: fuel-air equivalence ratios of 0.80 (lean), 1.0 (stoichiometric) and 1.25 (rich); pressure 40 torr. Conditions for the flames of Berg et al. [95]: fuel-air equivalence ratios of 0.81 (lean, 25 torr), 1.07 (stoichiometric, 25 torr) and 1.28 (rich, 30 torr).

NCN reactions, in particular NCN + H, are still in discussion. Consequently, the accuracy in predicting prompt NO formation in the combustion of methane or natural gas is probably not better than a factor of two. The uncertainty in predictions for other hydrocarbon fuels may be even larger, due to concerns about predicting accurately the concentration of CH [70].
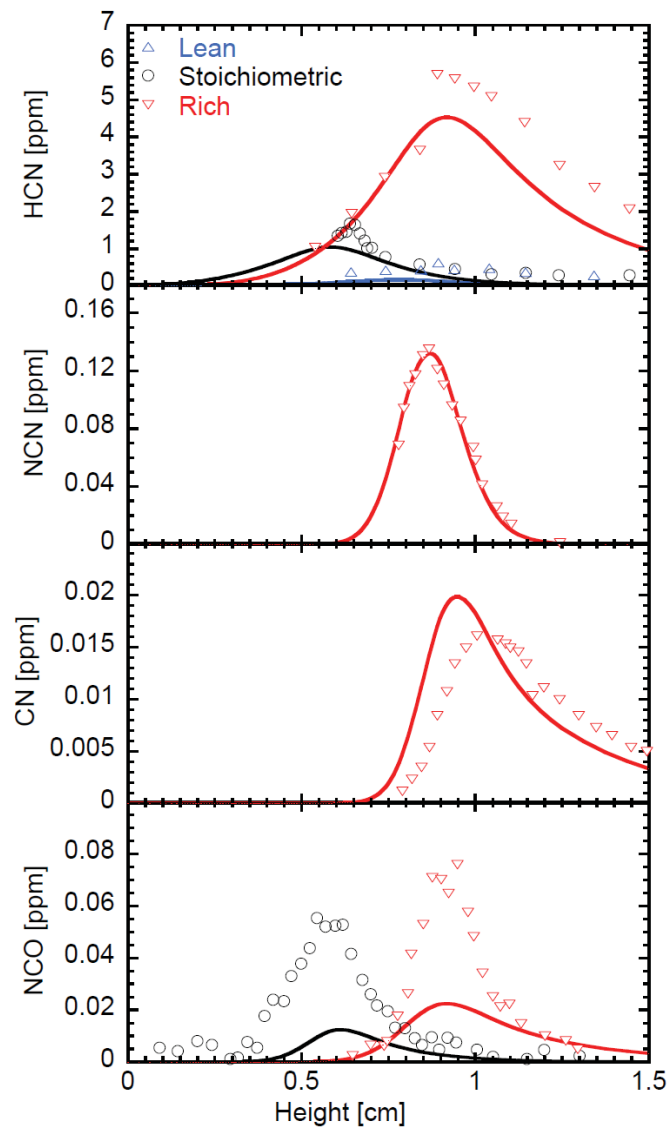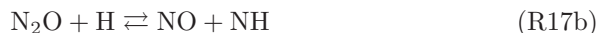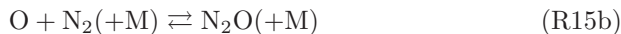
Figure 12: Comparison of measured [62, 72, 97] and predicted mole fractions of HCN, NCN, CN, and NCO in low-pressure premixed methane/air flames. The symbols denote experimental data, while the solid lines denote calculated values. Conditions: fuel-air equivalence ratios of 0.80 (lean), 1.0 (stoichiometric) and 1.25 (rich); pressure 40 torr.

3.3 The N_2O and NNH Mechanisms

Additional reaction paths to NO from atmospheric nitrogen are initiated by recombination of N_2 with atomic oxygen, $O + N_2 (+M) \rightarrow N_2O (+M)$ [101], or atomic hydrogen, $H + N_2 (+M) \rightarrow NNH (+M)$ [102], followed by oxidation of the nitrogen intermediate to NO. The N_2O scheme may be important under lean conditions at high pressure and moderate temperatures, while the NNH mechanism is most significant at slightly reducing conditions and higher temperatures, perhaps in particular in diffusion flames where NNH may form on the fuel-rich side of the flame sheet and then react with O inside the flame sheet [103]. While the N_2O mechanism is quite well established, the importance of NO formation through NNH remains controversial, as discussed below.

3.3.1 Reaction subset for NO formation via N_2O

The N_2O mechanism was proposed by Malte and Pratt [101]. It involves the steps

$$O + N_2(+M) \rightleftarrows N_2O(+M) \tag{R15b}$$

$$N_2O + H \rightleftarrows NO + NH \tag{R17b}$$

$$N_2O + O \rightleftarrows NO + NO \tag{R18}$$

The NH radical may react with OH or O_2 to form NO, or react with NO to form N_2 or N_2O. The NO forming reactions compete with steps recycling N_2O to N_2,

$$N_2O + H \rightleftarrows N_2 + OH \tag{R16}$$

$$N_2O + O \rightleftarrows N_2 + O_2 \tag{R19}$$

The N_2O subset of the mechanism is listed in Table 5. Data on the association reaction between N_2 and O (R15b) are very limited, but the reverse reaction,

dissociation of N_2O (R15), has been studied experimentally over a wide range of conditions. The data, reviewed by Baulch et al. [26], are in very good agreement. The selectivity for forming NO or N_2 from N_2O is largely controlled by the branching fractions of the reactions of N_2O with H and O, respectively.

		A	β	E	Source
15.	$N_2O(+M) \rightleftarrows O + N_2(+M)$	9.9E10	0.000	57901	[26]
	Low pressure limit:	6.0E14	0.000	57444	
16.	$N_2O + H \rightleftarrows N_2 + OH$	6.4E07	1.835	13492	[19]
17.	$NH + NO \rightleftarrows N_2O + H$	2.7E15	-0.780	20	See text
18.	$N_2O + O \rightleftarrows NO + NO$	9.2E13	0.000	27679	[104]
19.	$N_2O + O \rightleftarrows N_2 + O_2$	9.2E13	0.000	27679	See text

Table 5: Reactions involved in the N_2O mechanism. Parameters for use in the modified Arrhenius expression k = AT^{β} exp(-E/[RT]). Units are mol, cm, s, cal.

The N_2O + H reaction was studied theoretically by Klippenstein et al. [19]. Their calculated rate constant is in excellent agreement with the measurements of Marshall et al. [105]. The reaction yields predominantly N_2 + OH (R16), except at very low temperatures where addition occurs. The product channel to form NH + NO (R17b) is only minor and reliable data for the forward reaction are scarce. However, the NH + NO reaction has been studied extensively. The reaction has two major product channels:

$$NH + NO \rightleftarrows N_2O + H \tag{R17}$$

$$NH + NO \rightleftarrows N_2 + OH \tag{R71}$$
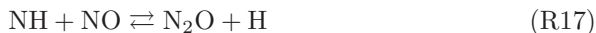
Reported results for the overall rate constant for NH + NO are summarized in Fig. 13. The low temperature measurements agree to within a factor of two, and the data of Lillich et al. [106] and Romming and Wagner [107], which are in good agreement, serve to extrapolate the data up to about 2200 K. Also the

theoretical rate constant from Klippenstein et al. [19] and the evaluation by Baulch et al. [26] are shown, both for k_{17} + k_{71}.

Experimental [106, 108–112] and theoretical [19] data for the branching ratio of the reaction show that N_2O + H (R17) is dominating in the 300-2200 K range, contributing 70-90% of the total rate. The N_2 + OH channel (R71) accounts for 10-30%; according to theory this value increases only slightly with temperature [19].
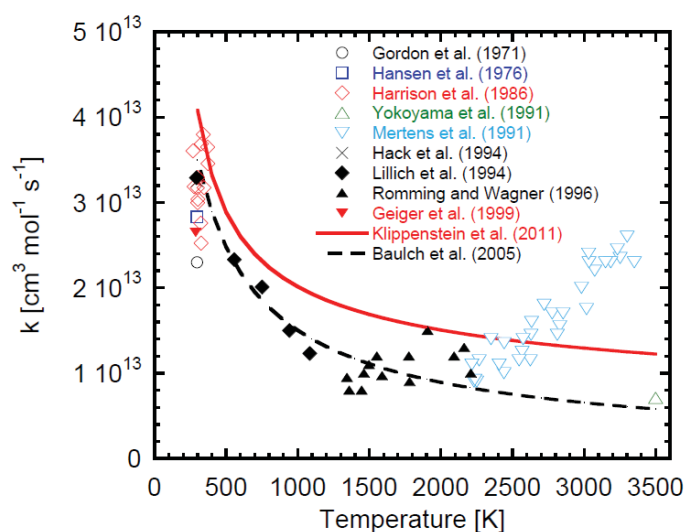

Figure 13: Arrhenius plot for the reaction NH + NO → products. The symbols denote measurements of the rate constant, while lines denote theoretical values (solid line) or evaluations (dashed line). The data are drawn from Gordon et al. [113], Hansen et al. [114], Harrison et al. [115], Yokoyama et al. [108], Mertens et al. [109], Hack et al. [116], Lillich et al. [106], Romming and Wagner [107], Geiger et al. [117], Klippenstein et al. [19] (k_{17} + k_{71}) and Baulch et al. [26] (k_{17} + k_{71}).

At temperatures above 2200 K there are only two reported studies of NH + NO, both conducted in a shock tube using HNCO as a source of NH. Mertens et al. [109] report overall rate measurements in the 2200-3350 K range, while Yokoyama et al. [108] report a single measurement at 3500 K. The data from Mertens et al., which are in good agreement with those of Romming and Wagner

in the overlapping temperature range, indicate an increase in the rate constant for NH + NO above 2200 K. The upturn in the rate constant is not consistent with the measurement of Yokoyama et al. Their result for k_{NH+NO} at 3500 K is about a factor of three lower than the data of Mertens et al., but in excellent agreement with the recommendation of Baulch et al. for $k_{17} + k_{71}$.

Baulch et al. [26] attributed the high temperature increase detected by Mertens et al. in the rate constant for NH + NO to a third product channel,

$$NH + NO \rightleftarrows NNH + O \qquad \text{(R23b)}$$
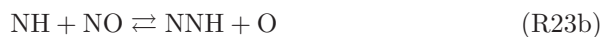
This would require a rate constant for NNH + O (R23) close to collision frequency at high temperatures. While this would be in agreement with early estimates [102, 118, 119], theoretical work [19, 120] indicates a value about an order of magnitude lower, making the NNH + O channel (R23) insignificant for the overall rate of NH + NO. Reaction R23 is discussed in detail in section 3.3.2 below.

We have adopted the value for $k_{17} + k_{71}$ and the branching fraction $k_{71}/(k_{17} + k_{71})$ from Baulch et al. [26]; these rate coefficients are in agreement with the theoretical work [19] within the uncertainty, but provide a slightly better agreement with the experiments of Lillich et al. and Romming and Wagner in the temperature range of interest in this study.

For the N_2O + O reaction, the rate constant for forming NO + NO (R18), measured both in the forward and reverse directions, and at high temperatures also the overall rate constant are well established [26, 104]. However, the predicted formation of NO from N_2O is sensitive to the branching fraction of the N_2O + O reaction between NO + NO (R18) and $N_2 + O_2$ (R19) and the value of k_{19} has significant error limits at intermediate temperatures [26]. In early evaluations by Baulch et al. [121] and Hanson and Salimian [122], it was concluded that k_{18} and k_{19} were similar over a wide temperature range. More recently, this

finding was questioned by Meagher and Anderson [104]. From a reevaluation of the available experimental results, they concluded that most likely reaction R19 had a significantly smaller activation energy than R18, causing formation of N_2 + O_2 to dominate at lower temperatures, while NO formation dominated at temperatures above 1900 K.

Reported experimental results obtained at lower temperatures do not support the conclusions of Meagher and Anderson regarding k_{19}. Kaufman et al. [123] conducted a batch reactor study of decomposition of N_2O and formation of NO at temperatures of 876-1031 K. Their data indicate that the NO producing channel (R18) constitutes at least 50% under these conditions. Meagher and Anderson discarded the batch reactor results due to concern about surface effects. However, according to Kaufman et al. an increase in the surface/volume ratio resulted in a decrease, not an increase, in formation of NO. The decrease in NO formation would be consistent with loss of atomic oxygen on the quartz surface (see App. A). In the present work, we have adopted the rate constant for reaction R18 from the review of Meagher and Anderson [104], but tentatively assumed that k_{18} = k_{19} based on the results of Kaufman et al. [123], Dindi et al. [124], and Rohrig et al. [125]. A high activation energy for reaction R19 is consistent with theoretical work [126], but more work on this reaction is desirable.

3.3.2 Reaction subset for NO formation via NNH

The reaction subset for NNH is listed in Table 6. The mechanism for forming NO via NNH consists of the reaction sequence [102],

$$H + N_2(+M) \rightleftarrows NNH(+M) \tag{R20b}$$
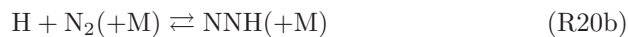
$$NNH + O \rightleftarrows NH + NO \tag{R23}$$

followed by oxidation of NH.

		A	β	E	Source
20.	$NNH \rightleftarrows N_2 + H$	1.0E09	0.000	0	[19]
21.	$NNH + O \rightleftarrows N_2O + H$	1.9E14	-0.274	-22	[19]
22.	$NNH + O \rightleftarrows N_2 + OH$	1.2E13	0.145	-217	[19]
23.	$NNH + O \rightleftarrows NH + NO$	5.2E11	0.381	-409	[19]
24.	$NNH + O_2 \rightleftarrows N_2 + HO_2$	5.6E14	-0.385	-13	[19]

Table 6: Selected reactions from the NNH subset. Parameters for use in the modified Arrhenius expression $k = AT^{\beta} \exp(-E/[RT])$. Units are mol, cm, s, cal.

The rate constant for NNH dissociation (R20) is discussed in more detail in section 4.1.1. With a lifetime of NNH of about 10^{-9} s [19], the NNH $\rightleftarrows N_2$ + H reaction equilibrates rapidly. Thereby, the yield of NO from the NNH mechanism becomes directly proportional to the rate constant for NNH + O $\rightleftarrows$ NH + NO (R23), as well as to the equilibrium constant $K_{C,20b}$ for reaction R20b [19,127]. The equilibrium constant $K_{C,20b}$ depends on the heat of formation of NNH, which is now well established at a value of $\Delta_f H^0_{298}(NNH) = 59.7$ kcal mol^{-1} [19]. Contrary to this, reported rate constants for the NNH + O $\rightarrow$ NH + NO reaction (R23) vary by more than an order of magnitude, as shown in Fig. 14.

There are no direct measurements of k_{23}. The data shown from Mertens et al. are calculated from their shock tube measurements of k_{NH+NO} by subtracting $k_{17} + k_{71}$ and then converting the resulting value for k_{23b} to k_{23} through the equilibrium constant. Hayhurst and Hutchinson reported values of $k_{23} \cdot K_{C,20b}$, derived from flame measurements, with error limits of a factor of five; we have used the present thermochemistry to obtain k_{23}. Konnov and De Ruyck [128] based their recommendation for k_{23} on a re-interpretation of flame data from Harrington et al. [129] at 1200 K. Their value is compatible with the results from Hayhurst and Hutchinson (1800-2500 K) and from Mertens et al.
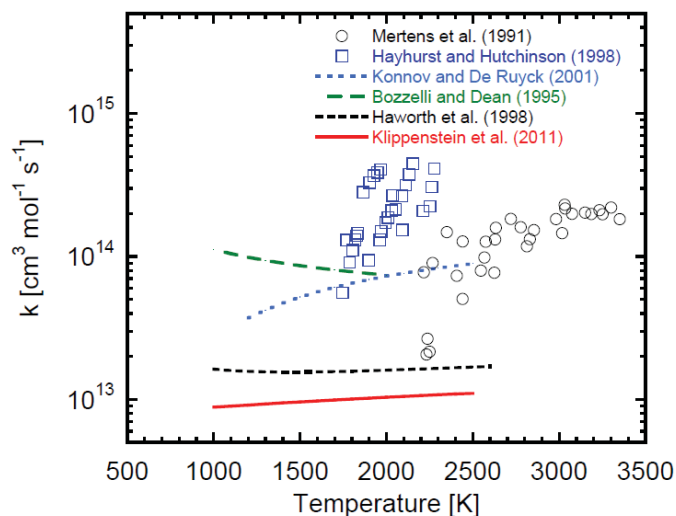
38

Figure 14: Arrhenius plot for the reaction NNH + O → NH + NO (R23). The data are drawn from the following sources: Mertens et al. [109] (shock tube study), Bozzelli and Dean [102], Hayhurst and Hutchinson [127] (flame study), Konnov and De Ruyck [128] (flame study), Haworth et al. [120] (theory), and Klippenstein et al. [19] (theory). The data from Mertens et al. are derived from their overall measurements of k_{NH+NO}, subtracting $k_{17} + k_{71}$ and converting through the equilibrium constant. The data from Hayhurst and Hutchinson are derived from their reported values of $k_{23} \cdot K_{C,20b}$, using the present thermochemistry.

These indirect experimental determinations of k_{23} all support a value close to collision frequency. However, the theoretical studies by Haworth et al. [120] and Klippenstein et al. [19] indicate a much lower rate constant for reaction R23 (Fig. 14). In the present work, we have drawn k_{23} from the theoretical study of Klippenstein et al. [19]. This value has an estimated 2σ uncertainty of a factor of two. The implications of this choice for predicting NO formation through the NNH mechanism is discussed below.

3.3.3 Modeling NO formation from the N_2O and NNH mechanisms

Under most conditions, formation of NO via N_2O or NNH is a minor source of nitric oxide compared to thermal NO and prompt NO. For this reason experi-

39

ments where the N_2O or NNH mechanisms dominate NO formation are scarce. To exclude the possibility of prompt-NO formation, we select validation data only from non-hydrocarbon systems, i.e. with H_2 or H_2/CO mixtures as fuel.

Following Haworth et al. [120] and Klippenstein et al. [19], we have selected the low-pressure, fuel-rich flames of Harrington et al. [129] and the lean jet-stirred reactor experiments of Steele et al. [130] for comparison with modeling predictions. The H_2/air flames of Harrington et al. were designed to minimize formation of NO through thermal NO and N_2O mechanisms while yielding measurable quantities of NO from NNH. To obtain this condition, the flames were operated at comparatively low temperature (about 1200 K) and under reducing conditions.

In Fig. 15, the measured NO profile from the 38 torr flame of Harrington et al. is compared with modeling predictions. The amount of NO formed is very low, below 1 ppm. Even so, the model underpredicts NO in the flame by almost an order of magnitude. We currently cannot explain the difference between the observed and calculated NO levels for this flame. With a value of k_{23} of about 10^{14} cm^3 mol^{-1} s^{-1}, the NO predictions become in agreement with experiment. However, such a fast step appears to be incompatible with the theoretical work [19,120], which clearly indicates that NH + NO is only a minor channel of the NNH + O reaction.

Malte and co-workers [101, 130] have conducted a range of jet-stirred reactor experiments to characterize NO formation in lean, premixed combustion. While NO is mostly formed via N_2O under these conditions, the CO/H_2 oxidation data of Steele et al. [130] is sensitive also to NO formation from the NNH mechanism [19,120]. Figure 16 compares measured and predicted NO and N_2O concentrations as a function of temperature. The model predicts both NO and N_2O within about 20%. Analysis of the calculations indicates that the N_2O mechanism dominates under the conditions of these experiments. However, augmented by the high levels of radicals in the reactor, the NNH mechanism is
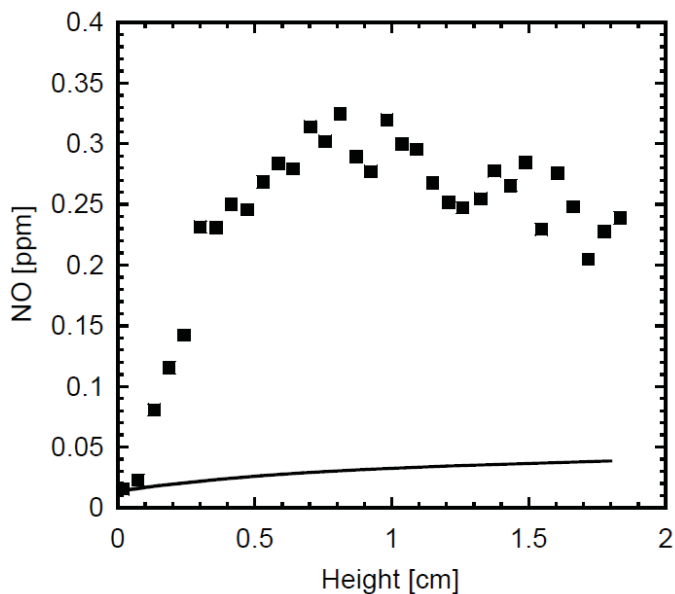
Figure 15: Comparison of measured [129] and predicted mole fractions of NO in a low-pressure premixed hydrogen/air flame. The symbols denote experimental data, while the solid lines denote calculated values. Conditions: pressure of 38 torr, fuel-air equivalence ratio of $\phi = 1.5$, and flame temperatures of the order of 1200 K.

also active, contributing about 25% to the formation of NO. It is noteworthy that modeling predictions with a high rate constant for the NNH + O $\rightleftarrows$ NH + NO reaction (R23) leads to a substantial overprediction of NO under these conditions [19, 120].

The N_2O mechanism is well established and predictions of NO formed from this scheme would be expected to be quite accurate at relevant temperatures and pressures. The main uncertainty relates to the activation energy for N_2O + O $\rightarrow N_2 + O_2$ (R19), which particularly at lower temperatures has some impact on the calculated NO.

The prediction of NO from NNH is significantly more uncertain. High level theoretical results for $\Delta_f H^0_{298}(NNH)$ [19] and for the NNH + O reaction [19,120] indicate that the NNH mechanism may be less important than indicated by early
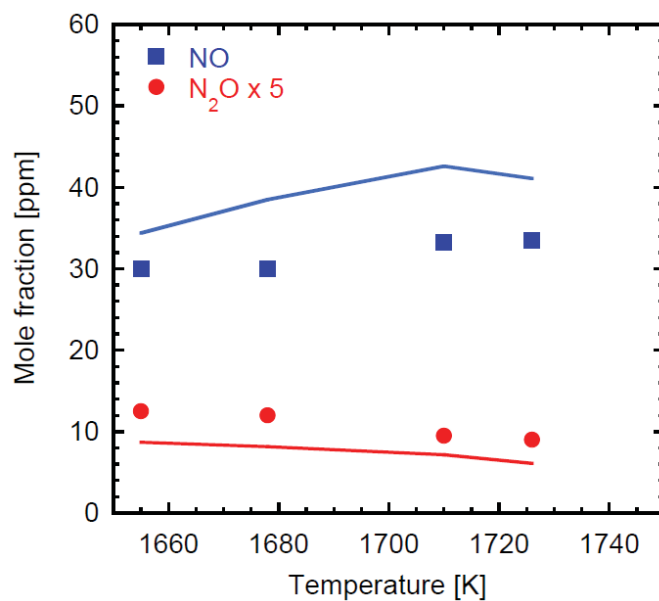
Figure 16: Comparison of measured [130] and predicted mole fractions of NO and N_2O in CO/H_2/air combustion in a jet-stirred reactor. The symbols denote experimental data, while the solid lines denote calculated values. Results are shown as a function of temperature with the following inlet composition: 17.4% CO, 82% air, 0.69-0.25% H_2 (decreasing with increasing temperature). The nominal residence time was about 4.0 ms.

modeling studies. Experimental results [129,130] are inconclusive and additional experimental work is called for to validate this subset.

3.4 Oxidation of HCN

In combustion processes, cyanides may be formed from reaction of CH and C with N_2 (the initiating steps in prompt NO formation), from reaction of reactive nitrogen species such as NO or amines with hydrocarbon radicals, from decomposition of hydrocarbon amines, or from devolatilization of fuels with organically bound nitrogen [1–4,131]. The predominant cyanide species in combustion is hydrogen cyanide (HCN) and the oxidation chemistry of this component has been studied extensively over the years [132–143]. Much of this work was reviewed by Dagaut et al. [20]. Recently the chemistry was re-examined by Glarborg and Marshall [143], who emphasized the role of the hydrogen isocyanide isomer HNC. The key issue in HCN chemistry is the selectivity towards forming other nitrogen species during oxidation, i.e., NH_3, HNCO, NO, N_2O, and N_2.

3.4.1 Reaction subset for HCN oxidation

Table 7 lists selected reactions from the HCN subset of the chemical kinetic model. It is based on the work of Dagaut et al. [20], adopting the modifications suggested by Glarborg and Marshall [143]. The major consumption steps for HCN are the reactions with O (R27-R29) and OH (R30-R33). Both of these reactions are complicated processes that involve multiple potential wells and multiple product channels [1]. While rate constant and product channels are fairly well established for the HCN + O reaction [1, 20, 144], few experimental data are available for HCN + OH. Only the H-abstraction reaction R30 is well characterized experimentally [143]. For the other product channels of HCN + OH (R31-33), rate constants are drawn from BAC-MP4 calculations by Miller and Melius [145].

Hydrogen isocyanide (HNC) has been proposed as an important intermediate in oxidation of HCN in combustion [154]. At higher temperatures, HCN and HNC equilibrate rapidly through isomerization (R25), and, being more reactive than

		A	β	E_a	Source
25.	$HCN + M \rightleftarrows HNC + M$	1.6E26	-3.230	54900	[146]
26.	$CN + H_2 \rightleftarrows HCN + H$	1.1E05	2.600	51908	[26]
27.	$HCN + O \rightleftarrows NCO + H$	1.4E04	2.640	4980	[1]
28.	$HCN + O \rightleftarrows NH + CO$	3.5E03	2.640	4980	[1]
29.	$HCN + O \rightleftarrows CN + OH$	4.2E10	0.400	20665	[146]
30.	$HCN + OH \rightleftarrows CN + H_2O$	3.9E06	1.830	10300	[147]
31.	$HCN + OH \rightleftarrows HOCN + H$	5.9E04	2.430	12500	[145]
32.	$HCN + OH \rightleftarrows HNCO + H$	2.0E-03	4.000	1000	[145]
33.	$HCN + OH \rightleftarrows NH_2 + CO$	7.8E-04	4.000	4000	[145]
34.	$HNC + H \rightleftarrows HCN + H$	7.8E13	0.000	0	[148]
35.	$HNC + O \rightleftarrows NH + CO$	4.6E12	0.000	2200	[146]
36.	$HNC + OH \rightleftarrows HNCO + H$	3.6E12	0.000	-479	[143, 149]
37.	$CN + O_2 \rightleftarrows NCO + O$	5.8E12	0.000	-417	[26, 150]
38.	$CN + O_2 \rightleftarrows NO + CO$	1.4E12	0.000	-417	[26, 150]
39.	$NCO + H \rightleftarrows NH + CO$	7.2E13	0.000	1000	[26]
40.	$NCO + O \rightleftarrows NO + CO$	2.0E15	-0.500	0	[151]
41.	$NCO + O_2 \rightleftarrows NO + CO_2$	2.0E12	0.000	20000	[152] est
42.	$NCO + NO \rightleftarrows N_2O + CO$	4.0E19	-2.190	1743	[153]
43.	$NCO + NO \rightleftarrows N_2 + CO_2$	1.5E21	-2.740	1824	[153]

Table 7: Selected reactions in the HCN oxidation subset. Parameters for use in the modified Arrhenius expression k=AT$^\beta$exp(-E/[RT]). Units are mol, cm, s, cal.

HCN, HNC offers an alternative route of oxidation for cyanides. The major issues regarding HNC have been the energy separation to HCN, important for the predicted concentration of HNC when equilibrated with HCN, and the rate constants for the reactions of HNC with OH and O_2. Both the thermodynamic properties of HNC and the key HNC reactions are known more accurately due to recent work. Nguyen et al. [12] determined the energy difference between HCN and HNC at 298 K to be 15.1±0.1 kcal mol^{-1}, 2.2 kcal mol^{-1} higher than that proposed in the early study by Lin et al. [154] and 0.3 kcal mol^{-1} higher than the recommendation of Dagaut et al. [20]. Reactions of HNC with OH (R36) [149] and O_2 [143] have been characterized theoretically and both steps appear to be slower at relevant temperatures than assumed in earlier modeling

studies. In particular, Glarborg and Marshall [143] report a high barrier of 44 kcal mol^{-1} for the latter reaction, making it irrelevant under most conditions of interest.

Compared to the HCN subset from previous work [20, 143], only a few changes have been made. The most important of these concerns the reaction of the CN radical with O_2. This step is fast and the overall rate constant is well established. However, the branching fraction to the two product channels NCO + O (R37) and NO + CO (R38) has been in discussion. Measurements of the branching fraction [150, 155, 156] are in good agreement at room temperature. Recently, Feng and Hershberger [150] verified that the NO + CO channel (R38) constituted 20% with little or no temperature dependence over the range 296-475 K, in contrast to earlier results from the same group [156], and we have adopted their recommendation.

3.4.2   Modeling HCN oxidation

In the following, modeling predictions for HCN oxidation are compared to experimental results from flames (high temperature, reducing conditions) and flow reactors (intermediate temperatures, oxidizing conditions).

Following Glarborg and Marshall [143], we compare modeling predictions for the post-flame zone with measurements from a rich ethylene flame doped with ammonia (Fig. 17). The conditions are representative of the high-temperature region in fuel-rich combustion prior to the rich-lean transition. The experimental data are from Haynes [157] who investigated the decay of hydrogen cyanide in the burnt gases of a number of fuel-rich, atmospheric pressure hydrocarbon flames, using nitrogen additives (ammonia or pyridine) as a source of HCN. In the reaction zone of the flame, the additive would be converted to HCN, with smaller amounts of NO. In the post-flame zone, HCN was slowly converted to NH_3. The temperature of the burnt gases was 2000 K. In the modeling,

it was assumed that both ethylene and oxygen were depleted in the reaction zone, resulting in an equilibrium mixture of CO, H_2, CO_2, and H_2O entering the post-flame zone together with measured concentrations of HCN, NH_3, and NO [143].

The modeling predictions are in good agreement with the measurements for HCN, NH_3, and NO. Hydrogen cyanide is consumed through a two step sequence,

$$HCN + M \rightleftharpoons HNC + M \tag{R25}$$

$$HNC + OH \rightarrow HNCO + H \tag{R36}$$
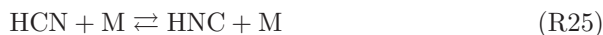
Under the conditions in the flame, HCN equilibrates rapidly with HNC. Atomic hydrogen and to a lesser extent OH are the dominant radicals in the flame but they consume little HCN because the reactions $HCN + H \rightleftharpoons CN + H_2$ (R26b) and $HCN + OH \rightleftharpoons CN + H_2O$ (R30) are both rapidly equilibrated. The HNCO formed in reaction R36 feeds rapidly into the amine pool, eventually forming NH_3:

$$HNCO + H \rightleftharpoons NH_2 + CO \tag{R44}$$

$$NH_2 + H_2 \rightleftharpoons NH_3 + H \tag{R53b}$$

A smaller fraction of the NH_2 is converted to NH and N through the sequence $NH_2 \xrightarrow{+H} NH \xrightarrow{+H} N$. The NH and N radicals may be oxidized to NO by reaction with OH or react with NO to form N_2O or N_2. This competition results overall in a small decrease in NO concentration.

In combustion, HCN is oxidized to NO and N_2 under excess air conditions, typically in the presence of combustibles. Figure 18 compares flow reactor results from Hulgaard and Dam-Johansen [136] and Glarborg and Miller [137] on lean oxidation of HCN with modeling predictions. The upper figure shows results for HCN oxidation in the absence of combustibles [137], while the lower figure shows the impact of adding CO as a reactant [136]. The agreement between
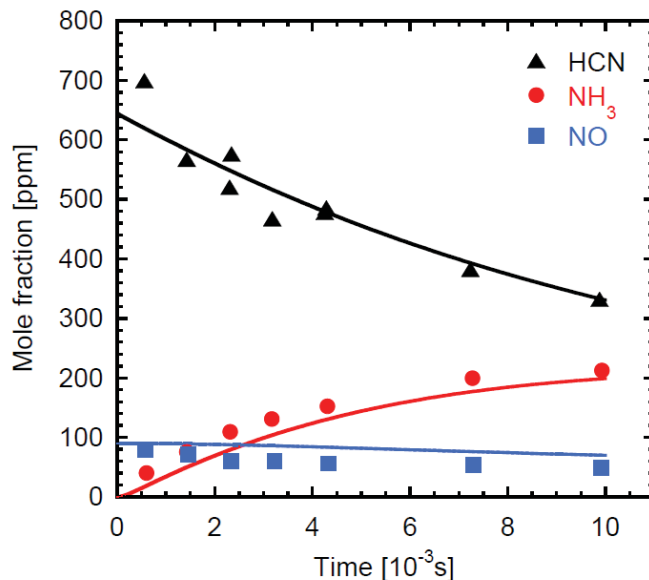
Figure 17: Comparison between experimental data [157] and modeling predictions for HCN oxidation in the post-flame region of an atmospheric pressure, premixed, fuel-rich ethylene-air flame doped with 680 ppm ammonia. Symbols denote experimental data while lines denote modeling predictions. Fuel-air equivalence ratio $\phi = 1.66$; temperature 2000 K.

model and experiment is good. In the absence of CO, the conversion of HCN to HNCO is underpredicted at lower temperatures, while predicted concentrations of NO and N_2O at higher temperatures are slightly too high.

Figure 19 shows a reaction path path diagram for HCN oxidation under the conditions of Fig. 18. In the absence of CO, predictions are sensitive to the generation of radicals. Due to the abundance of O_2 and H_2O in the flow reactor experiments, representative of the burnout region in combustion systems, H and O atoms are efficiently converted to OH, which becomes the dominant chain carrier. This occurs through the chain branching sequence H + O_2 → O + OH, O + H_2O → OH + OH. Consequently, removal of HCN is controlled primarily by reaction with OH (R30), followed by a fast reaction of CN with O_2 to form NCO + O (R37). The subsequent reactions of NCO largely determine

the fate of the N atom in the HCN oxidation process. Under the conditions of Fig. 18(upper), NCO reacts primarily with H_2O (R48b) at lower temperatures, thereby converting HCN to HNCO. Due to low radical concentrations, consumption of HNCO is very slow below 1150 K. As the temperature increases, the $NCO + H_2O \rightarrow HNCO + OH$ reaction is reversed at longer reaction times. In this way, reaction R48 becomes the main consumption channel for HNCO as well as the main source.
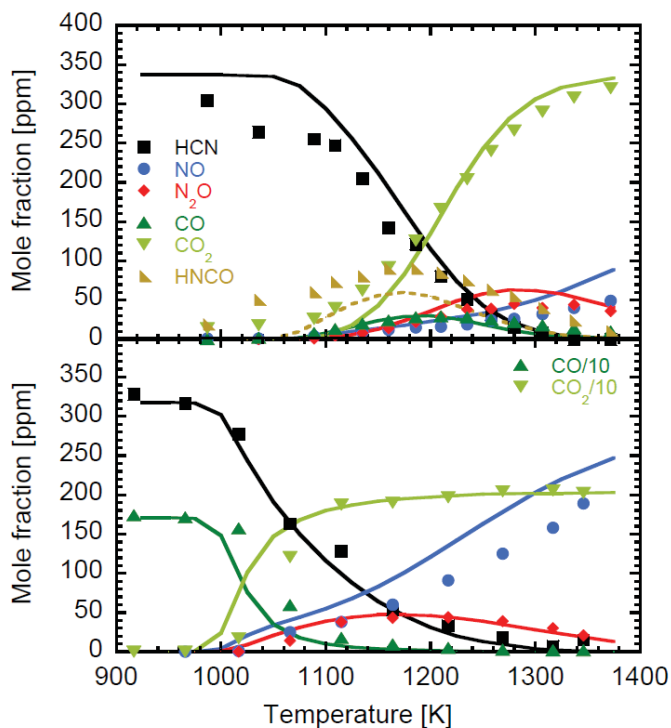

Figure 18: Comparison of experimental data [136,137] and modeling predictions for HCN oxidation in quartz a flow reactor, without (*upper figure*) and with (*lower figure*) CO in the inlet. Experimental data are shown as symbols, modeling predictions as lines. Inlet mole fractions: *upper figure* HCN = 337 ppm, O_2 = 2.6%, H_2O = 3.1%; *lower figure* HCN = 318 ppm, CO = 1710 ppm, O_2 = 2.4%, H_2O = 2.8%; balance N_2. P = 1.05 atm. Reaction times are 0.149 (upper) and 0.071 sec at 900 K (constant mass flow). Surface/volume ratios were 4.4 cm^{-1} (upper) and 8.0 cm^{-1} (lower).

In the presence of combustibles, here CO (Fig. 18 lower), the generation of chain carriers becomes less sensitive to reactions in the HCN subset. The sequence CO + $OH \rightarrow CO_2 + H$, $H + O_2 \rightarrow O + OH$ acts as a source of radicals and shifts

the HCN oxidation chemistry towards lower temperatures. It also suppresses the formation of HNCO. Since OH reacts rapidly with CO, atomic oxygen now assumes a more important role in the HCN oxidation. Reaction of HCN with O (R27, R28) becomes competitive with HCN + OH (R30) in removing HCN, and a minor oxidation route now proceeds through the amine pool via reaction R28. The increased O-atom concentration also shifts the balance between the NCO + O and NCO + NO reactions and causes a comparatively larger fraction of HCN to be oxidized to NO at higher temperatures.
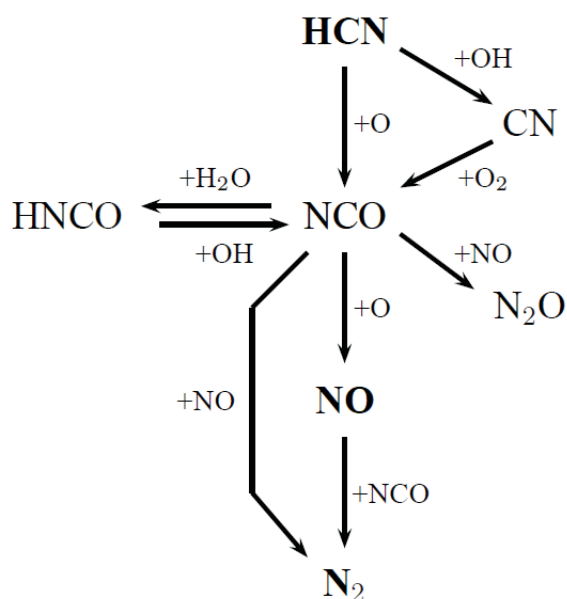
Figure 19: Reaction path diagram for oxidation of HCN under lean conditions.

For most practical purposes, the HCN oxidation chemistry is sufficiently well established. Hydrogen cyanide is very seldom a stand-alone combustible and the radical pool will typically be controlled by the oxidation of the main fuel or fuel intermediates, not by the HCN chemistry. The selectivity in HCN oxidation for forming NO, HNCO, NH_3, N_2O, or N_2 is predicted fairly accurately by the present model.

3.5 Oxidation of HNCO

Isocyanic acid (HNCO) is an important intermediate in fuel nitrogen oxidation [1,3,20,137–139]. It is also important in selective non–catalytic reduction of NO with cyanuric acid and urea, as it is a primary decomposition product of both these agents [152,158]. Previous modeling studies of HNCO oxidation [159] and reduction of NO by HNCO [1,152,159,160] have provided an understanding of the HNCO chemistry, but efforts to develop a reliable prediction tool have to some extent been hampered by the limited availability of suitable experimental data.

3.5.1 Reaction subset for HNCO oxidation

Table 8 lists selected reactions from the HNCO subset of the chemical kinetic model. The subset is mostly based on previous modeling studies by the authors [1,20,21,152,159], as well as on the evaluation by Baulch et al. [26]. Rate constants for several of the HNCO consumption reactions are fairly well established due to the low temperature work of Perry and coworkers [161,162], the medium-to-high temperature work of Lin's group [163–166], the high temperature work of Hanson and coworkers [167–170], and theoretical work, e.g., [171,172].

The main consumption step for HNCO is the reaction with OH [159],

$$HNCO + OH \rightleftarrows NCO + H_2O \tag{R48}$$

The rate constant for this reaction has been measured both at low [162] and high [170] temperatures and the results are in good agreement. Both experimental studies show that $NCO + H_2O$ is the major product channel. The importance of a secondary product channel to $NH_2 + CO_2$ has been in discussion, but the theoretical study of Sengupta and Nguyen [172] indicates that this channel is negligible.

|	A	β	E_a	Source
44. HNCO + H $\rightleftarrows$ NH$_2$ + CO	3.6E04	2.490	2345	[26]
45. HNCO + H $\rightleftarrows$ NCO + H$_2$	9.0E07	1.660	13900	[26]
46. HNCO + O $\rightleftarrows$ NH + CO$_2$	9.6E07	1.410	8520	[26]
47. HNCO + O $\rightleftarrows$ NCO + OH	2.2E06	2.110	11430	[26]
48. HNCO + OH $\rightleftarrows$ NCO + H$_2$O	3.5E07	1.500	3600	[170]
49. HNCO + O$_2$ $\rightleftarrows$ HNO + CO$_2$	2.0E13	0.000	58900	See text
50. HNCO + H$_2$O $\rightleftarrows$ NH$_3$ + CO$_2$	2.0E13	0.000	48500	[173, 174], est
51. HNCO + HNCO $\rightleftarrows$ HNCNH + CO$_2$	6.9E11	0.000	42100	[164]

Table 8: Selected reactions in the HNCO oxidation subset. Parameters for use in the modified Arrhenius expression k=AT$^\beta$exp(-E/[RT]). Units are mol, cm, s, cal.

The reaction between HNCO and O$_2$,

$$HNCO + O_2 \rightleftarrows HNO + CO_2 \tag{R49}$$

was proposed by Glarborg et al. [159] to explain the oxidation behavior of HNCO in the absence of other combustibles. They assumed an activation energy for reaction R49 of 35 kcal mol^{-1}. In the present work we estimate the barrier for the addition of triplet O$_2$ to HNCO to be about 58.9 kcal mol^{-1}. The overall barrier for reaction R49 might be even higher. Such a high barrier to reaction means that the HNCO + O$_2$ reaction is insignificant under the conditions of interest here.

Alternative reactions of HNCO include the self-reaction and the reaction with H$_2$O. Both of these reactions possibly yield CO$_2$,

$$HNCO + HNCO \rightleftarrows HNCNH + CO_2 \tag{R51}$$

$$HNCO + H_2O \rightleftarrows NH_3 + CO_2 \tag{R50}$$
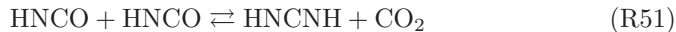
Reaction R51 has been studied both experimentally [164] and theoretically [164, 175] and data are in good agreement. The reaction is too slow to contribute

to HNCO consumption under most conditions of interest. The rate constant for formation of the HNCO dimer is predicted to be 1-2 orders of magnitude faster [175], but the dimer is not expected to be stable at elevated temperatures.

Hydrogenation of HNCO has been reported to occur readily in liquid phase [176], but there are no measurements of the gas-phase step. The reaction has been studied theoretically both in gas phase [173, 174, 177] and aqueous phase [178]. Wei et al. [173] and Cheng et al. [174] calculated barriers for R50 of 48.4 and 48.7 kcal mol^{-1}, respectively; significantly higher than the value of 35.3 kcal mol^{-1} predicted for the direct bimolecular reaction in aqueous phase [178]. Following Wei et al. [173] and Cheng et al. [174], we have included the reaction with an activation energy of 48.5 kcal mol^{-1}.

3.5.2 Modeling HNCO oxidation

The only experimental study of HNCO oxidation is the flow reactor work of Glarborg et al. [159]. However, results for the reduction of NO by HNCO (RapReNO$_x$) are also of importance for understanding the HNCO chemistry; these are discussed in section 4.1.2. Glarborg et al. investigated HNCO oxidation in the absence and presence of CO in the temperature range 1025–1425 K at atmospheric pressure. Figure 20 compares experimental results and predictions with the present model. Unfortunately, the source of HNCO in the experiments – saturation of a nitrogen stream at 195 K – was not completely stable, but the scatter in the data is limited. In order to facilitate interpretation, the experimental results are presented on a normalized basis in the figure, using the calculated concentrations of inlet HNCO. The corresponding calculations are carried out for each set with a fixed inlet composition.

Figure 20 (upper) shows results on HNCO oxidation in the absence of combustibles. Consumption of HNCO proceeds very slowly at temperatures below 1250 K. Above 1250 K the HNCO decay is faster, but even at 1400 K only of
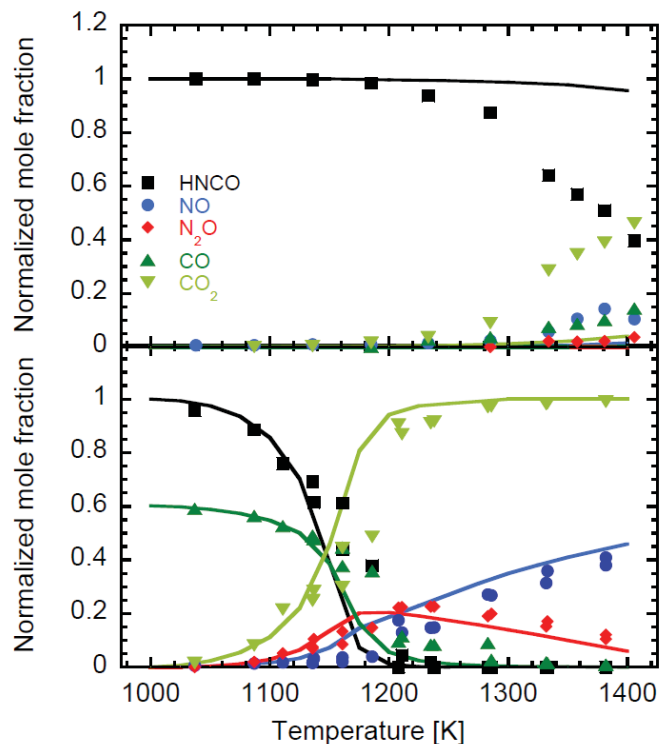
Figure 20: Comparison of experimental data [159] and modeling predictions for HNCO oxidation in a quartz flow reactor, without (*upper figure*) and with (*lower figure*) CO in the inlet. Experimental data are shown as symbols, modeling predictions as lines. The data have been normalized by the inlet HNCO concentration, calculated from a carbon balance (HNCO + CO + CO_2). Inlet mole fractions: *upper figure* HNCO = 228-336 ppm (320 ppm in the calculations), O_2 = 5.6%, H_2O = 0.5%; *lower figure* HNCO = 343-516 ppm (480 ppm in the calculations), CO = 730 ppm, O_2 = 5.5%, H_2O = 0.5%; balance N_2. P = 1.05 atm. Reaction time = 0.10 sec at 1200 K (constant mass flow). The reactor surface/volume ratio was 4.4 cm^{-1}.

the order of 50% of the inlet HNCO is consumed. Oxidation of HNCO leads to concentrations of CO_2 that are consistently larger than those of CO. Nitric oxide and N_2O constitute a comparatively small fraction of the products.

The model severely underpredicts the consumption rate of HNCO. The low predicted oxidation rate for HNCO even at high temperature is due to the fact that the major oxidation route for HNCO under these conditions is chain terminat-

ing. The OH radical is the main chain carrier, and HNCO is mainly consumed by the HNCO + OH reaction (R48), forming NCO and H_2O. The NCO radical is consumed by reaction with O (R40) and, at higher temperatures, possibly also O_2 (R41). These reactions are chain terminating and inhibit the oxidation process. Isocyanide oxidation is negligible even at 1400 K, if it proceeds exclusively through this sequence. The observed consumption of HNCO, and the formation of CO_2 rather than CO, support the importance of a reaction between HNCO and another stable species, i.e., O_2 (R49), H_2O (R50), or HNCO (R51). However, all of these steps appear to be too slow to account for the observed reaction. Formation of isomers of HNCO could potentially enhance oxidation, similarly to what is observed for HCN (see section 3.4). The isomerization pathways for HNCO have been studied theoretically by several groups [108,179,180] who find the pathway to HOCN to be energetically the most favorable. However, the overall barrier height is of the order of 90 kcal mol^{-1}, which is too high for the process to be significant at the present temperatures. Even though quartz surfaces are believed to be inert towards HNCO [158,160,181], it cannot be excluded that oxidation is promoted by heterogenous reactions on the surface.

Figure 20 (lower) shows results for HNCO oxidation in the presence of CO. The impact of CO on HNCO oxidation is similar to the effect it has on HCN oxidation, discussed in section 3.4. The presence of CO enhances the consumption rate of HNCO significantly and isocyanic acid is completely oxidized already at 1200 K, forming considerable amounts of NO and N_2O, in addition to N_2. The model describes the observations well. The predicted onset of reaction is slightly premature, but the product concentrations are in good agreement with experiment.

The CO oxidation chemistry acts to replenish the radical pool and shifts the chemistry towards lower temperatures. Similar to what was seen for HCN oxidation, this happens through the chain branching sequence CO + OH $\rightleftarrows$ CO_2

54

+ H, H + O$_2$ $\rightleftarrows$ O + OH, O+H$_2$O $\rightleftarrows$ OH + OH. Oxidation of CO is slightly inhibited by the presence of HNCO due to the chain terminating NCO reactions and the competition for OH–radicals between CO and HNCO. For this reason, CO enters the rapid oxidation regime only after most of the HNCO is depleted.

Figure 21 shows a pathway diagram for oxidation of HNCO in the presence of CO. Isocyanuric acid is consumed primarily by reaction with OH (R49), forming NCO. The NCO radical subsequently reacts either with O to form NO (R40) or with NO to form N$_2$O (R42) and N$_2$ (R43). At temperatures above 1250 K formation of N$_2$O diminishes while consumption reactions, in particular thermal dissociation, become competitive, causing a decrease in N$_2$O.
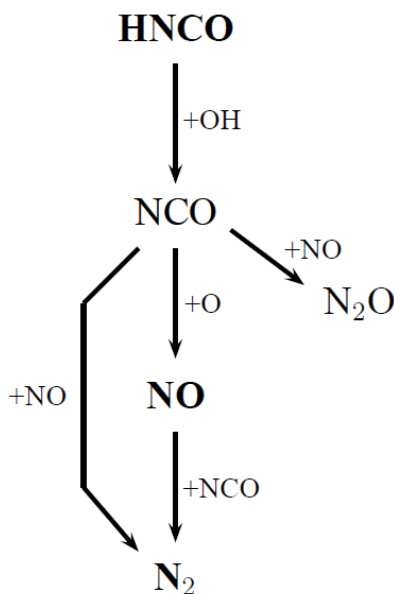
Figure 21: Reaction path diagram for oxidation of HNCO under lean conditions.

Similar to HCN, the reliability of the HNCO oxidation subset of the model is sufficient for most practical purposes. In combustion systems, HNCO is only a minor reactive nitrogen species, formed either in devolatilization of solid fuels or from partial oxidation of cyanides. The uncertainty in the HNCO oxidation chemistry is mainly related to the slow oxidation occurring in the absence of

other combustibles. However, as discussed in more detail in section 4.1.2, selective non-catalytic reduction of NO by cyanuric acid or urea is sensitive to the HNCO subset, and here the uncertainties in this chemistry limit the predictive capability of the model.

3.6 Oxidation of NH$_3$

Ammonia is the key volatile-N species in combustion. It is formed in devolatilization of solid fuels [3] or from conversion of cyanides at higher temperatures [1, 3, 131, 157]. At the rich-lean transition in staged combustion processes, NH$_3$ rather than HCN governs the nitrogen chemistry and controls the selectivity for forming NO and N$_2$ [182].

A number of modeling studies and reviews on ammonia oxidation chemistry have been reported, e.g. [1, 19, 48, 146, 183–185]. In addition, the chemistry of selective non-catalytic reduction of NO by reaction with ammonia has been studied extensively (see section 4.1.1). However, the development of reliable models for ammonia oxidation in combustion and flue gas cleaning has been hampered partly by issues concerning key reactions, in particular the branching fraction of the NH$_2$ + NO reaction and the lifetime of NNH [1,19], and partly by the strong sensitivity of ammonia to surfaces, potentially limiting the accuracy of reactor experiments (see App. A).

3.6.1 Reaction subset for NH$_3$ oxidation

Table 9 lists selected reactions in the amine subset of the chemical kinetic model. This subset was based mostly on the recent work by Klippenstein et al. [19], which again drew on previous modeling studies [22, 48, 186–189]. For many of the key reactions in the ammonia subset, rate constants have been calculated by Klippenstein and coworkers using high-level theory. These include NH$_2$ + NO [190, 191] and NH$_2$ + NO$_2$ [192], reactions on the ONNH potential energy surface (NH + NO, NNH + O, N$_2$O + H) [19], reactions of NH$_2$ and NNH with O$_2$ [19], and NH$_2$ + OH [193].

In the absence of hydrocarbons, ammonia is largely consumed by H-abstraction reactions with the O/H radical pool (R53-R55); these steps are all characterized

		A	β	E	Source
52.	$NH_2 + H(+M) \rightleftarrows NH_3(+M)$	1.6E14	0.000	0	[194]
	Low pressure limit:	3.6E22	-1.760	0	
	Troe parameters: 0.5 1.0E-30 1.0E30				
53.	$NH_3 + H \rightleftarrows NH_2 + H_2$	6.4E05	2.390	10171	[195]
54.	$NH_3 + O \rightleftarrows NH_2 + OH$	9.4E06	1.940	6460	[196]
55.	$NH_3 + OH \rightleftarrows NH_2 + H_2O$	2.0E06	2.040	566	[197]
56.	$NH_2 + HO_2 \rightleftarrows NH_3 + O_2$	1.7E04	1.550	2027	[198]
57.	$NH + H_2 \rightleftarrows NH_2 + H$	2.1E13	0.000	15417	[199]
58.	$NH_2 + O \rightleftarrows HNO + H$	6.6E14	-0.500	0	See text
59.	$NH_2 + O \rightleftarrows NH + OH$	7.0E12	0.000	0	See text
60.	$NH_2 + OH \rightleftarrows NH + H_2O$	3.3E06	1.949	-217	[19, 193]
61.	$NH_2 + HO_2 \rightleftarrows H_2NO + OH$	2.5E17	-1.280	1166	[198]
62.	$NH_2 + O_2 \rightleftarrows H_2NO + O$	2.6E11	0.487	29050	[19]
63.	$NH_2 + O_2 \rightleftarrows HNO + OH$	2.9E-2	3.764	18185	[19]
64.	$NH_2 + HNO \rightleftarrows NH_3 + NO$	5.9E02	2.950	-3469	[200]
65.	$NH_2 + NO \rightleftarrows NNH + OH$	4.3E10	0.294	-866	[201]
66.	$NH_2 + NO \rightleftarrows N_2 + H_2O$	2.6E19	-2.369	870	[201]
67.	$NH_2 + NO_2 \rightleftarrows N_2O + H_2O$	2.2E11	0.110	-1186	See text
68.	$NH_2 + NO_2 \rightleftarrows H_2NO + NO$	8.6E11	0.110	-1186	See text
69.	$NH + O_2 \rightleftarrows HNO + O$	4.6E05	2.000	6500	[202]
70.	$NH + O_2 \rightleftarrows NO + OH$	1.3E06	1.500	100	[202]
71.	$NH + NO \rightleftarrows N_2 + OH$	6.8E14	-0.780	20	See text
72.	$H_2NO + O_2 \rightleftarrows HNO + HO_2$	2.3E02	2.994	16500	See text
73.	$HNO + O_2 \rightleftarrows NO + HO_2$	2.0E13	0.000	16000	[146]

Table 9: Selected reactions in the NH_3 oxidation subset. Additional reactions are listed in Table 6. Parameters for use in the modified Arrhenius expression k=AT^{β}exp(-E/[RT]). Units are mol, cm, s, cal.

experimentally over a wide temperature range. The subsequent reactions of the NH_2 radical have a large impact on the consumption rate for NH_3 and on the selectivity for forming NO and N_2. Owing to the low reactivity of NH_2 towards O_2, the key step in the presence of even small amounts of NO is the fast NH_2 + NO reaction. Due to the importance of this reaction in the SNCR process (section 4.1.1), it has been studied extensively in the past [203]. An Arrhenius plot for the overall reaction between NH_2 and NO is shown in Fig. 22. The reaction has been measured over a wide temperature range, and data agree

roughly within a factor of two. The experimentally based value of Song et al. [204] and the theoretical rate constant from Klippenstein [191], which both provide an accurate representation of available measurements, are slightly lower than the value of Miller and Glarborg [188] used in our recent modeling work [19].
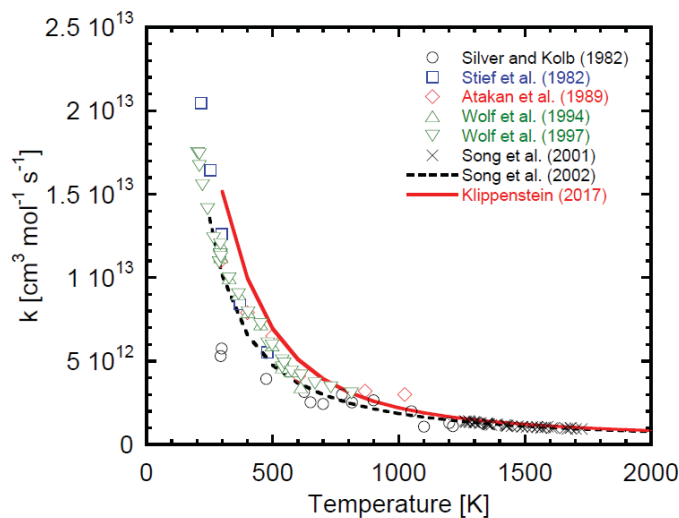
Figure 22: Arrhenius plot for the reaction $NH_2 + NO \rightarrow$ products. The symbols denote measurements of the rate constant while lines denote theoretical values. The data are drawn from Silver and Kolb [205], Stief et al. [206], Atakan et al. [207], Wolf et al. [208, 209], Song et al. [201, 204], and Klippenstein [191].

The $NH_2 + NO$ reaction has two product channels,

$$NH_2 + NO \rightleftarrows NNH + OH \tag{R65}$$

$$NH_2 + NO \rightleftarrows N_2 + H_2O \tag{R66}$$

Reaction R65 is chain branching while R66 is terminating, and for this reason, modeling predictions are very sensitive to the branching fraction for the reaction, defined as $\alpha = k_{65}/(k_{65} + k_{66})$. Figure 23 compares experimental data for the branching fraction with the theoretical ratio from Miller and Klippenstein [190] and Klippenstein [191]. The recent experimental data [201, 204, 210–213] and

the theoretical values are in very good agreement.

In the present work, we have adopted the rate constants for reactions R65 and R66 from Song et al. [201]. Their branching ratio was chosen to match the theoretical value from Miller and Klippenstein [190]. In the temperature window for the Thermal DeNO$_x$ process (around 1250 K), this value is slightly lower than the value of the CASPT2 calculation from Klippenstein [191] (see Fig. 23). Due to the very high sensitivity to α in modeling predictions for Thermal DeNO$_x$, even a very small change has a significant impact (see section 4.1.1).
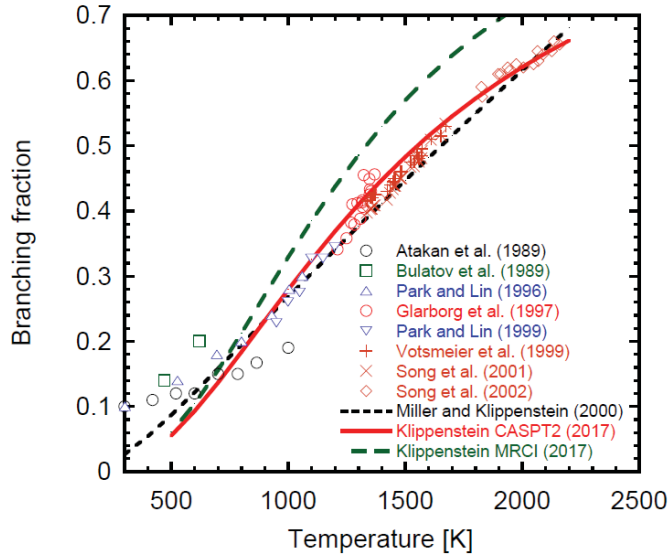
Figure 23: Arrhenius plot for the branching fraction of the reaction NH$_2$ + NO $\rightarrow$ products, defined as $\alpha = k_{65}/(k_{65} + k_{66})$. The symbols denote measurements of the rate constant while lines denote theoretical values. The data are drawn from Atakan et al. [207], Bulatov et al. [214], Park and Lin [210, 211], Glarborg et al. [212], Votsmeier et al. [213], Song et al. [201, 204], Miller and Klippenstein [190], and Klippenstein [191]. The Klippenstein branching fractions are based on the following rate constants: $k_{65} = 6.2 \cdot 10^{15}$ T$^{-1.150}$ exp(-1267/T); $k_{66} = 1.2 \cdot 10^{20}$ T$^{-2.576}$ exp(-365/T) (CASPT2); $k_{65} = 1.3 \cdot 10^{16}$ T$^{-1.216}$ exp(-1360/T); $k_{66} = 3.3 \cdot 10^{21}$ T$^{-3.029}$ exp(-588/T) (MRCI+Q).

At large excess air ratios, the HO$_2$ radical may be formed in significant quan-

tities, promoting oxidation of NO to NO_2. This occurs via the reaction NO + $HO_2 \rightleftarrows NO_2$ + OH, which is well characterized both in the forward [26, 215] and reverse [216] direction. The NH_2 + NO_2 reaction has been studied over a wide range of temperature. Similar to NH_2 + NO, it has two major product channels,

$$NH_2 + NO_2 \rightleftarrows N_2O + H_2O \qquad (R67)$$

$$NH_2 + NO_2 \rightleftarrows H_2NO + NO \qquad (R68)$$

Values for the overall rate constant have been reported over a wide range of conditions [192, 217–226], but the scatter in the data is considerable. However, even though data at 500 K differ by more than an order of magnitude (Fig. 24), most recent determinations are in fairly good agreement. The rate constant calculated by Klippenstein et al. [192] provides a good description of most of the data below 1000 K, but it is a factor of three below the high temperature (1300-1600 K) shock tube determination of Song et al. [226]. In the present work, we have adopted the overall rate constant from Glarborg et al. [223], which is compatible with the rate constants from both Song et al. and Klippenstein et al. within their uncertainties.

Also the branching fraction for the NH_2 + NO_2 reaction, defined as $k_{67}/(k_{67} + k_{68})$, has been in discussion but most studies support a value around 20% [223, 225–229], in agreement with the theoretical analysis of Klippenstein et al. [192].

Competing consumption steps of NH_2 include reactions with the O/H radical pool (R57-R61), with amine radicals leading to formation of N_2-amines, and, at high excess oxygen levels, with O_2 (R62, R63). The NH_2 + H reaction (R57b) has been measured both in the forward [230,231] and reverse [199,232] direction at elevated temperatures. The data for the NH + H_2 reaction [199, 232] is in excellent agreement over an extended temperature range and consistent with the only low temperature measurement of k_{57b} [233]. The NH_2 + O reaction (R58,
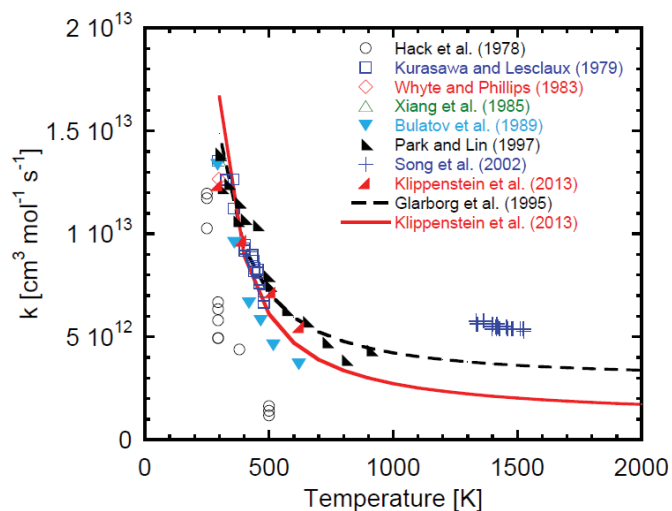
Figure 24: Arrhenius plot for the reaction $NH_2 + NO_2 \rightarrow$ products. The symbols denote measurements of the rate constant while lines denote theoretical values. The data are drawn from Hack et al. [217], Kurasawa and Lesclaux [218], Whyte and Phillips [219], Xiang et al. [220], Bulatov et al. [221], Park and Lin [225], Song et al. [226], Klippenstein et al. [192], and Glarborg et al. [223].

R59) has only been measured at low temperature where the overall rate constant has been shown to be fast [234–236] and HNO + H (R58) is the dominating product channel, with a minor contribution from NH + OH (R59) [234, 235]. Based on unpublished data by Temps (cited by Miller et al. [183]), we have assumed a $T^{-0.5}$ temperature dependence for reaction R58. Since the NH_2 + O reaction is important for formation of NO from NH_3 at high temperatures, a measurement of the rate of this step at elevated temperature is desirable. The NH_2 + OH reaction (R60) was studied experimentally and theoretically by Klippenstein et al. [193].

The NH radical, formed by hydrogen atom abstraction from NH_2, may react with NO to form N_2O (R17) or N_2 (R71), as discussed in section 3.3.1, or with O_2 leading to formation of NO,

$$NH + O_2 \rightleftarrows NO + OH \tag{R70}$$

$$\text{NH} + \text{O}_2 \rightleftarrows \text{HNO} + \text{O} \qquad\qquad\qquad \text{(R69)}$$

The competition between the different consumption reactions of NH is important for the overall selectivity for forming NO or N_2 in ammonia oxidation, in particular at higher temperatures.

Under conditions with high O_2 concentrations [19] or high pressure [237], nitroxide (H_2NO) may be formed in significant quantities from reaction of NH_2 with HO_2 or NO_2. The H_2NO subset of the reaction mechanism is not well established and consists largely of reactions with estimated rate constants. The most important reaction of H_2NO is that with O_2,

$$\text{H}_2\text{NO} + \text{O}_2 \rightleftarrows \text{HNO} + \text{HO}_2 \qquad\qquad\qquad \text{(R72)}$$
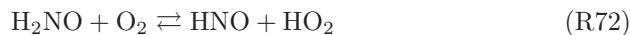
There are no experimental data available for this reaction. Recently, it was studied theoretically by Song et al. [237] who calculated the rate constant from ab initio theory. To facilitate modeling predictions of NH_3 oxidation and Thermal DeNO_x at high oxygen concentrations, we have lowered the activation energy for reaction (R72) by 2.5 kcal mol^{-1}; this change is within the estimated uncertainty in the calculated barrier height.

Also for HNO, reaction with O_2 (R73) is an important consumption step. For this reaction we rely on a rate constant derived from QRRK theory [146]. Experimental determinations of the rate constants for both HNO + O_2 and H_2NO + O_2 are desirable.

3.6.2 Modeling NH_3 oxidation

Oxidation of ammonia has been studied extensively in the past, both experimentally and through modeling. The experimental work include studies in flames [238–245], shock tubes [185, 246–253] and flow reactors [136, 140, 237, 254, 255].

Due to the potential impact of surface reactions on the induction time in NH_3 oxidation even for quartz (see [254] and App. A), flow and batch reactor experiments can be used only cautiously for model validation. For this reason, we supplement flow reactor data with results from experiments conducted in premixed flames and shock tubes for validation of the NH_3 oxidation subset.

Following Miller and Bowman [1], we evaluate the model against the low-pressure flame data of Bian et al. [244]. They measured the structure of a flame burning in a near equimolar ammonia-oxygen mixture at reduced pressure (35 Torr), using using a molecular beam sampling technique coupled with a mass spectrometer. Figure 25 compares the measured species profiles with modeling predictions.

Overall, the agreement between the experimental results and the modeling predictions is good. The concentrations of both reactants (NH_3, O_2) and products (NO, N_2O, N_2, and H_2O) are predicted quite accurately, while calculations for the amine radicals NH_2 and NH are within the experimental uncertainty. The only major discrepancies, not shown, occur for HNO and N, which are both severely overpredicted.

Figure 26 shows a reaction path diagram for oxidation of NH_3. Ammonia is converted to NH_2 by reaction with the radical pool. The NH_2 radical may be converted to NH and N in the sequence $NH_2 \xrightarrow{+OH,H} NH \xrightarrow{+OH,H} N$; these reactions become more competitive with increasing temperature. Subsequently, the NH_i radicals may react with NO, leading to N_2, or with O, OH, or O_2, forming NO. The selectivity for forming NO or N_2 in oxidation of ammonia is determined by the competition of the amine radicals for reacting with NO or with the O/H radical pool (or O_2).

Mathieu and Petersen [185] measured the ignition delay for NH_3 as a function of stoichiometry and pressure. In Fig. 27, their results for a pressure of 1.4 atm are compared with modeling predictions. The calculations are in good
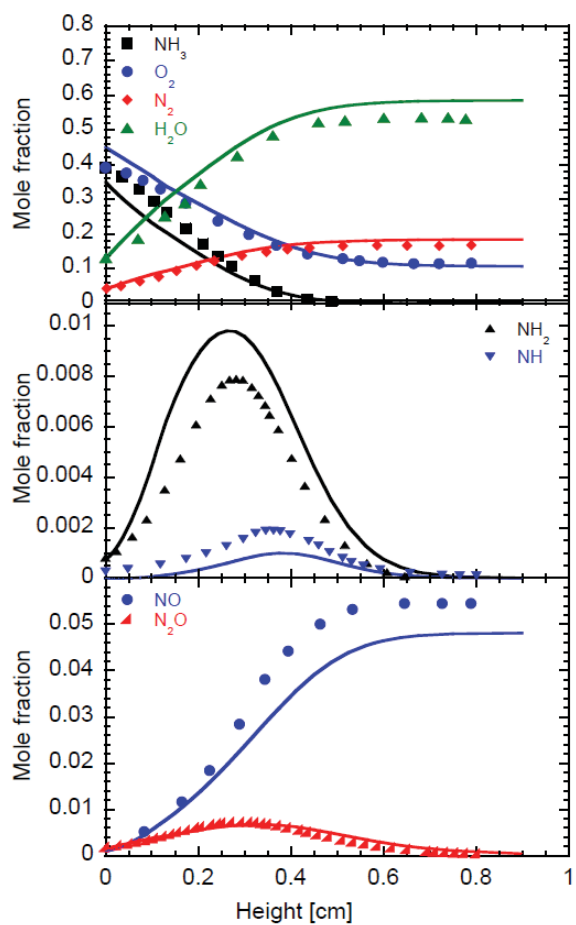
Figure 25: Comparison of measured [244] and predicted mole fractions of stable species and selected radicals in a low-pressure premixed ammonia/oxygen flame. The symbols denote experimental data, while the solid lines denote calculated values. Conditions: pressure of 35 torr; inlet composition 48% NH_3, 51% O_2, and 1% Ar. The gas velocity was 60.8 cm s^{-1} and the peak flame temperature was about 2250 K.

agreement with measurements at lean and rich conditions, but curiously show a larger deviation at stoichiometric conditions. As pointed out by Mathieu and Petersen, the predicted ignition delays for NH_3 are sensitive to the N_2H_x subset of the mechanism. This subset is quite uncertain and more work on the N_2-amine chemistry is desirable.
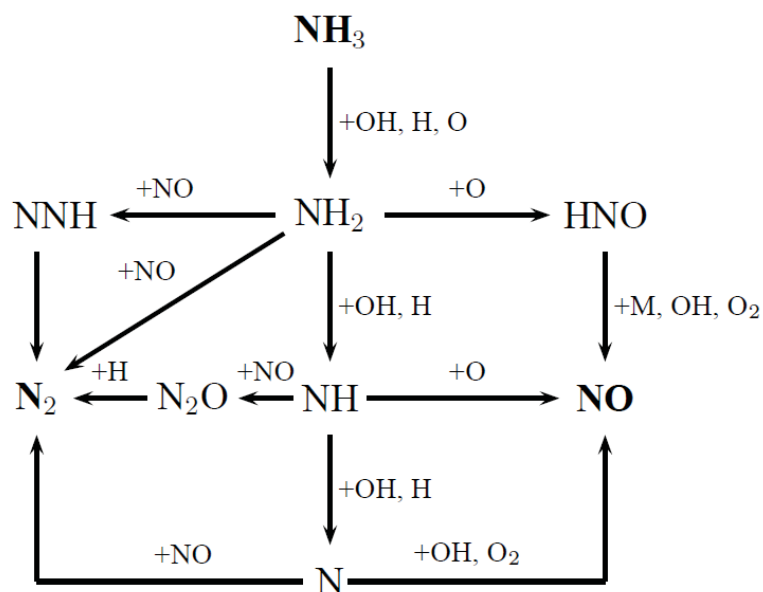
Figure 26: Reaction path diagram for oxidation of NH_3.

In the presence of even small amounts of NO, NH_3 oxidation becomes insensitive to initiation reactions and the impact of the surface in flow reactor experiments is minimized [1, 159]. Figure 28 shows results for NH_3 oxidation in the presence of NO varying in the range 25-100 ppm, with the NH_3 and O_2 inlet levels maintained at 1000 ppm and 40%, respectively [256]. The onset temperature for reaction is independent of the NO level. Even at the smallest NO concentration of 25 ppm, a minimum in NO is observed just above the initiation temperature, and inspection of the data shows that the fractional conversion of NO at the minimum is quite similar over the range of NO levels from 25 to 100 ppm. At higher temperatures (> 1200 K), the exit NO concentration asymptotically approaches a value, which is independent of the inlet level. A similar observation was reported by Lyon and Benn [257]. The modeling predictions capture all these trends well.

The comparisons with the flame structure data (Fig. 25), the shock tube ignition delays (Fig. 27), and the flow reactor data (Fig. 28) indicate that the important
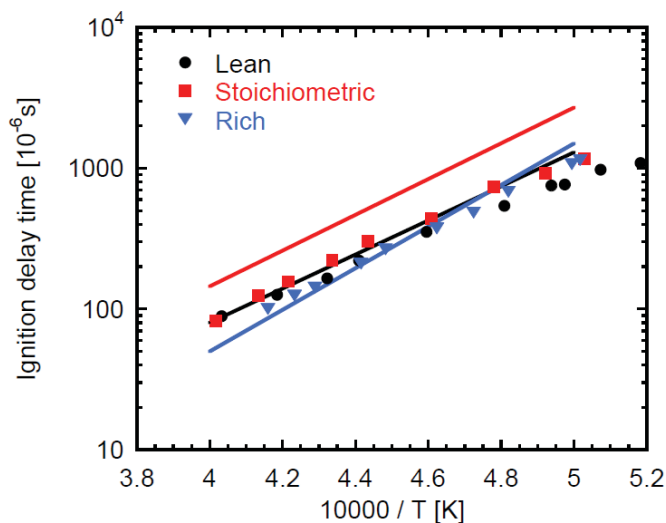
Figure 27: Experimental [185] and predicted ignition delays for mixtures of NH_3 and O_2 in Ar (99%) as a function of fuel-air equivalence ratio (lean (ϕ=0.5), stoichiometric (ϕ=1.0), and rich (ϕ=2.0)) and temperature. The data were obtained in a shock tube at a pressure of 1.4 bar. Symbols denote experimental data, while solid lines denote modeling predictions.

features of NH_3 oxidation, including the selectivity for forming NO and N_2, are described well by the model. However, in combustion processes ammonia formed from fuel-nitrogen will typically be present only in small amounts compared to other combustibles. The oxidation chemistry of these combustibles will control the generation of chain carriers, and, particularly under reducing conditions, hydrocarbon/amine interactions may be important.

Figure 29 compares modeling predictions with the experimental results from Mendiara and Glarborg [22] for oxidation of CH_4 doped with NH_3 in a flow reactor as a function of temperature and stoichiometry. The conditions of these experiments are expected to be more representative of practical combustion systems. The methane inlet level was about 2500 ppm, with about 500 ppm NH_3. The stoichiometry is seen to have a major impact on the NO formation. Under fuel-rich conditions, the amount of NO formed is negligible. Carbon monoxide is formed above 1230 K and reaches a plateau level at a temperature
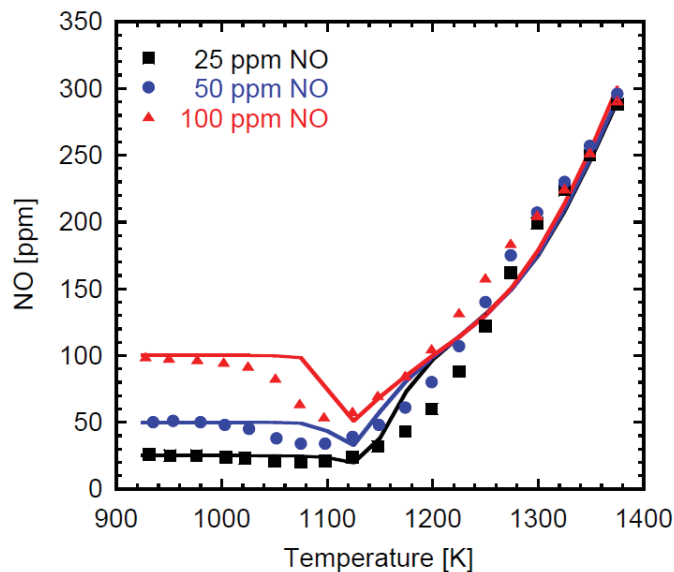
Figure 28: Comparison of experimental data [256] and modeling predictions for oxidation of NH_3 in a quartz flow reactor: effect of inlet NO concentration. Symbols denote experimental data, while solid lines denote modeling predictions. Inlet concentrations: $NH_3 = 1000\pm100$ ppm, $O_2 = 40\pm1.2\%$, H_2O = trace, NO varying (25, 50, 100 ppm); balance N_2. Residence time (s) = 48.7/T[K].

close to 1300 K. Ammonia oxidation is initiated at 1130 K, but the consumption rate of NH_3 is slow until CH_4 is completely converted to CO. For stoichiometric conditions, the initiation of the reaction occurs at a slightly lower temperature. Nitric oxide is formed following the disappearance of NH_3, reaching a level of 180 ppm at 1400 K and then leveling out. Carbon monoxide exhibits a peak at 1230 K and then reaches a plateau. For fuel-lean conditions, reaction is initiated at much lower temperatures. Carbon monoxide peaks already at 1030 K, and no CO is observed above 1075 K. Following the depletion of NH_3 at about 1050 K, NO is formed. The NO concentration increases with temperature up to 1250 K and then levels out.

Modeling predictions are generally in good agreement with experiments. The model captures well the initiation of methane and ammonia oxidation and the onset of NO formation, except under lean conditions where the onset tempera-

68
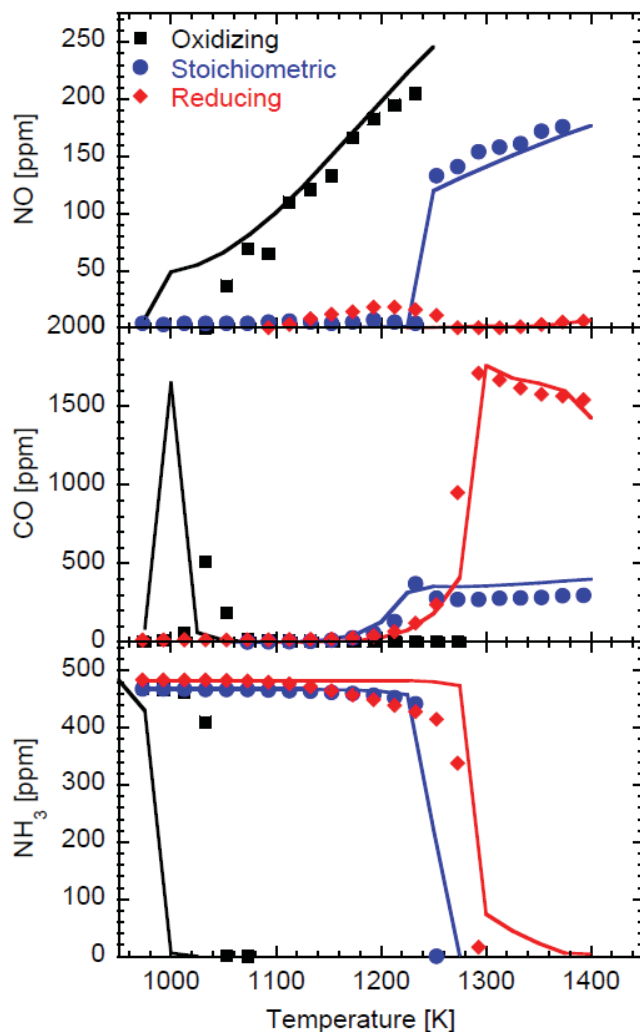
Figure 29: Comparison of experimental data [22] and modeling predictions for oxidation of a mixture of CH_4 and NH_3 as a function of stoichiometry and temperature. Symbols denote experimental data, while solid lines denote modeling predictions. Inlet concentrations (reducing ($\phi = 1.55$) / stoichiometric ($\phi = 1.07$) / oxidizing ($\phi = 0.13$)): $CH_4 = 2508$ / 2513 / 2515 ppm, $O_2 = 3480$ / 5040 / 40100 ppm, $NH_3 = 484$ / 468 / 468 ppm; balance N_2. All experiments were conducted in a 12 mm inner diameter alumina reactor at 1.05 atm with a residence time in the isothermal zone of 1296/T(K).

69

ture is underpredicted. The amount of NO formed is predicted quite accurately over the range of temperature and stoichiometry.

The presence of hydrocarbons opens up additional oxidation pathways for NH_3, compared to the diagram in Fig. 26. These interactions are discussed in more detail elsewhere [22, 131, 189]. In particular the methyl radical plays an active role, converting amine radicals to hydrocarbon amines,

$$CH_3 + NH_2(+M) \rightleftarrows CH_3NH_2(+M)$$

$$CH_3 + NH \rightleftarrows CH_2NH + H$$
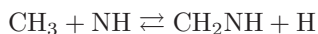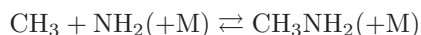
and hydrogen cyanide to acetonitrile,

$$CH_3 + HCN \rightleftarrows CH_3CN + H$$
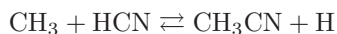
The level of accuracy shown in Fig. 29 is presumably representative of the reliability of the model in simulating ammonia oxidation, in particular the selectivity for forming NO and N_2, in most practical systems. This is encouraging, as NH_3 can be considered the most important fuel-nitrogen species in the gas-phase. However, the interaction of NH_3 with the hydrocarbon oxidation chemistry, particularly under reducing conditions, is quite complicated [22, 131, 189] and uncertainties in this chemistry may limit the accuracy of modeling predictions under reducing conditions.

4 In-situ reduction of NO

As legislation on nitrogen oxide emissions becomes increasingly stringent, primary measures based on staged combustion may become inadequate, making it necessary to employ either catalytic flue gas cleaning or in-situ control technologies such as selective non-catalytic reduction (SNCR) or reburning. Both SNCR [1, 152, 258, 259] and reburning [21, 260–273] have been studied extensively. They are available as commercial technologies, typically offering NO_x reductions of the order of 50% [274]. In the following sections, the chemistry of these processes are outlined and the reliability of the model in describing the NO reduction is evaluated.

4.1 Selective Non-Catalytic Reduction of NO

Selective, non-catalytic reduction of NO (SNCR) is widely used for NO_x control in combustion of fuels such as biomass and waste, where catalytic cleaning may be prohibitive due to poisoning of the catalyst. The reducing agents used to react with NO are ammonia, urea and cyanuric acid. Also ammonium sulfate has been proposed [274], but little is known about the performance of this agent.

4.1.1 SNCR with NH_3 (Thermal DeNO$_x$)

Selective, non-catalytic reduction of NO using NH_3 as the reducing agent was developed by Lyon [258] who termed the process Thermal DeNO$_x$. The chemistry of Thermal DeNO$_x$ has been studied extensively [1,19,187,188,258,259,275–277]. Characteristic of the process is that nitric oxide removal is possible only in a narrow temperature range centered at 1250 K and only in the presence of oxygen. At temperatures below 1100 K, reaction is too slow to be significant, and above 1400 K the NH_3 is oxidized to NO rather than to N_2.

The kinetic model for Thermal DeNO$_x$ is the same as that for the H/N/O chemistry discussed in previous sections. The major difference between the present subset, adopted largely from Klippenstein et al. [19], and previous kinetic models for Thermal DeNO$_x$, e.g., [1, 188], is that the chain branching in the process is now mainly restricted by the small value of the branching fraction α of the NH$_2$ + NO reaction, rather than by reactions of NNH with O$_2$ or NO. Following Klippenstein et al. [19], we use a value for the NNH lifetime of 10^{-9} s, much lower than values commonly used in modeling. This value corresponds to k$_{20}$ = 1x10^9 s^{-1}. A lower limit rate for prompt dissociation can be estimated to around 2x10^8 s^{-1}. An accurate determination of the dissociation rate for NNH (R20) would be very valuable for modeling ammonia oxidation and selective non-catalytic reduction of NO.

Figure 30 compares experimental and modeling results for the Thermal DeNO$_x$ process. The upper figure shows data obtained in a laminar flow reactor [278], while the results in the lower figure were obtained in a jet-stirred reactor [276]. Despite the difference in reaction conditions, the temperature window for the process is similar in the two reactor configurations. Presence of water vapor is seen to have only a limited impact on the process.

The present model provides a satisfactory prediction of the experimental results, even though it predicts a larger impact of H$_2$O than observed experimentally. While NO is predicted fairly accurately in the presence of water vapor, in particular for the flow reactor conditions, the model tends to underpredict the temperature for onset of reaction in the absence of H$_2$O. The reason for this discrepancy is not clear. Loss of atomic oxygen on the reactor wall under dry conditions could conceivably play a role; this is discussed in App. A. The predicted inhibition by water vapor is mostly caused by its high collider efficiency in the reaction H + O$_2$ + M $\rightarrow$ HO$_2$ + M. Presently, the collider efficiency is based on low temperature measurements, but there is likely a considerable temperature dependence to it.
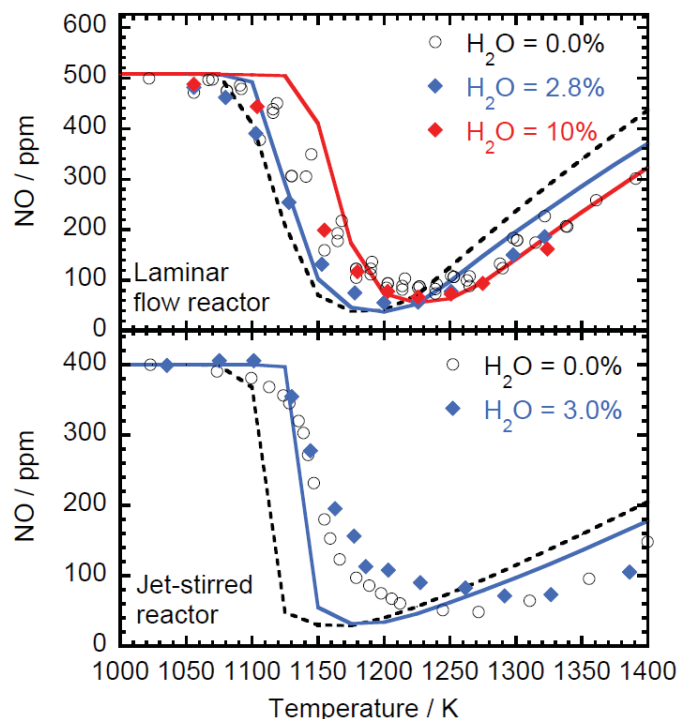
Figure 30: Comparison of experimental data [276,278] and modeling predictions for reduction of NO by NH_3: effect of H_2O concentration. Symbols denote experimental data, while solid lines denote modeling predictions. *Upper figure* (laminar quartz flow reactor [278]): Inlet concentrations: NH_3 = 832 ppm, NO = 507 ppm, O_2 = 4.0%, H_2O = 0% or 2.8% or 10%, balance N_2. Residence time (s) = 92.7/T(K). *Lower figure* (jet-stirred reactor [276]): Inlet concentrations: NH_3 = 960 ppm, NO = 400 ppm, O_2 = 0.8%, H_2O = 0% or 3%, balance N_2. Nominal residence time (s) = 370/T(K).

Figure 31 shows a pathway diagram for the Thermal $DeNO_x$ process in the presence of water vapor. Ammonia is converted to NH_2 by reaction with the O/H radical pool, primarily OH (R55). The subsequent reaction between NH_2 and NO is the key step in the process. This reaction must simultaneously remove NO and produce free radicals to sustain reaction [1,19]. As discussed above, it has two product channels

$$NH_2 + NO \rightleftarrows NNH + OH \qquad (R65)$$

73

$$NH_2 + NO \rightleftarrows N_2 + H_2O \qquad (R66)$$

Dissociation of NNH initiates a reaction sequence, which secures that reaction (R65) leads to a net formation of three hydroxyl radicals [1,19]:

$$NNH \rightleftarrows N_2 + H \qquad (R20)$$

$$H + O_2 \rightleftarrows O + OH$$

$$O + H_2O \rightleftarrows OH + OH$$
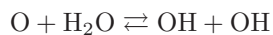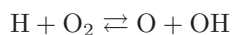
For the overall process to be self-sustainable, it is required that the branching fraction of the $NH_2 + NO$ reaction, $\alpha = k_{65}/(k_{65} + k_{66})$, must be at least 25%. Early experiments [207, 279] indicated a smaller branching fraction, but it is now well established that α attains values of 0.3-0.4 in the 1100-1400 K range (Fig. 23).
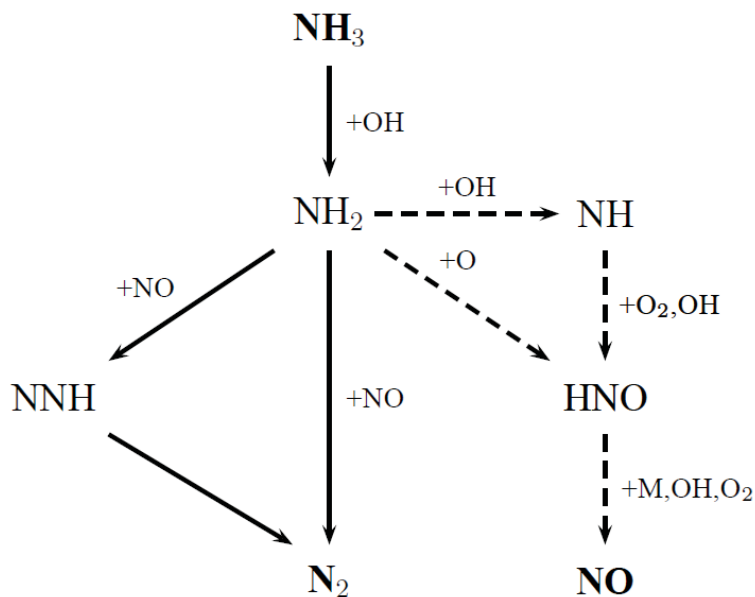

Figure 31: Reaction path diagram for the Thermal DeNO$_x$ process. Dashed lines denote pathways only important at high temperatures.

The process is limited in the high temperature end by the chain branching cycle

74

occurring too rapidly, thus leading to a strong growth in the O/H radical pool. This promotes conversion of NH_2 to NH,

$$NH_2 + OH \rightleftarrows NH + H_2O \tag{R60}$$

which becomes competitive with the NH_2 + NO reaction. The NH formed is partly oxidized to NO through the sequence NH $\xrightarrow{+O_2}$ HNO $\xrightarrow{+M,OH,O_2}$ NO. Also the NH_2 + O reaction (R58, R59) contributes to formation of NO. At sufficiently high temperatures, typically around 1400 K, these reactions lead to a net formation of NO.

Figure 32 shows a sensitivity analysis for NO for the conditions of the experiments of Duo (Fig. 30). Results for three water vapor concentrations are shown for temperatures slightly above the onset temperature for the process and below the optimum temperature for NO reduction. Chain branching processes enhance the reduction, whereas termination processes inhibit it. Reaction R65, NH_2 + NO $\rightarrow$ NNH + OH, is favorable to NO reduction, and reaction R66, NH_2 + NO $\rightarrow$ N_2 + H_2O, is equally unfavorable. Similarly, but with much lower sensitivity coefficients, H + O_2 $\rightarrow$ O + OH promotes reaction while H + O_2 (+M) $\rightarrow$ HO_2 (+M) inhibits reduction of NO.

The sensitivity coefficients for the NH_2 + NO reaction, and in particular for the branching fraction for the reaction, $\alpha = k_{65}/(k_{65} + k_{66})$, are very large, showing the unusually large sensitivity of modeling predictions for Thermal DeNO$_x$ to this parameter. Apart from the H + O_2 reaction, no other steps in the mechanism are nearly as important.

Figures 33 and 34 compare modeling predictions for NO with experimental data from Kasuya et al. [280]. They performed a series of flow reactor experiments where they investigated the effect of O_2 concentration from close to zero to 50% on the Thermal DeNO$_x$ process, measuring both NO, NO_2, and N_2O.

Figures 33 shows results for NO. An increase in the oxygen concentration shifts
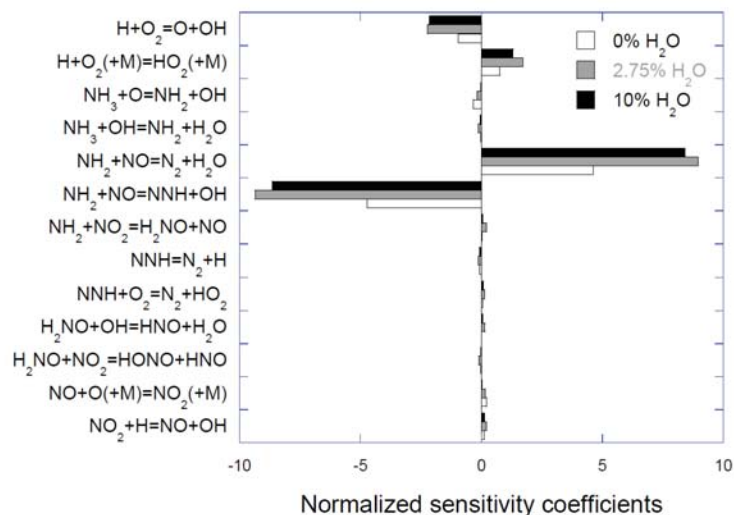
Figure 32: Sensitivity coefficients for prediction of NO in Thermal DeNO$_x$ for the conditions of the experiments of Duo [278] as a function of the water vapor concentration at a temperature slightly above the temperature for onset of reaction: 0% (1100 K), 2.75% (1125 K), and 10% (1150 K).

the window towards lower temperatures and widens it. At the same time, the maximum amount of NO removal decreases. Similar results were reported by Lu and Lu [277]. These characteristics are described well by the model. Similar to what was observed by Klippenstein et al. [19], the predicted temperature for onset of reaction is slightly shifted for some conditions. The very short NNH lifetime of the present mechanism causes the predicted onset temperature to be less sensitive to the O$_2$ level than observed experimentally, but the difference is probably within experimental uncertainty.

Figure 34 compares predicted and observed concentrations of NO$_2$ and N$_2$O for the conditions of Fig. 33. Kasuya et al. were the first to report detection of NO$_2$ in the Thermal DeNO$_x$ process; NO$_2$ is now believed to be a key intermediate in the process [19, 187, 188]. Nitrogen dioxide is seen to form in significant quantities at high concentrations of O$_2$, but the level drops off rapidly as O$_2$ decreases.

76

Figure 33: Comparison of experimental data [280] and modeling predictions for reduction of NO by NH_3 in a quartz flow reactor: effect of O_2 concentration. Symbols denote experimental data, while solid lines denote modeling predictions. Inlet concentrations: NH_3 = 1000$\pm$60 ppm, NO = 500$\pm$30 ppm, H_2O = 5%, balance N_2. Residence time (s) = 88.0/T(K). The reactor surface/volume ratio was 7.8 cm^{-1}.

The modeling predictions are in qualitative agreement with the measurements, but the predicted window for NO_2 extends to higher temperatures than observed experimentally. Nitrogen dioxide is formed through the sequence,

$$NNH + O_2 \rightleftarrows N_2 + HO_2 \qquad (R24)$$

77

Figure 34: Comparison of experimental data [280] and modeling predictions for formation of NO_2 and N_2O in the reduction of NO by NH_3 in a quartz flow reactor: effect of O_2 concentration. Symbols denote experimental data, while solid lines denote modeling predictions. Conditions are the same as in Fig. 33. Inlet concentrations: $NH_3 = 1000\pm60$ ppm, $NO = 500\pm30$ ppm, $H_2O = 5\%$, balance N_2. Residence time (s) $= 88.0/T(K)$. The reactor surface/volume ratio was 7.8 cm^{-1}.

$$NO + HO_2 \rightleftarrows NO_2 + OH \qquad\qquad (R17)$$

Formation of HO_2, and thereby NO_2, is then replenished through the reactions,

$$NH_2 + NO_2 \rightleftarrows H_2NO + NO \qquad\qquad (R68)$$

78

$$H_2NO + O_2 \rightleftarrows HNO + HO_2 \tag{R72}$$

$$HNO + O_2 \rightleftarrows NO + HO_2 \tag{R73}$$

The competition between reactions of HNO and H_2NO with O_2 (neither of which are well characterized) and with the radical pool is important for the peak concentration of NO_2, as well as the width of the NO_2 formation window [19].

The formation of N_2O is a complex function of temperature and oxygen concentration. The N_2O peak shifts from high temperature to low temperature as $[O_2]$ increases. At 10% O_2, a double peak in N_2O can be detected, indicating that two mechanisms of N_2O formation are active. The two sources of N_2O are the reactions [187, 188]

$$NH_2 + NO_2 \rightleftarrows N_2O + H_2O \tag{R67}$$

active predominantly at lower temperatures and larger $[O_2]$ where NO_2 is readily available, and

$$NH + NO \rightleftarrows N_2O + H \tag{R17}$$

which competes with NH + O_2 at higher temperatures and lower values of $[O_2]$. The predictions with the current mechanism agree qualitatively with the measured profiles, but the model overpredicts N_2O under conditions where the NH + NO reaction is the main source.

Presence of combustibles such as H_2 or CO shifts the window for NO removal towards lower temperatures by replenishing the radical pool. Furthermore, it leads to a narrowing of the process window, because the enhanced radical levels cause oxidation of NH_3 to NO to compete more efficiently with the NO removal reactions. These effects are illustrated in Fig. 35, which compares modeling predictions for the effect of CO addition on Thermal $DeNO_x$ with the experimental results of Alzueta et al. [281]. Both the shift in onset temperature and the narrowing of the temperature window are captured quite well by the model.
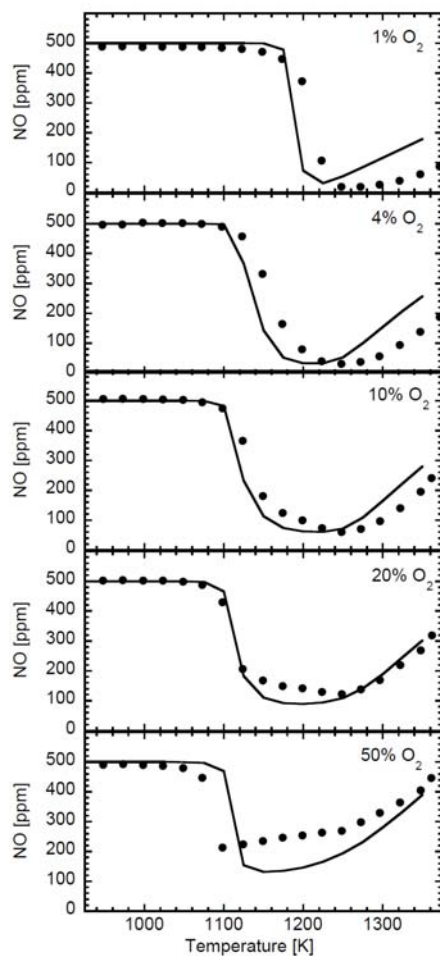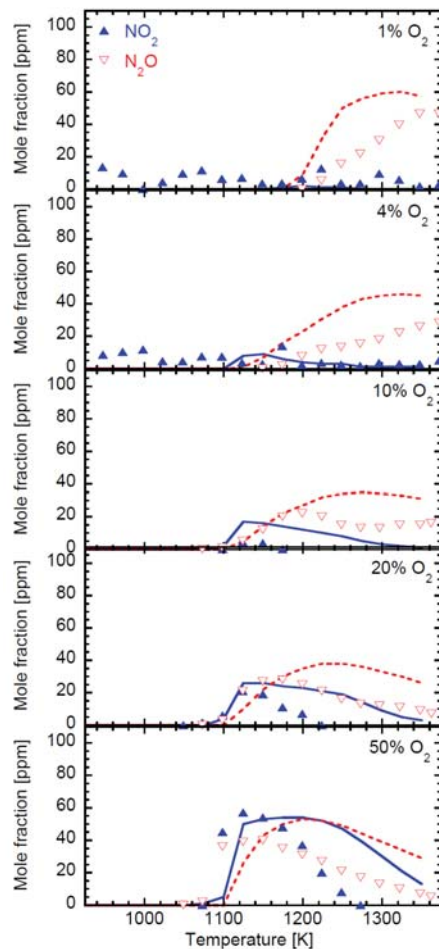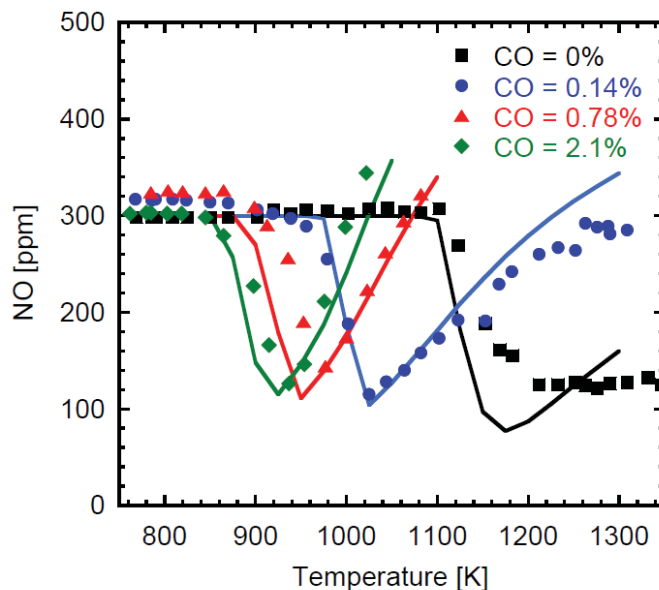
Figure 35: Comparison of experimental data [281] and modeling predictions for reduction of NO by NH$_3$ in a quartz flow reactor: effect of CO concentration. Symbols denote experimental data, while solid lines denote modeling predictions. Inlet concentrations: 300 ppm NH$_3$, 300 ppm NO, 4.0% O$_2$, 4.5% H$_2$O; balance N$_2$. Pressure is 1.1 atm. Residence time at 1200 K (constant molar rate) is about 150 ms. The reactor surface/volume ratio was 4.4 cm^{-1}.

Even though the Thermal DeNO$_x$ mechanism is now well understood and the main features of the process are predicted satisfactorily by the model, quantitative modeling predictions over a wider range of conditions are still elusive. As discussed in section 3.6.1, the rate constants and branching fractions of some of the key reactions were re-evaluated in the present work, most importantly the NH$_2$ + NO reaction (R65, R66). This reaction is probably one of the best characterized reactions in combustion chemistry, with rate constants for the two product channels determined very accurately from both experiment and theory. Still, this level of accuracy ($\pm$ 10%) is not sufficient to guarantee a good prediction of NO in the Thermal DeNO$_x$ process. A small lowering of the branching fraction from 0.37 (best theoretical value [191]) to 0.34 (lower end of experimental range) at 1200 K considerably improves predictions for the process by

increasing the onset temperature for reaction by 25-50 K. It is probably a unique feature of nitrogen chemistry - due to the selectivity in products (NO, N_2, N_2O, etc.) - that such a small correction has a major impact on predictions. The accuracy of modeling predictions for Thermal $DeNO_x$ is limited also by uncertainties in other reactions, for instance at increased oxygen concentrations the steps $HNO + O_2$ and $H_2NO + O_2$.

4.1.2 SNCR with Cyanuric Acid (RapReNO$_x$)

Cyanuric acid, (HOCN)$_3$, is an alternative to ammonia and urea as an SNCR agent. Above 600 K, cyanuric acid decomposes to isocyanic acid (HNCO), which at sufficiently high temperature initiates a reaction sequence that can take out NO [152]. The process was discovered by Perry [282] and termed RapReNO$_x$. Compared to the Thermal DeNO$_x$ process, RapReNO$_x$ is efficient at slightly higher temperatures, due to the self-inhibiting nature of HNCO oxidation discussed in section 3.5. A concern with the process is the formation and possible emission of nitrous oxide, N$_2$O.

A number of flow reactor studies of the reduction of NO by HNCO have been performed in order to investigate the characteristics of this process [158–160,181, 283]. The most comprehensive data were obtained by Caton and Siebers [158] who investigated the effect of temperature and exhaust gas composition on the process. Modeling studies for the RapReNO$_x$ process have been reported by Miller and Bowman [1, 152], Lyon and Cole [160], and Glarborg et al. [159]. These studies have provided an overall understanding of the reduction of NO by HNCO, but details of the chemistry remain uncertain.

The subset used in the present work for studying the RapReNO$_x$ is the same as that discussed in sections 3.4 and 3.5 for oxidation of HCN and HNCO, respectively. In the modeling, cyanuric acid is assumed to decompose instantaneously at the temperatures relevant for the process. The key reaction for removing NO is NCO + NO, which has two product channels,

$$NCO + NO \rightleftarrows N_2O + CO \tag{R42}$$

$$NCO + NO \rightleftarrows N_2 + CO_2 \tag{R43}$$

The overall rate constant has been measured over a wide range of temperature [161, 284, 285] and the main uncertainty relates to the branching ratio for the

reaction. We have adopted the recommendation of Baulch et al. [26], which is based on the theoretical work by Zhu and Lin [153]. The nitrous oxide formed in reaction (R42) may be emitted from the process and it is a concern for RapReNO$_x$.

For model validation, we compare predictions with the flow reactor data of Caton and Siebers [158]. They systematically investigated the effect of the initial concentrations of CO, H$_2$O, and O$_2$. Their data are characterized by a high HNCO/NO ratio and long reaction times, promoting NO reduction and widening the temperature window for the process. However, uncertainties related to the mixing conditions, the temperature profile, and the decomposition of cyanuric acid imply that their results should be used with caution for model evaluation purposes [152].

Figure 36 shows the effect of adding water vapor and carbon monoxide to the process. In the absence of H$_2$O and CO, the process window occurs at temperatures above 1300 K. Under these conditions, atomic oxygen is the main radical, and the HNCO + O reaction yields both NCO (R47) and NH (R46). The subsequent NCO + NO reaction (R42, R43) is chain terminating. Even though the reaction removes NO, it serves to limit NO reduction, shifting the process to higher temperatures. In addition, the sequence NO + O (+M) $\rightarrow$ NO$_2$ (+M), NO$_2$ + O $\rightarrow$ NO + O$_2$ is chain terminating and slows down reaction. The NH radical is consumed primarily by reaction with O$_2$ and NO in chain propagating reactions; the NH + NO reaction makes a considerable contribution to reducing NO under dry conditions.

Addition of H$_2$O shifts the window approximately 50 K towards lower temperatures. The presence of water vapor causes a shift from O to OH as the major chain carrier due to the reaction O + H$_2$O $\rightarrow$ OH + OH, diminishing the importance of the chain terminating sequence involving NO$_2$. Also, the direct reaction between HNCO and H$_2$O serves to promote reaction, even though it is slow.
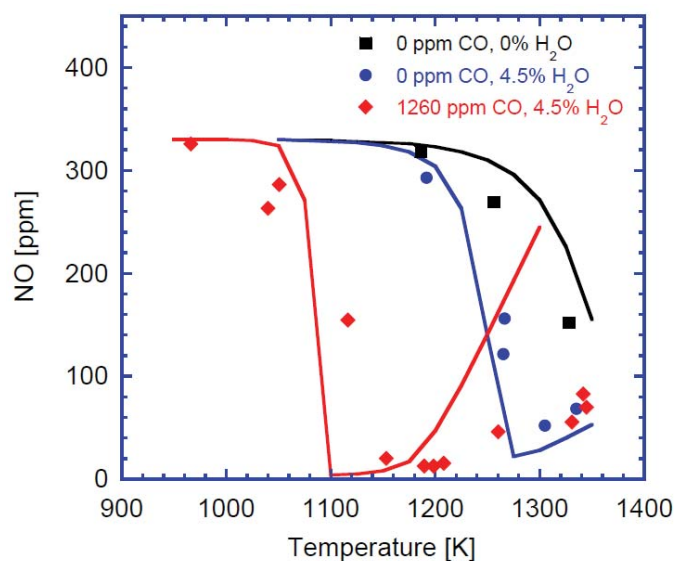
Figure 36: Comparison of modeling predictions and experimental data for the RapReNO$_x$ process in a quartz flow reactor: effect of the initial mole fractions of CO and H$_2$O. The experimental data, taken from Caton and Siebers [158], are shown as symbols, modeling predictions as lines. Inlet mole fractions: (HOCN)$_3$ = 470 ppm, NO = 330 ppm, CO = 0 or 1260 ppm, O$_2$ = 12.3%, H$_2$O = 0 or 4.5%, balance N$_2$. Reaction time = 0.72 s at 1200 K (constant mass flow). The surface to volume ratio was 1.2. In the calculations, it is assumed that (HOCN)$_3$ is instantaneously converted to HNCO (1410 ppm).

When CO is added as a combustible, the temperature window is lowered further, with onset of reaction occurring below 1100 K. Figure 37 shows comparison of experimental data and modeling predictions for HNCO, NO, N$_2$O, CO, and CO$_2$ for these conditions. Due to the large excess of HNCO compared to NO, as well as the long residence time, the temperature window for the process is unusually wide, extending from 1100 K to beyond 1350 K. A significant fraction of the NO is converted to N$_2$O; only at the highest investigated temperature of 1350 K is N$_2$O depleted.

Despite the uncertainties in the subset for HNCO, the model describes the data of Caton and Siebers satisfactorily, particularly in the presence of combustibles. Nitric oxide is generally overpredicted in the higher end of the temperature

84
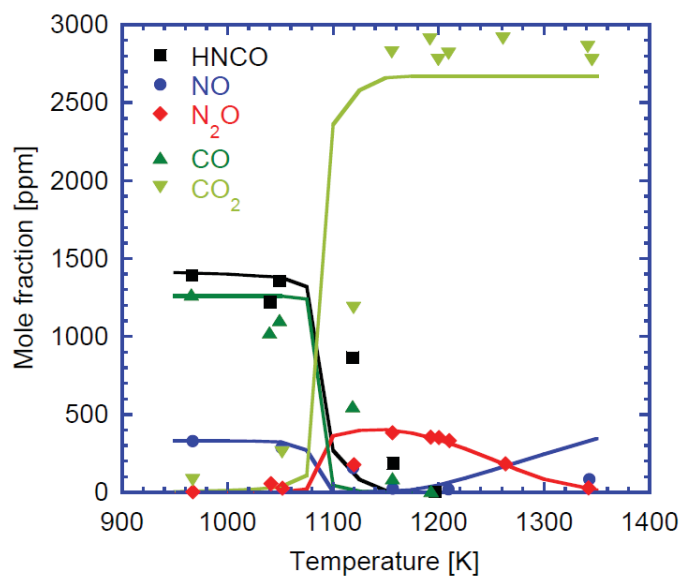
Figure 37: Comparison of modeling predictions and experimental data for the RapReNO$_x$ process in a quartz flow reactor. The experimental data, taken from Caton and Siebers [158], are shown as symbols, modeling predictions as lines. Inlet mole fractions: (HOCN)$_3$ = 470 ppm, NO = 330 ppm, CO = 1260 ppm, O$_2$ = 12.3%, H$_2$O = 4.5%, balance N$_2$. Reaction time = 0.72 s at 1200 K (constant mass flow). In the calculations, it is assumed that (HOCN)$_3$ is instantaneously converted to HNCO (1410 ppm).

window, but N$_2$O is predicted well. However, the availability of reliable experimental data for RapReNO$_x$ is limited and it is difficult to fully assess the predictive capabilities of the model.

4.1.3 SNCR with urea (NO_xOut)

Selective non-catalytic reduction of NO using urea as a reducing agent was proposed by Muzio and coworkers [286] who termed the process NO_xOut. At high temperatures, urea decomposes rapidly to NH_3 and HNCO [158], and thus the chemistry of the process shares important similarities with both Thermal $DeNO_x$ and $RapReNO_x$. Compared to ammonia, the use of urea has the advantage of easier handling and reduced safety hazards. In addition, the urea SNCR process has a slightly wider temperature window than SNCR with NH_3. A disadvantage of the process is that, similarly to $RapReNO_x$, N_2O will be formed and may be emitted from the process.

The urea SNCR process is not as well characterized as Thermal $DeNO_x$, even though its commercial impact is similar. Experimental data for NO_xOut, obtained under well-defined conditions in the laboratory, are limited, partly because urea is typically added to the reactor either in solid form or dissolved in water. In laboratory scale, flow reactor experiments have been reported by Alzueta et al. [287] and Lee et al. [288], while Rota et al. [289, 290] conducted experiments in a jet-stirred reactor.

Chemical kinetic models for the NO_xOut process have been reported by several groups [287, 289, 291]. The reaction mechanism involves reactions for urea decomposition, along with the H/N/O subset for Thermal $DeNO_x$ and the HNCO subset for $RapReNO_x$. Data for urea decomposition at high temperatures and high heating rates representative of the SNCR process are limited, but results indicate that it is fast [291, 292]; we assume it to happen instantaneously. When urea is added in an aqueous solution or as a solid, the decomposition presumably happens in condensed phase; reported activation energies of 15-20 kcal mol^{-1} [292] seem to be too low to be compatible with a gas-phase dissociation. Details of the condensed phase decomposition of urea still need to be verified, but a preliminary reaction mechanism has been proposed based on TGA exper-

Figure 38 compares modeling predictions to the experimental data from Alzueta et al. [287], obtained in a laminar flow reactor, and from Rota et al. [289], measured in a jet-stirred reactor. Despite differences in reactor configuration and urea/NO molar ratio, the two data sets agree fairly well. The onset of reaction (in the absence of combustibles) occurs at around 1150 K, with the highest NO reduction observed at about 1250 K.
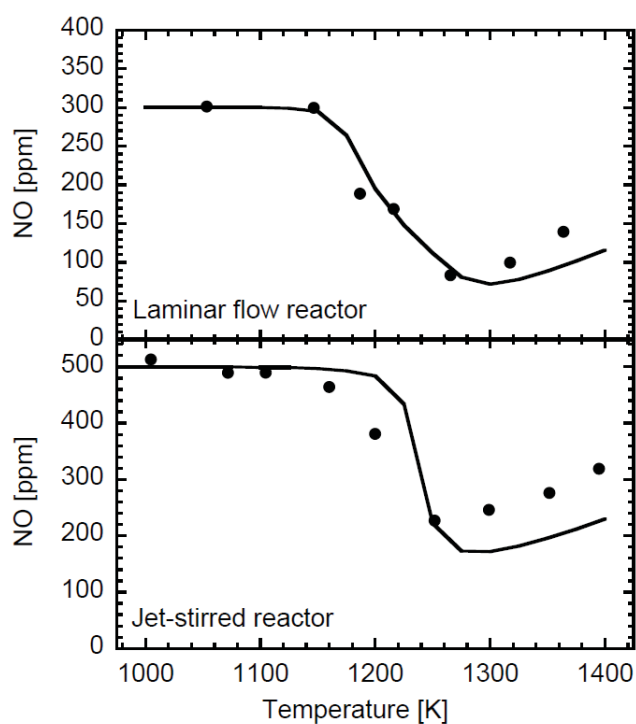
Figure 38: Comparison of experimental data [287, 289] and modeling predictions for reduction of NO by urea. Symbols denote experimental data, while solid lines denote modeling predictions. *Upper figure* (laminar flow quartz reactor (S/V = 2.3) [287]): Inlet concentrations: urea = 150 ppm, NO = 300 ppm, O_2 = 4.0%, H_2O = 4%, balance N_2. Residence time (s) = 200/T(K). *Lower figure* (jet-stirred reactor [289]): Inlet concentrations: urea = 300 ppm, NO = 500 ppm, O_2 = 4.0%, H_2O = 19%, balance N_2. Nominal residence time (s) = 200/T(K).

The model captures the trends well and the agreement with experiment is satisfactory. The minimum in NO is predicted at slightly higher temperatures than

observed and the level of reduction is overpredicted at higher temperatures, but the differences are not large.

Similar to the situation for RapReNO$_x$, the availability of experimental data for NO$_x$Out is limited and the predictive capability of the model is difficult to assess. However, conceivably the uncertainty in predictions is similar to that for Thermal DeNO$_x$, since this subset, in particular the choice of rate constants for the NH$_2$ + NO reaction and NNH dissociation, controls the temperature window for the process.

4.2 Reburning

Sixty years ago Myerson et al. [294] discovered that hydrocarbon radicals react fast with NO. A low-NO$_x$–technique that exploits this reaction was outlined by Wendt et al. [295], who termed the method reburning. In reburning NO is removed from the combustion products by using fuel as reducing agent. By adding part of the fuel and combustion air to the post flame region instead of the main combustion zone a three stage combustion process is obtained. The first stage, where around 80% of the heat is released, is normally run with stoichiometric or excess air. The reburn fuel, which usually constitutes 10-20% of the total fuel, is added after the primary combustion zone to form a fuel-rich second stage where NO is reduced. Downstream of the reburn zone secondary combustion air is added to secure complete burnout.

The reburning process has been studied extensively, both experimentally and through modeling work [296]. The reported experimental work includes data from flow reactors [21, 23, 265–267, 297, 298], jet-stirred reactors [100, 268, 270, 272], and low-pressure flames [299–303]. The stages in the reburn process involves mixing of the reburn fuel into the flue gas from the primary zone, decomposition of the reburn fuel and formation of flame radicals to react with NO, and conversion of the formed cyano and amine species to molecular nitrogen. The reburn chemistry is quite complex, sharing similarities with both prompt NO and fuel-NO chemistry. Despite this complexity, reported modeling studies for reburning [1,21,23,24,262,266,268–273] have generally provided satisfactory results, at least for smaller hydrocarbons.

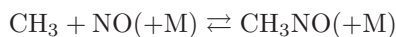### 4.2.1 Reaction subset for reburning

Table 10 lists selected reactions from the reburning subset of the model. Significant progress has been made in characterizing the reactions that reduce NO.

In the 1200–1500 K range typical of the reburn process it is primarily the reactions HCCO + NO, CH_3 + NO and $^3CH_2$ + NO that are active in reducing NO [21, 23]. At higher temperatures, for instance in well–stirred reactors or flames, NO is primarily reduced by smaller hydrocarbon radicals, i.e., $^3CH_2$, CH, and C [1]. Many of these steps are complex, multi-step reactions.

		A	β	E	Source
74.	$CH_3 + NO \rightleftharpoons HCN + H_2O$	1.5E-1	3.520	3950	[304]
75.	$CH_3 + NO \rightleftharpoons H_2CN + OH$	1.5E-1	3.520	3950	[304]
76.	$^3CH_2 + NO \rightleftharpoons HCNO + H$	3.1E12	0.000	-378	[305, 306]
77.	$^3CH_2 + NO \rightleftharpoons HCN + OH$	3.9E11	0.000	-378	[305, 306]
78.	$^1CH_2 + NO \rightleftharpoons HCN + OH$	2.0E13	0.000	0	est
79.	$^1CH_2 + NO \rightleftharpoons {}^3CH_2 + NO$	1.0E14	0.000	0	[307]
80.	$CH + NO \rightleftharpoons CO + NH$	9.1E12	0.000	0	[26]
81.	$CH + NO \rightleftharpoons NCO + H$	1.8E13	0.000	0	[26]
82.	$CH + NO \rightleftharpoons HCN + O$	7.9E13	0.000	0	[26]
83.	$CH + NO \rightleftharpoons CN + OH$	1.1E12	0.000	0	[26]
84.	$CH + NO \rightleftharpoons HCO + N$	6.8E12	0.000	0	[26]
85.	$C + NO \rightleftharpoons CN + O$	2.0E13	0.000	0	[307]
86.	$C + NO \rightleftharpoons CO + N$	2.8E13	0.000	0	[307]
87.	$C_2H_3 + NO \rightleftharpoons HCN + CH_2O$	7.0E21	-3.382	1025	[308]
88.	$C_2H + NO \rightleftharpoons HCN + CO$	4.6E13	0.000	570	[309, 310]
89.	$C_2H + NO \rightleftharpoons CN + HCO$	1.4E13	0.000	570	[309, 310]
90.	$C_2 + NO \rightleftharpoons C_2O + N$	2.3E13	0.000	8640	[311]
91.	$HCCO + NO \rightleftharpoons HCNO + CO$	7.5E12	0.000	-676	[312–314]
92.	$HCCO + NO \rightleftharpoons HCN + CO_2$	2.1E12	0.000	-676	[312–314]
93.	$C_2O + NO \rightleftharpoons CO + NCO$	1.0E14	0.000	670	[315]
94.	$HCNO + H \rightleftharpoons HCN + OH$	7.2E10	0.841	8612	[316]
95.	$HCNO + O \rightleftharpoons HCO + NO$	6.3E13	0.000	0	[317]
96.	$HCNO + O \rightleftharpoons NCO + OH$	7.0E12	0.000	0	[316]
97.	$HCNO + OH \rightleftharpoons CO + H_2NO$	1.0E13	0.000	-1490	[318]
98.	$HCNO + OH \rightleftharpoons HCO + HNO$	6.0E12	0.000	-1490	[318]

Table 10: Selected reactions in the reburn subset. Parameters for use in the modified Arrhenius expression k=AT^βexp(-E/[RT]). Units are mol, cm, s, cal.

The reaction between CH_3 and NO has three product channels:

$$CH_3 + NO(+M) \rightleftharpoons CH_3NO(+M)$$

$$CH_3 + NO \rightleftarrows HCN + H_2O \qquad \text{(R74)}$$

$$CH_3 + NO \rightleftarrows H_2CN + OH \qquad \text{(R75)}$$

It has been studied extensively, both at low temperatures, where only the recombination reaction is competitive, and at high temperatures, where cyanides are formed (R74, R75). In the temperature range of the present work, the CH_3NO complex dissociates rapidly, and only reactions R74 and R75 serve to remove NO. The overall rate for these two steps is fairly well established. We use a rate constant for the overall reaction derived theoretically by Miller et al. [304], which is in good agreement with high temperature experimental data [319, 320], together with a branching fraction of 50% [21].

The reaction between $^3CH_2$ and NO has two major product channels, presumably

$$^3CH_2 + NO \rightleftarrows HCNO + H \qquad \text{(R76)}$$

$$^3CH_2 + NO \rightleftarrows HCN + OH \qquad \text{(R77)}$$

Despite a number of experimental studies [305, 321–323] both reaction rate and product channels for this reaction remain uncertain. In particular, the static reactor laser photolysis measurements of Atakan et al. [305] deviate significantly from the shock tube results of Bauerle et al. [323] at the overlapping temperature of 1000 K, both in the overall rate constant and in the contribution of an OH producing channel. Following Mendiara and Glarborg [23], we adopt the overall rate constant from Atakan et al., using the branching fraction reported by Fikri et al. [306]. The reaction of singlet CH_2 with NO yields primarily inter-system crossing to triplet CH_2, with a possible minor channel forming HCN [21]. For the reaction of CH with NO that appears to have five product channels (R80-R84), we rely on the recommendations of Baulch et al. [26].

The reaction between ketenyl and NO,

$$HCCO + NO \rightleftarrows HCNO + CO \qquad \text{(R91)}$$

$$HCCO + NO \rightleftarrows HCN + CO_2 \qquad\qquad (R92)$$
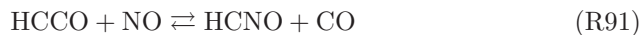
has been characterized experimentally in a number of studies [312–314, 324–328] and both the overall rate constant and the branching fraction is fairly well established. Measurements of the branching fraction indicate that the HCNO + CO channel (R91) dominates, with reported yields of 64-88% [313, 314, 326, 327]. We have combined the total rate coefficient measurement of Carl et al. [312] with the reported branching fraction, which appears to be independent of temperature [313, 314], to arrive at the rate coefficients used in the present work.

The reactions between hydrocarbon radicals and NO mostly feed into the cyanide pool, forming mainly hydrogen cyanide; the cyanide chemistry is discussed in section 3.4. However, both HCCO + NO (R76) and $^3CH_2$ + NO (R91) form HCNO and the fate of this intermediate is important for the NO reduction efficiency. In earlier reburn modeling work [21], it was assumed that the reactions of HCNO with O and OH were fast and that both of them produced NO as the major product. Later, Miller et al. [316] proposed NCO as an alternative product for the HCNO + OH reaction. However, recent experimental [318] and theoretical [329] work indicate that the HCNO + OH reaction forms mainly H_2NO (R97) and HNO (R98). Thereby the reactions of HCNO with O (R95) and OH (R97, R98) largely recycle HCNO back to NO, and consequently the reactions that form HCNO have only a minor impact on the NO reduction efficiency.

4.2.2 Modeling reburning

Even though the reburning process has been studied extensively, experimental data obtained under well-controlled conditions in laboratory scale are limited. For the present purposes, we have selected data from well–stirred reactor and flow reactor experiments.

Chen and Malte [330] studied combustion of $CH_4/O_2/N_2$–mixtures doped with NO in a jet-stirred flow reactor. They measured the emissions of NO, HCN and NH_3 as a function of fuel-air equivalence ratio and temperature. Figure 39 shows comparison between their measurements and modeling predictions for reactor temperatures of 1580 K and 1800 K.
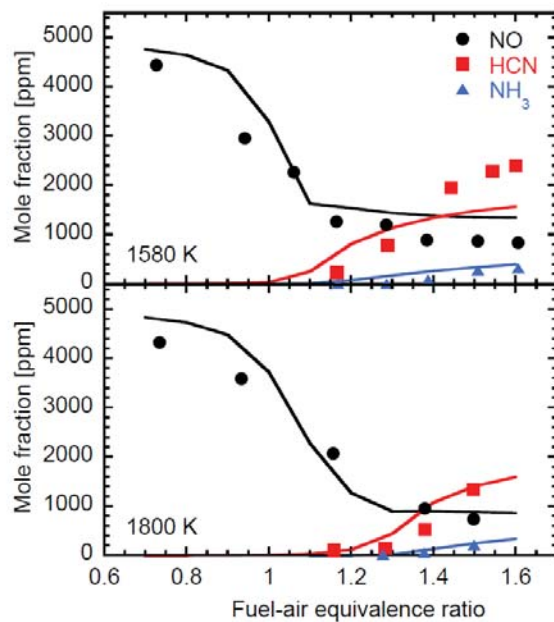

Figure 39: Comparison of measured [330] and predicted emissions of fixed nitrogen species in combustion of methane doped with 5000 ppm NO in a well–stirred reactor. The symbols denote experimental data, while the solid lines denote calculated values. Reactor conditions: temperatures of 1580 K or 1800 K, nominal residence time 9.0 ms, and pressure 1.0 atm.

The behavior of the reburning system is similar at the two investigated temperatures. Under lean conditions 60-100% of the NO is emitted, while under fuel-rich conditions the emission of NO is considerably lower, constituting less than 20% of the inlet NO at fuel-air equivalence ratios larger than 1.4. Here, a major part of the NO is converted to cyanides, with minor amounts of ammonia formed. There is a minimum in total fixed nitrogen (TFN), taken here as the sum HCN + NH_3 + NO, as a function of the equivalence ratio. The minimum

93

at 1580 K occurs at a fuel-air equivalence ratio below 1.2, while at 1800 K the minimum is observed at more reducing conditions, $\phi \approx 1.3$. The agreement between experimental data and modeling predictions is good. Both NO, HCN and NH_3 are predicted well over the whole range of equivalence ratios, in particular at the higher temperature.

The importance of competing reaction pathways depends strongly on the actual reburn conditions, particularly reburn fuel, temperature, and stoichiometry. However, the results can all be interpreted in terms of three most important overall steps:

- Decomposition of the reburn fuel and formation of hydrocarbon radicals

- Fast reaction of hydrocarbon radicals with NO, forming cyanide species

- Comparatively slow conversion of cyanide species via isocyanic and amine species partly to N_2 and partly back to NO

Figure 40 shows a reaction path diagram for the reburn chemistry, for methane as a reburn fuel. Nitric oxides are converted into cyanides and isocyanides by reactions with a wide range of hydrocarbon radicals, mainly CH_3, $^3CH_2$, CH, C, and HCCO. At high radical concentrations (high temperatures and/or jet-stirred reactor conditions), the smaller hydrocarbon radicals are most active in reducing NO, while in a less reactive environment (lower temperatures and/or flow reactor conditions) reactions of NO with CH_3 and HCCO dominate.

The cyanide pool is oxidized in a sequence of reactions similar to that discussed for prompt-NO formation (section 3.2) and HCN oxidation (section 3.4). Under high-temperature, reducing conditions a significant fraction of the HCN is converted through the isomer HNC in the sequence HCN $\xrightarrow{+M,H}$ HNC $\xrightarrow{OH}$ HNCO $\xrightarrow{H}$ NH_2 $\xrightarrow{H,OH}$ NH. This sequence is shown as a single dashed line in Fig. 40.

Reactions of $^3CH_2$ and HCCO with NO yield HCNO, which becomes an important nitrogen intermediate under certain conditions. The HCNO is partly con-
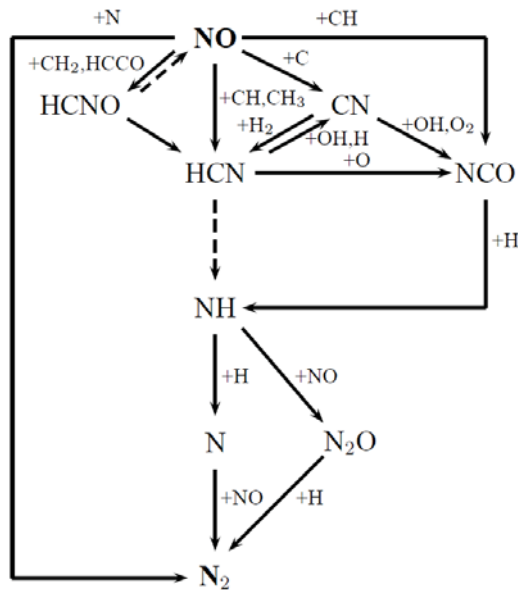
Figure 40: Reaction path diagram for NO reduction by reburning with methane. Dashed lines denote multi-step pathways (see discussion).

verted to HCN by reaction with atomic hydrogen and possibly also by thermal dissociation. However, a significant fraction of the HCNO is recycled directly or indirectly (via HNO and H_2NO) to NO through reaction with OH (R97, R98) and O (R95); these recycling pathways are shown in Fig. 40 as a single dashed line.

Figure 41 shows sensitivity coefficients for NO for the conditions of the Chen and Malte experiments for fuel-air equivalence ratios of 1.1 and 1.3. The analysis shows that the reactions of importance for NO removal depends on the stoichiometry, but there are some common trends. Nitric oxide is consumed by mainly hydrocarbon radicals and prediction of NO is sensitive to these steps, in particular CH_3 + NO (R74, R75), $^3CH_2$ + NO (R76), and CH + NO (R82). Consequently, also reactions promoting formation of CH_n exhibit negative sensitivity coefficients; these steps include CH_3 + H (R99, R100b), CH_3 + OH (R103) and $^3CH_2$ + H (R106). Oxidation of hydrocarbon radicals to oxygenated in-

termediates inhibits NO removal; this takes place mainly through the reactions $CH_3 + O$ (R101), $^3CH_2 + OH$ (R107), $CH + H_2O$ (R115), and $CH + CO_2$ (R116). Nitric oxide may also be reduced by reaction with amine radicals, NH + NO (R17) and N + NO (R1), or reformed by the reaction N + OH (R3).
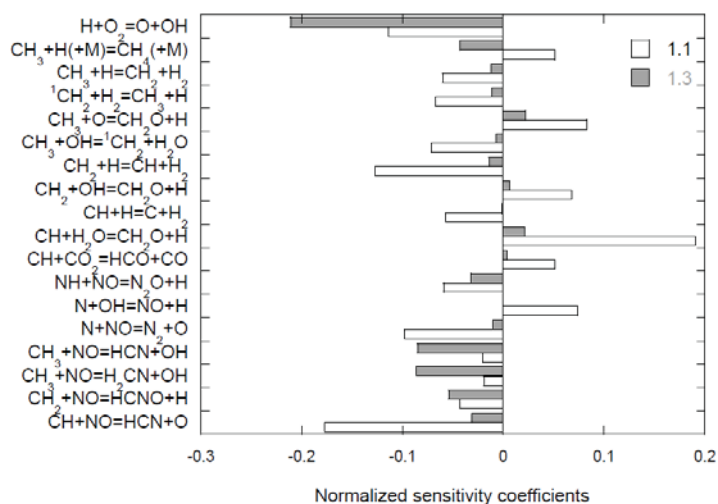
Figure 41: Sensitivity coefficients for prediction of NO under the conditions of the Chen and Malte reburn experiments [330] at 1580 K as a function of the stoichiometry ($\phi = 1.1$ or 1.3).

Figure 42 shows a comparison between the flow reactor data of Myerson [297] and calculations for combustion of methane in a simulated flue gas containing CO, CO_2, O_2 and N_2, together with 1150 ppm NO. The figure shows the effect of oxygen concentration on the emission of total fixed nitrogen (NO + HCN + NH_3) from the reactor. Myerson observed significant temperature gradients in the reactor and the reported temperature of 1423 K was only accurate within ±70 K.

Myerson showed that for a variety of fuels, there was a most effective molar ratio between the oxygen and the reburn fuel at which a minimum TFN could be obtained. The observed minimum for methane occurs at an O_2/CH_4–ratio of 1.0 (Figure 42). The agreement between experimental data and calculations
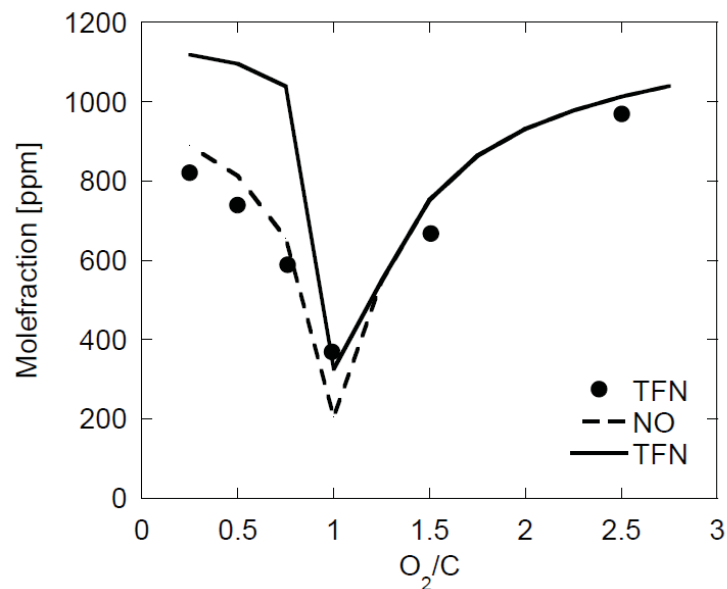
Figure 42: Comparison of measured [297] and predicted emissions of total fixed nitrogen species ($HCN + NH_3 + NO$) for reaction of methane with a simulated flue gas in a flow reactor (mullite or alumina). The symbols denote experimental data, while the solid line denotes calculated values. The dashed line denotes the predicted NO emission. Reactor conditions: temperature 1423 ± 70 K (assumed 1450 K in calculations), residence time 189 ms, and pressure 1.0 atm. Inlet mole fractions: 0.46% CH_4, 1.0% CO, 13.2% CO_2, 0.115% NO 0.0012, O_2 varying; N_2 balance.

is good, except at very reducing conditions ($O_2/CH_4 < 1.0$) where the concentration of total fixed nitrogen is overpredicted. Both modeling predictions and experimental data indicate that the fixed nitrogen under these conditions consists almost entirely of NO and HCN; only negligible amounts of NH_3 are formed.

Alzueta and coworkers [21,267] studied the reburn chemistry for different hydrocarbon fuels in flow reactor experiments under reducing conditions. In Fig. 43 a comparison is shown between their data and calculations for NO in combustion of methane and C_2-hydrocarbons as a function of temperature.

The results show that the ability to remove NO varies significantly between the

97

investigated hydrocarbons. Under the conditions of the experiments, CH_4 is only active above 1350 K, reducing NO by about 30%. A simulated natural gas (methane with about 10% of ethane) is more efficient in reducing NO and with a lower onset temperature, about 1300 K. Among the C_2-hydrocarbons, acetylene and ethylene behave similarly, with an NO reduction of up to about 50% from 1150 K. Ethane is able to reduce NO above 1100 K, with the efficiency increasing with temperature. Nitric oxide is partly converted to hydrogen cyanide for all fuels, but the HCN concentrations are comparatively low.

The modeling predictions capture the trends well and are mostly in good agreement with the experimental results. The only major discrepancy is seen for reburning with ethane, where both the reduction of NO and the formation of HCN is underpredicted. Part of this difference may be attributed to mixing effects in the reactor, as discussed by Glarborg et al. [21].

Prediction of the potential of reburning for reducing NO relies on the ability of the model to describe the chemistry in the reducing zone, where hydrocarbon radicals are formed and act to reduce NO, and at the rich-lean transition, where the formed cyanides and amines are converted to NO and N_2. The accuracy in predicting the fuel-derived radical concentrations is still in discussion, even for oxidation of methane (see section 3.2 and App. B). However, since most of the C_1 and C_2 radicals typically participate in removing NO and the radical + NO reactions generally are fairly well characterized, the model would be expected to predict the NO consumption in the reducing zone perhaps within 30% for methane, with a slightly higher uncertainty for other hydrocarbons. The burnout chemistry at the rich-lean transition, which is discussed in more detail by Kristensen et al. [182], involves oxidation of HCN and NH_3 in the presence of the remaining combustibles as well as of NO. It shares similarities with selective non-catalytic reduction of NO (see section 4.1). The radical generation in the burnout region is controlled by oxidation of CO and H_2 rather than by the nitrogen chemistry, and the selectivity for forming NO and N_2 from the reactive

nitrogen species would be expected to be captured well by the model.
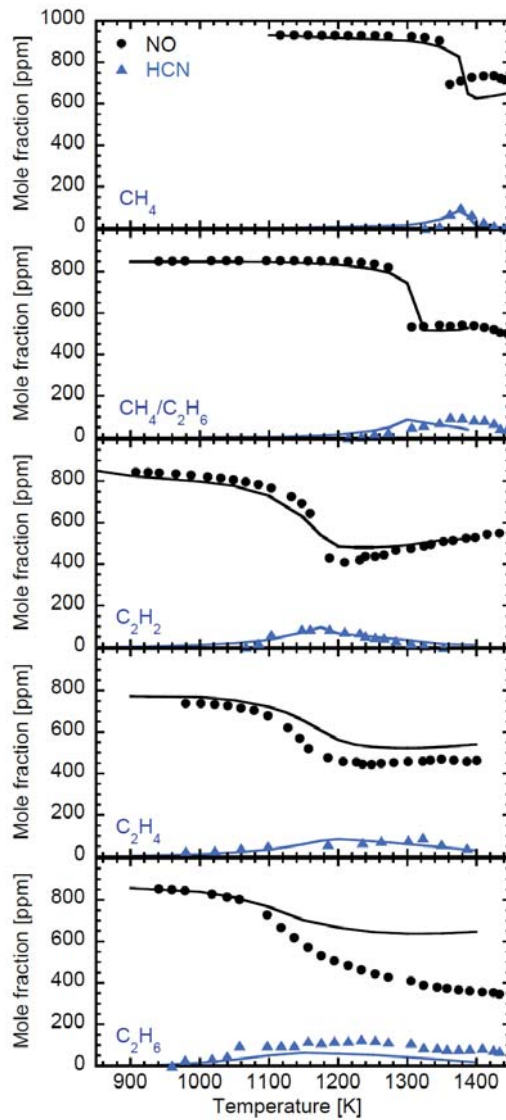
Figure 43: Comparison of experimental data [21, 267] and modeling predictions for reduction of NO by hydrocarbons under reburning conditions in a quartz flow reactor. Symbols denote experimental data, while solid lines denote modeling predictions. Inlet concentrations: $CH_4 = 2800$ ppm, $O_2 = 4830$ ppm, NO = 920 ppm ($\tau = 181[K]/T$); $CH_4 = 2770$ ppm, $C_2H_6 = 260$ ppm, $O_2 = 4885$ ppm, NO = 850 ppm ($\tau = 170[K]/T$); $C_2H_2 = 890$ ppm, $O_2 = 1700$ ppm, NO = 835 ppm ($\tau = 162[K]/T$); $C_2H_4 = 1020$ ppm, $O_2 = 2015$ ppm, NO = 790 ppm ($\tau = 165[K]/T$); $C_2H_6 = 1530$ ppm, $O_2 = 3970$ ppm, NO = 870 ppm ($\tau = 167[K]/T$). All experiments were conducted with 2% H_2O, balance N_2, at 1.05 atm.

Concluding remarks

Close to thirty years ago, Miller and Bowman published their epochal review on nitrogen chemistry in combustion. They concluded that future changes to their proposed mechanism were likely to be quantitative rather than qualitative. Since then, our knowledge of the thermochemistry and rate constants important for formation and destruction of nitrogen oxides has increased considerably, facilitated by the development of high-level theoretical tools. However, to a large extent the statement of Miller and Bowman has turned out to be accurate. The subsets describing formation of NO by the thermal mechanism, via N_2O, or from oxidation of cyanides and amines are now more reliable due to advances in our knowledge of specific reactions, but qualitatively they are similar to those proposed by Miller and Bowman. The same applies for the reburn type chemistry that serves to destroy NO in staged combustion. Major discoveries post Miller and Bowman concern the formation of prompt NO, where the products of the rate controlling reaction between CH and N_2 is now known to be NCN + H rather than HCN + N, and the Thermal $DeNO_x$ process, where the predicted lifetime of NNH has been reduced from 10^{-4} s to 10^{-9} s, so reaction now is restrained by the branching fraction α of the NH_2 + NO reaction rather than by reaction of NNH with NO or O_2. Despite the advances in the accuracy of specific rate constants, there are still subsets of the nitrogen chemistry where modeling predictions are less reliable than desired; these include primarily prompt NO formation and selective non-catalytic reduction of NO (SNCR). However, overall the present non-optimized model offers reliable predictions for formation and destruction of NO over a wide range of conditions and can be used with a significant degree of confidence in engineering calculations for industrial processes.

Future challenges in nitrogen chemistry include extension of the model to more complicated fuels (emphasizing, for instance, formation of hydrocarbon radicals that may interact with nitrogen species), more complex nitrogen compounds

such as cyclic species, and, not least, extension to the high pressures encountered in engines and gas turbines.

Acknowledgments

References

[1] J.A. Miller and C.T. Bowman. Mechanism and modeling of nitrogen chemistry in combustion. *Prog. Energy Combust. Sci.*, 15:287–338, 1989.

[2] C.T. Bowman. Control of combustion-generated nitrogen oxide emissions: technology driven by regulation. *Symp. (Int.) Combust.*, 24:859–878, 1992.

[3] P. Glarborg, A.D. Jensen, and J.E. Johnsson. Fuel nitrogen conversion in solid fuel fired systems. *Prog. Energy Combust. Sci.*, 29:89–113, 2003.

[4] P. Glarborg. Hidden interactions - trace species governing combustion and emissions. *Proc. Combust. Inst.*, 31:77–98, 2007.

[5] J.E. Johnsson. Formation and Reduction of Nitrogen Oxides in Fluidized-Bed Combustion. *Fuel*, 73:1398–1415, 1994.

[6] S.C. Hill and L.D. Smoot. Modeling of nitrogen oxides formation and destruction in combustion systems. *Prog. Energy Combust. Sci.*, 26:417–458, 2000.

[7] F.L. Dryer, F.M. Haas, J. Santner, T.I. Farouk, and M. Chaos. Interpreting chemical kinetics from complex reaction-advection-diffusion systems: Modeling of flow reactors and related experiments. *Prog. Energy Combust. Sci.*, 44:19–39, 2014.

[8] B. Ruscic, R.E. Pinzon, M.L. Morton, G. von Laszewski, S. Bittner, S.G. Nijsure, K.A. Amin, M. Minkoff, and A.F. Wagner. Introduction to Active Thermochemical Tables: Several "key" enthalpies of formation revisited. *J. Phys. Chem. A*, 108:9979–9997, 2004.

[9] B. Ruscic, R.E. Pinzon, G. von Laszewski, D. Kodeboyina, A. Burcat, D. Leahy, D. Montoya, and A.F. Wagner. Active Thermochemical Tables: thermochemistry for the 21st century. *J. Phys. Conf. Ser.*, 16:561–570, 2005.

[10] B. Ruscic. Active Thermochemical Tables: Sequential bond dissociation Enthalpies of methane, ethane, and methanol and the related thermochemistry. *J. Phys. Chem. A*, 119:7810–7837, 2015.

[11] B. Ruscic and D. H. Bross. *Active Thermochemical Tables (ATcT) values based on ver. 1.122 of the Thermochemical Network*. (available at ATcT.anl.gov), 2016.

[12] T. L. Nguyen, J. H. Baraban, B. Ruscic, and J. F. Stanton. On the HCN - HNC energy difference. *J. Phys. Chem. A*, 119:10929–10934, 2015.

[13] S.J. Klippenstein, L.B. Harding, and B. Ruscic. Ab initio computations and Active Thermochemical Tables hand in hand: Heats of formation of core combustion species. *J. Phys. Chem. A*, 121:6580–6602, 2017.

[14] B. J. McBride and S. Gordon. *Properties and coefficients, computer program for calculating and fitting thermodynamic functions*. National Aeronautics and Space Administration, Glenn Research Center, Cleveland, OH, 1999.

[15] E. Goos, A. Burcat, , and B. Ruscic. *Ideal gas thermochemical database with updates from Active Thermochemical Tables*. (<ftp://ftp. technion. ac. il/pub/supported/aetdd/thermodynamics> mirrored at <http://-garfield. chem. elte. hu/burcat/burcat. html>, 2016.

[16] H. Hashemi, J.M. Christensen, S. Gersen, H. Levinsky, S.J. Klippenstein, and P. Glarborg. High-pressure oxidation of methane. *Combust. Flame*, 172:349–364, 2016.

[17] J. Gimenez-Lopez, C. T. Rasmussen, H. Hashemi, M.U. Alzueta, Y. Gao, P. Marshall, C.F. Goldsmith, and P. Glarborg. Experimental and kinetic modeling study of C_2H_2 oxidation at high pressure. *Int. J. Chem. Kinet.*, 48:724–738, 2016.

[18] H. Hashemi, J. G. Jacobsen, C. T. Rasmussen, J. M. Christensen, P. Glarborg, S. Gersen, M. van Essen, H.B. Levinsky, and S.J. Klippenstein. High-pressure oxidation of ethane. *Combust. Flame*, 182:150–166, 2017.

[19] S.J. Klippenstein, L.B. Harding, P. Glarborg, and J.A. Miller. The role of NNH in NO formation and control. *Combust. Flame*, 158:774–789, 2011.

[20] P. Dagaut, P. Glarborg, and M.U. Alzueta. The oxidation of hydrogen cyanide and related chemistry. *Prog. Energy Combust. Sci.*, 34:1–46, 2008.

[21] P. Glarborg, M.U. Alzueta, K. Dam-Johansen, and J.A. Miller. Kinetic modeling of hydrocarbon/nitric oxide interactions in a flow reactor. *Combust. Flame*, 115:1–27, 1998.

[22] T. Mendiara and P. Glarborg. Ammonia chemistry in oxy-fuel combustion of methane. *Combust. Flame*, 156:1937–1949, 2009.

[23] T. Mendiara and P. Glarborg. NO reduction in oxy-fuel combustion of methane. *Energy Fuels*, 23:3565–3572, 2009.

[24] P. Glarborg, J.A. Miller, and R.J. Kee. Kinetic modeling and sensitivity analysis of nitrogen oxide formation in well–stirred reactors. *Combust. Flame*, 65:177–202, 1986.

[25] Y.B. Zeldovich. The oxidation of nitrogen in combustion and explosions. *Acta. Physicochem. USSR*, 21:577–628, 1946.

[26] D.L. Baulch, C.T. Bowman, C.J. Cobos, R.A. Cox, T. Just, J.A. Kerr, M.J. Pilling, D. Stocker, J. Troe, W. Tsang, R.W. Walker, and J. Warnatz. Evaluated kinetic data for combustion modeling: Supplement II. *J. Phys. Chem. Ref. Data*, 34:757–1397, 2005.

[27] J.P. Monat, R.K. Hanson, and C.H. Kruger. Shock tube determination of the rate coefficient for the reaction $N_2+O \rightarrow NO+N$. *Symp. (Int.) Combust.*, 17:543–552, 1979.

[28] K. Thielen and P. Roth. Resonance absorption measurements of N and O atoms in high temperature NO dissociation and formation kinetics. *Symp. (Int.) Combust.*, 20:685–693, 1984.

[29] C.P. Fenimore. Formation of nitric oxide in premixed hydrocarbon flames. *Symp. (Int.) Combust.*, 13:373–380, 1971.

[30] J.B. Livesey, A.L. Roberts, and A. Williams. The formation of oxides of nitrogen in some oxy-propane flames. *Combust. Sci. Technol.*, 4:9–15, 1971.

[31] F. Bachmaier, K.H. Eberius, and Th. Just. The formation of nitric oxide and the detection of HCN in premixed hydrocarbon-air flames at 1 atmosphere. *Combust. Sci. Technol.*, 7:77–84, 1973.

[32] D. Iverach, K.S. Basden, and N.Y. Kirov. Formation of nitric oxide in fuel-lean and fuel-rich flames. *Symp. (Int.) Combust.*, 14:767–775, 1973.

[33] R.J. Harris, M. Nasralla, and A. Williams. Formation of oxides of nitrogen in high-temperature CH_4-O_2-N_2 flames. *Combust. Sci. Technol.*, 14:85–94, 1976.

[34] P.V. Heberling. Prompt NO measurements at high pressures. *Symp. (Int.) Combust.*, 16:159–166, 1977.

[35] J. Blauwens, B. Smets, and J. Peeters. Mechanism of prompt NO formation in hydrocarbon flames. *Symp. (Int.) Combust.*, 16:1055–1064, 1976.

[36] M.F. Zabielski and D.J. Seery. The direct measurement of the rate of nitric oxide formation in a high temperature, oxygen enriched methane flame. *ASME Fossil Fuels Combust. Symp.*, 25:91–94, 1989.

[37] M.A.A. Clyne and B.A. Thrush. Kinetics of reactions of active nitrogen with oxygen and with nitric oxide. *Proc. R. Soc. London A*, 261:259–273, 1961.

[38] M.A.A. Clyne and I.S. McDermid. Mass-spectrometric determinations of rates of elementary reactions of NO and of NO_2 with ground-state N atoms. *J. Chem. Soc. Faraday Trans. 1*, 71:2189–2202, 1975.

[39] C.T. Cheah and M.A.A. Clyne. Reactions forming electronically-excited free-radicals. 2. Formation of N4s, N_2d and N_2p atoms in the H + NF_2 reaction, and N-atom reactions. *J. Chem. Soc. Faraday Trans. 2*, 76:1543–1560, 1980.

[40] J. Brunning and M.A.A. Clyne. Elementary reactions of the SF radical. Part 1. Rate constants for the reactions F + OCS → SF + CO and SF + SF → SF_2 + S. *J. Chem. Soc. Faraday Trans. 2*, 80:1001–1014, 1984.

[41] J.H. Lee, J.V. Michael, W.A. Payne, and L.J. Stief. Absolute rate of the reaction of N with NO from 196-400 K with DF-RF and FP-RF techniques. *J. Chem. Phys.*, 69:3069–3076, 1978.

[42] M. Koshi, M. Yoshimura, K. Fukuda, H. Matsui, K. Saito, M. Watanabe, A. Imamura, and C. Chen. Reactions of N atoms with NO and H_2. *J. Chem. Phys.*, 93:8703–8708, 1990.

[43] D.F. Davidson and R.K. Hanson. High-temperature reaction-rate coefficients derived from N-atom ARAS measurements and excimer photolysis of NO. *Int. J. Chem. Kinet.*, 22:843–861, 1990.

[44] J.V. Michael and K.P. Lim. Rate constants for the N_2O reaction system - thermal-decomposition of N_2O, N+NO → N_2+O and implications for O+N_2 → NO+N. *J. Chem. Phys.*, 97:3228–3234, 1992.

[45] H.J. Mick, H. Matsui, and P. Roth. High-temperature kinetics of Si atom oxidation by NO based on Si, N, and O atom measurements. *J. Phys. Chem.*, 97:6839–6842, 1993.

[46] M. Abian, M.U. Alzueta, and P. Glarborg. Formation of NO from N_2/O_2 mixtures in a flow reactor: Towards an accurate prediction of Thermal NO. *Int. J. Chem. Kinet.*, 47:518–532, 2015.

[47] P. Gamallo, M. Gonzalez, and R. Says. Ab initio study of the two lowest triplet potential energy surfaces involved in the N + NO reaction. *J. Chem. Phys.*, 118:10602–10610, 2003.

[48] O. Skreiberg, P. Kilpinen, and P. Glarborg. Ammonia chemistry under fuel-rich conditions in a flow reactor. *Combust Flame*, 136:501–518, 2004.

[49] A. Fernandez, A. Goumri, and A. Fontijn. Kinetics of the reactions of N atoms with O_2 and CO_2 over wide temperature ranges. *J. Phys. Chem. A*, 102:168–172, 1998.

[50] A.A. Konnov. On the relative importance of different routes forming NO in hydrogen flames. *Combust Flame*, 134:421–424, 2003.

[51] A. Frassoldati, T. Faravelli, and E. Ranzi. A wide range modeling study of NO_x formation and nitrogen chemistry in hydrogen combustion. *Int. J. Hydrogen Energy*, 31:2310–2328, 2006.

[52] N. Arai, T. Higashi, M. Hasatani, and S. Sugiyama. Formation of thermal NO_x in a binary system of nitrogen and oxygen. *Int. Chem. Eng.*, 18:661–665, 1978.

[53] J.B. Homer and M.M. Sutton. Nitric oxide formation and radical overshoot in premixed hydrogen flames. *Combust Flame*, 20:71–76, 1973.

[54] A.N. Hayhurst and I.M. Vince. Nitric-oxide formation from N_2 in flames - the importance of prompt NO. *Prog. Energy Combust. Sci.*, 6:35–51, 1980.

[55] M.R. Roomina and R.W. Bilger. Conditional moment closure (CMC) predictions of a turbulent methane-air jet flame. *Combust. Flame*, 125:1176–1195, 2001.

[56] L. Cui, K. Morokuma, J.M. Bowman, and S.J. Klippenstein. The spin-forbidden reaction $CH+N_2 \rightarrow HCN+N$ revisited. II. Nonadiabatic transition state theory and application. *J. Chem. Phys.*, 110:9469–9482, 1999.

[57] L.V. Moskaleva and M.C. Lin. The spin-conserved reaction $CH + N_2 \rightarrow H + NCN$: A major pathway to prompt NO studied by quantum/statistical theory calculations and kinetic modeling of rate constant. *Proc. Combust. Inst.*, 28:2393–2401, 2000.

[58] S. Xu and M. C. Lin. Ab initio chemical kinetics for singlet CH_2 reaction with N_2 and the related decomposition of diazomethane. *J. Phys. Chem. A*, 114:5195–5204, 2010.

[59] B.A. Williams and J.W. Fleming. Experimental and modeling study of NO formation in 10 torr methane and propane flames: Evidence for additional prompt-NO precursors. *Proc. Combust. Inst.*, 31:1109–1117, 2007.

[60] J.A. Sutton and J.W. Fleming. Towards accurate kinetic modeling of prompt NO formation in hydrocarbon flames via the NCN pathway. *Combust. Flame*, 154:630–636, 2008.

[61] A.A. Konnov. Implementation of the NCN pathway of prompt-NO formation in the detailed reaction mechanism. *Combust. Flame*, 156:2093–2105, 2009.

[62] N. Lamoureux, P. Desgroux, A. El Bakali, and J.F. Pauwels. Experimental and numerical study of the role of NCN in prompt-NO formation in low-pressure CH_4-O_2-N_2 and C_2H_2-O_2-N_2 flames. *Combust. Flame*, 157:1929–1941, 2010.

[63] R. S. Zhu, S. C. Xu, and M. C. Lin. Ab initio chemical kinetics for the reactions of N_2 with singlet and triplet C_2O radicals. *Chem. Phys. Lett.*, 488:121–125, 2010.

[64] T. Sommer, T. Kruse, P. Roth, and H. Hippler. Perturbation study on the reaction of C_2 with N_2 in high-temperature C_{60}/Ar+N_2 mixtures. *J. Phys. Chem. A*, 101:3720–3725, 1997.

[65] Yu. A. Kolbanovskii and Yu. A. Borisov. Quantum chemical calculations on the mechanism of the reaction between dicarbene C_2 and molecular nitrogen. *Russ J. Phys. Chem. B*, 9:29–35, 2015.

[66] M. Köhler, A. Brockhinke, M. Braun-Unkhoff, and K. Kohse-Höinghaus. Quantitative laser diagnostic and modeling study of C_2 and CH chemistry in combustion. *J. Phys. Chem. A*, 114:4719–4734, 2010.

[67] A. el Bakali, L. Pillier, P. Desgroux, B. Lefort, L. Gasnot, J.F. Pauwels, and I. da Costa. NO prediction in natural gas flames using GDF-Kin3.0 mechanism NCN and HCN contribution to prompt-NO formation. *Fuel*, 85:896–909, 2006.

[68] I.G. Zsely, J. Zador, and T. Turanyi. Uncertainty analysis of NO production during methane combustion. *Int. J. Chem. Kinet.*, 40:754–768, 2008.

[69] S. Gersen, A.V. Mokhov, and H.B. Levinsky. Diode laser absorption measurement and analysis of HCN in atmospheric-pressure, fuel-rich premixed methane/air flames. *Combust. Flame*, 155:267–276, 2008.

[70] J.A. Sutton, B.A. Williams, and J.W. Fleming. Investigation of NCN and prompt-NO formation in low-pressure C_1-C_4 alkane flames. *Combust. Flame*, 159:562–576, 2012.

[71] E. Goos, C. Sickfeld, F. Mauss, L. Seidel, B. Ruscic, A. Burcat, and T. Zeuch. Prompt NO formation in flames: The influence of NCN thermochemistry. *Proc. Combust. Inst.*, 34:657–666, 2013.

[72] N. Lamoureux, H. El Merhubi, L. Pillier, S. de Persis, and P. Desgroux. Modeling of NO formation in low pressure premixed flames. *Combust. Flame*, 163:557–575, 2016.

[73] E.P. Clifford, P.G. Wenthold, W.C. Lineberger, G.A. Petersson, and G.B. Ellison. Photoelectron spectroscopy of the NCN- and HNCN- ions. *J. Phys. Chem. A*, 101:4338–4345, 1997.

[74] R.T. Bise, H. Choi, and D.M. Neumark. Photodissociation dynamics of the singlet and triplet states of the NCN radical. *J. Chem. Phys.*, 111:4923–4932, 1999.

[75] R.T. Bise, A.A. Hoops, and D.M. Neumark. Photodissociation and photoisomerization pathways of the HNCN free radical. *J. Chem. Phys.*, 114:9000–9011, 2001.

[76] S. Canneaux, A. Wallet, M. Ribaucour, and F. Louis. A theoretical study of the NCN biradical thermochemical properties: Implications for combustion chemistry. *Comput. Theo. Chem.*, 967:67–74, 2011.

[77] L.B. Harding, S.J. Klippenstein, and J.A. Miller. Kinetics of CH + N_2 revisited with multireference methods. *J. Phys. Chem. A*, 112:522–532, 2008.

[78] N. Fassheber, J. Dammeier, and G. Friedrichs. Direct measurements of the total rate constant of the reaction NCN + H and implications for the product branching ratio and the enthalpy of formation of NCN. *Phys. Chem. Chem. Phys.*, 16:11647–11657, 2014.

[79] B. Ruscic. *Active Thermochemical Tables (ATcT) values based on ver. 1.112 of the Thermochemical Network.* (available at ATcT.anl.gov), 2013.

[80] B. Ruscic. *Active Thermochemical Tables (ATcT) values based on ver. 1.118 of the Thermochemical Network.* (available at ATcT.anl.gov), 2015.

[81] B. Ruscic, D. Feller, and K. A. Peterson. Active Thermochemical Tables: Dissociation energies of several homonuclear first-row diatomics and related thermochemical values. *Theor. Chem. Acc.*, 133:1415/1–12, 2014.

[82] S. J. Klippenstein, M. Pfeifle, A.W. Jasper, and P. Glarborg. Theory and Modeling of Relevance to Prompt-NO Formation at High Pressure. *submitted for publication.*

[83] J. Dammeier, N. Fassheber, and G. Friedrichs. Direct measurements of the high temperature rate constants of the reactions NCN + O, NCN + NCN, and NCN + M. *Phys. Chem. Chem. Phys.*, 14:1030–1037, 2012.

[84] R.S. Zhu and M.C. Lin. Ab initio study on the oxidation of NCN by O: prediction of the total rate constant and product branching ratios. *J. Phys. Chem. A*, 111:6766–6771, 2007.

[85] N. Fassheber and G. Friedrichs. Shock tube Measurements of the rate constant of the reaction NCN + O_2. *Int. J. Chem. Kinet.*, 47:586–595, 2015.

[86] J. Dammeier and G. Friedrichs. Direct measurements of the rate constants of the reactions NCN plus NO and NCN + NO_2 behind shock waves. *J. Phys. Chem. A*, 115:14382–14390, 2011.

[87] A.J. Dean, R.K. Hanson, and C.T. Bowman. High temperature shock tube study of reactions of CH and C-atoms with N_2. *Symp. (Int.) Combust.*, 23:259–265, 1991.

[88] V. Vasudevan, R.K. Hanson, C.T. Bowman, D.M. Golden, and D.F. Davidson. Shock tube study of the reaction of CH with N_2: Overall rate and branching ratio. *J. Phys. Chem. A*, 111:11818–11830, 2007.

[89] J.A. Miller and S.P. Walch. Prompt NO: Theoretical prediction of the high-temperature rate coefficient for CH+N_2 $\rightarrow$ HCN+N. *Int. J. Chem. Kinet.*, 29:253–259, 1997.

[90] J.A. Miller, M.J. Pilling, and J. Troe. Unravelling combustion mechanisms through a quantitative understanding of elementary reactions. *Proc. Combust. Inst.*, 30:43–88, 2005.

[91] D. Lindackers, M. Burmeister, and P. Roth. Prturbation studies of high temperature C and CH reactions with N_2 and NO. *Symp. (Int.) Combust.*, 23:251–257, 1991.

[92] W.-S. Teng, L.V. Moskaleva, H.-L. Chen, and M.C. Lin. Ab initio chemical kinetics for H + NCN: Prediction of NCN heat of formation and reaction product branching via doublet and quartet surfaces. *J. Phys. Chem. A*, 117:5775–5784, 2013.

[93] R.S. Zhu, H.M.T. Nguyen, and M.C. Lin. Ab initio study on the oxidation of NCN by OH: Prediction of the individual and total rate constants. *J. Phys. Chem. A*, 113:298–304, 2009.

[94] R.S. Zhu and M.C. Lin. Ab initio study of the oxidation of NCN by O_2. *Int. J. Chem. Kinet.*, 37:593–598, 2005.

[95] P.A. Berg, D.A. Hill, A.R. Noble, G.P. Smith, J.B. Jeffries, and D.R. Crosley. Absolute CH concentration measurements in low-pressure methane flames: Comparisons with model results. *Combust. Flame*, 121:223–235, 2000.

[96] N. Lamoureux, X. Mercier, C. Western, J.F. Pauwels, and P. Desgroux. NCN quantitative measurement in a laminar low pressure flame. *Proc. Combust. Inst.*, 32:937–944, 2009.

[97] N. Lamoureux, P. Desgroux, A. El Bakali, and J.F. Pauwels. Experimental and numerical study of the role of NCN in the prompt-NO formation in low pressure $CH_4/O_2/N_2$ and $C_2H_2/O_2/N_2$ flames. *Combust. Flame*, 160:745–746, 2013.

[98] N. Lamoureux, C.M. Western, X. Mercier, and P. Desgroux. Reinvestigation of the spectroscopy of the $Å^3\Pi_u$-$X^3\Sigma_g$-transition of the NCN radical at high temperature: application to quantitative NCN measurement in flames. *Combust. Flame*, 160:755–765, 2013.

[99] N. Lamoureux, H. El Merhubi, L. Gasnot, C. Schoemaecker, and P. Desgroux. Measurements and modelling of HCN and CN species profiles in laminar $CH_4/O_2/N_2$ low pressure flames using LIF/CRDS techniques. *Proc. Combust. Inst.*, 35:745–752, 2015.

[100] W. Bartok, V. S. Engleman, R. Goldstein, and E. G. del Valle. Basic kinetic studies and modeling of nitrogen oxide formation in combustion processes. *AIChE Symp. Ser.*, 126 (68):30–38, 1972.

[101] P. Malte and D.T. Pratt. Measurements of atomic oxygen and nitrogen oxides in jet-stirred combustion. *Symp. (Int.) Combust.*, 15:1061–1070, 1975.

[102] J.W. Bozzelli and A.M. Dean. O + NNH: A possible new route for NO_x formation in flames. *Int. J. Chem. Kinet.*, 27:1097–1109, 1995.

[103] M.S. Day, J.B. Bell, X. Gao, and P. Glarborg. Numerical simulation of nitrogen oxide formation in lean premixed turbulent $H_2/O_2/N_2$ flames. *Proc. Combust. Inst.*, 33:1591–1599, 2011.

[104] N.E. Meagher and W.R. Anderson. Kinetics of the O(3P) + N_2O reaction. 2. Interpretation and recommended rate coefficients. *J. Phys. Chem. A*, 104:6013–6031, 2000.

[105] P. Marshall, A. Fontijn, and C.F. Melius. High-temperature photochemistry and BAC-MP4 studies of the reaction between ground-state H-atoms and N_2O. *J. Chem. Phys.*, 86:5540–5549, 1987.

[106] H. Lillich, A. Schuck, H-R. Volpp, J. Wolfrum, and P.D. Naik. Kinetic studies of the reactions NH + NO and NH + O_2 at elevated temperatures. *Symp. (Int.) Combust.*, 25:993–1001, 1994.

[107] H.J. Romming and H.G. Wagner. A kinetic study of the reactions of NH with O_2 and NO in the temperature range from 1200 to 2200 K. *Symp. (Int.) Combust.*, 26:559–566, 1996.

[108] K. Yokoyama, Y. Sakane, and T. Fueno. Formations of OH in the reaction of NH with NO in incident shock waves. *Bull. Chem. Soc. Jpn.*, 64:1738–1742, 1991.

114

[109] J. D. Mertens, A. Y. Chang, R. K. Hanson, and C. T. Bowman. A shock tube study of the reactions of NH with NO, O_2, and O. *Int. J. Chem. Kinet.*, 23:173–196, 1991.

[110] J.L. Durant. Product branching fractions in the reaction of NH (ND) with NO. *J. Phys. Chem.*, 98:518–521, 1994.

[111] S. Okada, A. Tezaki, A. Miyoshi, and H. Matsui. Product branching fractions in the reactions of NH with NO. *J. Chem. Phys.*, 101:9582–9588, 1994.

[112] R. W. Quandt and J. F. Hershberger. Product branching ratios of the NH + NO and NH + NO_2 reactions. *J. Phys. Chem.*, 99:16939–16944, 1995.

[113] S. Gordon, W. Mulac, and P. Nangia. Pulse radiolysis of ammonia gas. II. Rate of disappearance of the NH_2 radical. *J. Phys. Chem.*, 75:2087–2093, 1971.

[114] I. Hansen, K. Hoinghaus, C. Zetzsch, and F. Stuhl. Detection of NH by resonance fluorescence in the pulsed vacuum UV photolysis of NH_3 and its application to reactions of NH radicals. *Chem. Phys. Lett.*, 42:370–372, 1976.

[115] J.A. Harrison, A.R. Whyte, and L.F. Phillips. Kinetics of reactions of NH with NO and NO_2. *Chem. Phys. Lett.*, 129:346–352, 1986.

[116] W. Hack, H.Gg. Wagner, and A. Zaspypkin. Elementary reactions of NH with N, O and NO. *Ber. Bunsenges. Phys. Chem.*, 98:156–164, 1994.

[117] H. Geiger, P. Wiesen, and K.H. Becker. A product study of the reaction of CH radicals with nitric oxide at 298 K. *Phys. Chem. Chem. Phys.*, 1:5601–5606, 1999.

[118] A.A. Konnov, G. Colson, and J. De Ruyck. The new route forming NO via NNH. *Combust. Flame*, 121:548–550, 2000.

[119] A.A. Konnov, I.V. Dyakov, and J. De Ruyck. Nitric oxide formation in premixed flames of H_2+CO+CO_2 and air. *Proc. Combust. Inst.*, 29:2171–2177, 2002.

[120] N.L. Haworth, J.C. Mackie, and G.B. Bacskay. An ab initio quantum chemical and kinetic study of the NNH + O reaction potential energy surface: How important is this route to NO in combustion? *J. Phys. Chem. A*, 107:6792–6803, 2003.

[121] D.L. Baulch, D.D. Drysdale, D.G. Horne, and A.C. Lloyd. *Evaluated kinetic data for high temperature reactions. Vol 2, Homogeneous gas phase reactions of the H_2-N_2-O_2 system.* Butterworths, London, 1973.

[122] R.K. Hanson and S. Salimian. Combustion chemistry of nitrogen. In Jr. W.C. Gardiner, editor, *Combustion chemistry.* Springer-Verlag, New York, 1984.

[123] F. Kaufman, N.J. Gerri, and R.E. Bowman. Role of nitric oxide in the thermal decomposition of nitrous oxide. *J. Chem. Phys.*, 25:106–115, 1956.

[124] H. Dindi, H.-M. Tsai, and M.C. Branch. Combustion mechanism of carbon monoxide-nitrous oxide flames. *Combust. Flame*, 87:13–20, 1991.

[125] M. Rohrig, E. L. Petersen, D. F. Davidson, and R. K. Hanson. The pressure dependence of the thermal decomposition of N_2O. *Int. J. Chem. Kinet.*, 28:599–608, 1996.

[126] M. Gonzalez, R. Sayos, and R. Valero. Ab initio and kinetics study of the ground potential energy surface of the O(D-1) + N_2O $\rightarrow$ 2NO, N_2 + O_2 reactions. *Chem. Phys. Lett.*, 355:123–132, 2002.

[127] A.N. Hayhurst and E.M. Hutchinson. Evidence for a new way of producing NO via NNH in fuel-rich flames at atmospheric pressure. *Combust. Flame*, 114:274–279, 1998.

[128] A.A. Konnov and J. De Ruyck. Temperature-dependent rate constant for the reaction NNH + O → NH + NO. *Combust. Flame*, 125:1258–1264, 2001.

[129] J.E. Harrington, G.P. Smith, P.A. Berg, A.B. Noble, J.B. Jeffries, and D.R. Crosley. Evidence for a new NO production mechanism in flames. *Symp. (Int.) Combust.*, 26:2133–2138, 1996.

[130] R. Steele, P. Malte, D. Nicol, and J. Kramlich. NO_x and N_2O in lean-premixed jet stirred flames. *Combust. Flame*, 100:440–449, 1995.

[131] A. Lucassen, K. Zhang, J. Warkentin, K. Moshammer, P. Glarborg, P. Marshall, and K. Kohse-Höinghaus. Fuel-nitrogen conversion in the combustion of small amines using dimethylamine and ethylamine as biomass-related model fuels. *Combust. Flame*, 159:2254–2279, 2012.

[132] Murakami N., Tokunaga K., and Sakai M. Formation of NO by the oxidation of HCN. *Nenryo Kyokaishi*, 61:759–769, 1982.

[133] T. Higashihara, K. Saito, and I. Murakami. Oxidation of hydrogen-cyanide in shock-waves - formation of nitrogen monoxide. *J. Phys. Chem.*, 87:3707–3712, 1983.

[134] J.A. Miller, M.C. Branch, W.J. McLean, Chandler D.W., M.D. Smooke, and Kee R.J. The conversion of HCN to NO and N_2 in H_2-O_2-HCN-Ar flames at low pressure. *Proc. Combust. Inst.*, 20:673–684, 1984.

[135] K. Thielen and P. Roth. Resonance absorption measurements of N, O, and H atoms in shock heated $HCN/O_2/Ar$ mixtures. *Combust. Flame*, 69:141–154, 1987.

[136] T. Hulgaard and K. Dam-Johansen. Homogeneous nitrous oxide formation and destruction under combustion conditions. *AIChE J.*, 39:1342–1354, 1993.

[137] P. Glarborg and J.A. Miller. Mechanism and modeling of hydrogen cyanide oxidation in a flow reactor. *Combust. Flame*, 99:475–483, 1994.

[138] P. Dagaut, F. Lecomte, S. Chevailler, and M. Cathonnet. Mutual sensitization of the oxidation of nitric oxide and simple fuels over an extended temperature range: experimental and detailed kinetic modeling. *Combust Sci Technol*, 148:27–57, 1999.

[139] P. Dagaut, F. Lecomte, S. Chevailler, and M. Cathonnet. The oxidation of HCN and reactions with nitric oxide: Experimental and detailed kinetic modeling. *Combust. Sci. Technol.*, 155:105–127, 2000.

[140] V. J. Wargadalam, G. Löffler, F. Winter, and H. Hofbauer. Homogeneous formation of NO and N_2O from the oxidation of HCN and NH_3 at 600-1000^oC. *Combust. Flame*, 120:465–478, 2000.

[141] J. Gimenez-Lopez, A. Millera, R. Bilbao, and M.U. Alzueta. HCN oxidation in an O_2/CO_2 atmosphere: An experimental and kinetic modeling study. *Combust. Flame*, 157:267–276, 2010.

[142] J. Gimenez-Lopez, A. Millera, R. Bilbao, and M. U. Alzueta. Interactions of HCN with NO in a CO_2 Atmosphere Representative of Oxy-fuel Combustion Conditions. *Energy Fuels*, 29:6593–6597, 2015.

[143] P. Glarborg and P. Marshall. Importance of the HNC isomer in modeling HCN oxidation in combustion. *Energy Fuels*, 31:2156–2163, 2017.

[144] J.A. Miller, C. Parrish, , and N.J. Brown. A statistical-theoretical investigation of the thermal rate coefficient and branching ratio for the reaction O + HCN $\rightarrow$ products. *J. Phys. Chem.*, 90:3339–3345, 1986.

[145] J.A. Miller and C.F. Melius. A theoretical analysis of the reaction between hydroxyl and hydrogen cyanide at high temperature. *Symp. (Int.) Combust.*, 21:919–927, 1986.

[146] A.M. Dean and J.W. Bozzelli. Combustion chemistry of nitrogen. In W.C. Gardiner, editor, *Gas phase combustion chemistry*, chapter 2. Springer-Verlag, 2000.

[147] S.T. Wooldridge, R.K. Hanson, and C.T. Bowman. Simultaneous laser-absorption measurements of CN and OH in a shock-tube study of HCN+OH $\rightarrow$ products. *Int. J. Chem. Kinet.*, 27:1075–1087, 1995.

[148] R. Sumathi and M.T. Nguyen. A theoretical study of the CH_2N system: Reactions in both lowest lying doublet and quartet states. *J. Phys. Chem. A*, 102:8013–8020, 1998.

[149] A.J.C. Bunkan, Y. Tang, S.R. Sellevag, and C.J. Nielsen. Atmospheric gas phase chemistry of CH_2=NH and HNC. A first-principles approach. *J. Phys. Chem. A*, 118:5279–5288, 2014.

[150] W. Feng and J. F. Hershberger. Reinvestigation of the branching ratio of the CN + O_2 reaction. *J. Phys. Chem. A*, 113:3523–3527, 2009.

[151] Y. Gao and G. MacDonald. Determination of the rate constant for the NCO + O reaction at 292 K. *J. Phys. Chem. A*, 107:4625–4635, 2003.

[152] J. A. Miller and C. T. Bowman. Kinetic modeling of the reduction of nitric oxide in combustion products by isocyanic acid. *Int. J. Chem. Kinet.*, 23:289–313, 1991.

[153] R. S. Zhu and M. C. Lin. The NCO + NO reaction revisited: Ab inito MO/VRRKM calculations for total rate constant and product branching ratios. *J. Phys. Chem. A*, 104:10807–10811, 2000.

[154] M.C. Lin, Y. He, and C.F. Melius. Communication - implications of the HCN $\rightarrow$ HNC process to high-temperature nitrogen-containing fuel chemistry. *Int. J. Chem. Kinet.*, 24:1103–1107, 1992.

[155] F. Mohammad, V.R. Morris, W.H. Fink, and W.M. Jackson. On the mechanism and branching ratio of the CN+O_2 $\rightarrow$ CO+NO reaction channel

119

using transient IR emission spectroscopy. *J. Phys. Chem.*, 97:11590–11598, 1993.

[156] K.T. Rim and J.F. Hershberger. Temperature dependence of the product branching ratio of the CN+O_2 reaction. *J. Phys. Chem. A*, 103:3721–3725, 1999.

[157] B. S. Haynes. The oxidation of hydrogen cyanide in fuel-rich flames. *Combust. Flame*, 28:113–121, 1977.

[158] J. A. Caton and D. L. Siebers. Comparison of nitric oxide removal by cyanuric acid and ammonia. *Combust. Sci. Technol.*, 65:277–293, 1989.

[159] P. Glarborg, P.G. Kristensen, S.H. Jensen, and K. Dam-Johansen. A flow reactor study of HNCO oxidation chemistry. *Combust. Flame*, 98:241–258, 1994.

[160] R.K. Lyon and J.A. Cole. A reexamination of the $RapreNO_x$ process. *Combust. Flame*, 82:435–443, 1990.

[161] R.A. Perry. Kinetics of the reactions of NCO radicals with H_2 and NO using laser photolysis-laser induced fluorescence. *J. Chem. Phys.*, 82:5485–5488, 1985.

[162] F.P. Tully, R.A. Perry, L.R. Thorne, and M.D. Allendorf. Free-radical oxidation of isocyanic acid. *Symp. (Int.) Combust.*, 22:1101–1106, 1988.

[163] C. H. Wu, H. T. Wang, M. C. Lin, and R. A. Fifer. Kinetics of CO and H atom production from the decomposition of HNCO in shock-waves. *J. Phys. Chem.*, 94:3344–3347, 1990.

[164] Y. He, X.P. Liu, M.C. Lin, and C.F. Melius. The thermal reaction of HNCO at moderate temperatures. *Int. J. Chem. Kinet.*, 23:1129–1149, 1991.

[165] Y. He, M. C. Lin, C. H. Wu, and C. F. Melius. The reaction of HNCO with NO_2 in shock waves. *Symp. (Int.) Combust.*, 24:711–717, 1992.

[166] Y. He, X.P. Liu, M.C. Lin, and C.F. Melius. Thermal-reaction of HNCO with NO_2 at moderate temperatures. *Int. J. Chem. Kinet.*, 25:845–863, 1993.

[167] J. D. Mertens, A. Y. Chang, R. K. Hanson, and C. T. Bowman. Reaction-kinetics of NH in the shock-tube pyrolysis of HNCO. *Int. J. Chem. Kinet.*, 21:1049–1067, 1989.

[168] J. D. Mertens, A. Y. Chang, R. K. Hanson, and C. T. Bowman. A shock-tube study of H + HNCO → NH_2 + CO. *Int. J. Chem. Kinet.*, 23:655–668, 1991.

[169] J. D. Mertens, R. K. Hanson, and C. T. Bowman. A shock-tube study of reactions of atomic oxygen with isocyanic acid. *Int. J. Chem. Kinet.*, 24:279–295, 1992.

[170] S.T. Wooldridge, R.K. Hanson, and C.T. Bowman. A shock tube study of CO+OH → CO_2+H and HNCO+OH → products via simultaneous laser adsorption measurements of OH and CO_2. *Int. J. Chem. Kinet.*, 28:361–372, 1995.

[171] J.A. Miller and C.F. Melius. A theoretical analysis of the reaction between hydrogen atoms and isocyanic acid. *Int. J. Chem. Kinet.*, 24:421–432, 1992.

[172] D. Sengupta and M. T. Nguyen. Mechanism of NH_2+CO_2 formation in OH+HNCO reaction: Rate constant evaluation via ab initio calculations and statistical theory. *J. Chem. Phys.*, 106:9703–9707, 1997.

[173] X.-G. Wei, X.-M. Sun, X.-P. Wu, S. Geng, Y. Ren, N.-B. Wong, and W.-K. Li. Cooperative effect of water molecules in the self-catalyzed neutral hydrolysis of isocyanic acid: a comprehensive theoretical study. *J. Mol. Model.*, 17:2069–2082, 2011.

[174] X. Cheng, Y. Zhao, W. Zhu, and Y. Liu. Theoretical investigation on the synthesis mechanism of cyanuric acid from NH_3 and CO_2. *J. Mol. Model.*, 19:5037–5043, 2013.

[175] W.L. Feng, Y. Wang, and S.-W. Zhang. Theoretical study of the mechanism and rate constant of the dimerization of isocyanic acid. *J. Mol. Structure (Theochem)*, 342:147–151, 1995.

[176] N. Borduas, B. Place, G. R. Wentworth, J. P. D. Abbatt, and J. G. Murphy. Solubility and reactivity of HNCO in water: insights into HNCO's fate in the atmosphere. *Atmos. Chem. Phys.*, 16:703–714, 2016.

[177] A. Zabardasti and M. Solimannejad. Theoretical study and aim analysis of hydrogen bonded clusters of water and isocyanic acid. *J. Mol. Structure THEOCHEM*, 819:52–59, 2007.

[178] A. Nicolle, S. Cagnina, and T. de Bruin. First-principle based modeling of urea decomposition in aqueous solutions. *Chem. Phys. Lett.*, 664:149–153, 2016.

[179] A.M. Mebel, A. Luna, M.C. Lin, and K. Morokuma. A density functional study of the global potential energy surfaces of the [HCNO] system in singlet and triplet states. *J. Chem. Phys.*, 105:6439–6454, 1996.

[180] J. Cao, Z.X. Wang, L.J. Gao, and F. Fu. Water-assisted isomerization of the [H,C,N,O] system. *J. Mol. Model.*, 21:66, 1–8, 2015.

[181] B. G. Wicke, K. A. Grady, and J. W. Ratcliffe. Cyanuric acid + nitric oxide reaction at 700^oC and the effects of oxygen. *Combust. Flame*, 78:249–255, 1989.

[182] P.G. Kristensen, P. Glarborg, and K. Dam-Johansen. Nitrogen chemistry during burnout in fuel-staged combustion. *Combust. Flame*, 107:211–222, 1996.

[183] J. A. Miller, M. D. Smooke, R. M. Green, and R. J. Kee. Kinetic modeling of the oxidation of ammonia in flames. *Combust. Sci. Technol.*, 34:149–176, 1983.

[184] R. P. Lindstedt, F. C. Lockwood, and M. A. Selim. A detailed kinetic study of ammonia oxidation. *Combust. Sci. Technol.*, 108:231–254, 1995.

[185] O. Mathieu and E.L. Petersen. Experimental and modeling study on the high-temperature oxidation of Ammonia and related NO_x chemistry. *Combust. Flame*, 162:554–570, 2015.

[186] P. Glarborg, K. Dam-Johansen, J.A. Miller, R.J. Kee, and M.E. Coltrin. Modeling the Thermal $DeNO_x$ process in flow reactors. Surface effects and nitrous oxide formation. *Int. J. Chem. Kinet.*, 26:421–436, 1994.

[187] J. A. Miller and P. Glarborg. Modeling the formation of N_2O and NO_2 in the Thermal $De-NO_x$ process. *Springer Ser. Chem. Phys.*, 61:318–333, 1996.

[188] J. A. Miller and P. Glarborg. Modeling the Thermal $DeNO_x$ process: Closing in on a final solution. *Int. J. Chem. Kinet.*, 31:757–765, 1999.

[189] Z. Tian, Y. Li, L. Zhang, P. Glarborg, and F. Qi. An experimental and kinetic modeling study of premixed $NH_3/CH_4/O_2/Ar$ flames at low pressure. *Combust. Flame*, 156:1413–1426, 2009.

[190] J. A. Miller and S. J. Klippenstein. Theoretical considerations in the NH_2 + NO reaction. *J. Phys. Chem. A*, 104:2061–2069, 2000.

[191] S. J. Klippenstein. From theoretical reaction dynamics to chemical modeling of combustion. *Proc. Combust. Inst.*, 36:77–111, 2017.

[192] S. J. Klippenstein, L. B. Harding, P. Glarborg, Y. Gao, and P. Marshall. Rate constant and branching fraction for the NH_2 + NO_2 reaction. *J. Phys. Chem. A*, 117:9011–9022, 2013.

[193] S.J. Klippenstein, L.B. Harding, B. Ruscic, R. Sivaramakrishnan, N.K. Srinivasan, M.-C. Su, and J.V. Michael. Thermal decomposition of NH_2OH and subsequent reactions: Ab initio transition state theory and reflected shock tube experiments. *J. Phys. Chem. A*, 113:10241–10259, 2009.

[194] G. Altinay and R. G. Macdonald. Determination of the rate constants for the $NH_2(X^2B_1)$ + $NH_2(X^2B_1)$ and $NH_2(X^2B_1)$ + H recombination reactions in N_2 as a function of temperature and pressure. *J. Phys. Chem. A*, 119:7593–7610, 2015.

[195] J. V. Michael, J. W. Sutherland, and R. B. Klemm. Rate constant for the reaction H + NH_3 over the temperature range 750-1777 K. *J. Phys. Chem.*, 90:497–500, 1986.

[196] J. W. Sutherland, P. M. Patterson, and R. B. Klemm. Flash photolysis-shock tube kinetic investigation of the reaction of O(3P) atoms with ammonia. *J. Phys. Chem.*, 94:2471–2475, 1990.

[197] S. Salimian, R. K. Hanson, and C. H. Kruger. High-temperature study of the reactions of O and OH with NH_3. *Int. J. Chem. Kin.*, 16:725–739, 1984.

[198] R. Sumathi and S. D. Peyerimhoff. A Quantum Statistical Analysis of the Rate Constant for the HO_2+NH_2 Reaction. *Chem. Phys. Lett.*, 263:742–748, 1996.

[199] A. Fontijn, S.M. Shamsuddin, D. Crammond, P. Marshall, and W.R. Anderson. Kinetics of the NH reaction with H_2 and reassesment of HNO formation from NH + CO_2, H_2O. *Combust. Flame*, 145:543–551, 2006.

[200] S. Xu and M. C. Lin. Ab initio chemical kinetics for the NH_2 + HNO_x reactions, Part I: Kinetics and mechanism for NH_2 + HNO. *Int. J. Chem. Kin.*, 41:667–677, 2009.

[201] S. Song, R. K. Hanson, C. T. Bowman, and D. M. Golden. Shock tube determination of the overall rate of $NH_2 + NO \rightarrow$ products in the Thermal De-NO_x temperature window. *Int. J. Chem. Kinet.*, 33:715–721, 2001.

[202] J.A. Miller and C.F Melius. The reactions of imidogen with nitric oxide and molecular oxygen. *Symp. (Int.) Combust.*, 24:719–726, 1992.

[203] D.-C. Fang, L.B. Harding, S.J. Klippenstein, and J.A. Miller. A direct transition state theory analysis of the branching in $NH_2 + NO$. *Faraday Disc. Royal Soc. Chem.*, 119:207–222, 2001.

[204] S. Song, R. K. Hanson, C. T. Bowman, and D. M. Golden. A shock tube study of the product branching ratio of the $NH_2 + NO$ reaction at high temperatures. *J. Phys. Chem. A*, 106:9233–9235, 2002.

[205] J. A. Silver and C. E. Kolb. Kinetic measurements for the reaction of $NH_2 + NO$ over the temperature range 294-1215 K. *J. Phys. Chem.*, 86:3240–3246, 1982.

[206] L. J. Stief, W. D. Brobst, D. F. Nava, R. P. Borkowski, and J. V. Michael. Rate constant for the reaction NH_2+NO from 216 K to 480 K. *J. Chem. Soc. Faraday Trans. 2*, 78:1391–1401, 1982.

[207] B. Atakan, A. Jacobs, M. Wahl, R. Weller, and J. Wolfrum. Kinetic measurements and product branching ratio for the reaction NH_2+NO at 294-1027 K. *Chem. Phys. Lett.*, 155:609–613, 1989.

[208] M. Wolf, D. L. Yang, and D. L. Durant. Kinetic studies of NH_x radical reactions. *J. Photochem. Photobiol. A: Chem.*, 80:85–93, 1994.

[209] M. Wolf, D. L. Yang, and D. L. Durant. A comprehensive study of the reaction $NH_2+NO \rightarrow$ products: Reaction rate coefficients, product branching fractions, and ab initio calculations. *J. Phys. Chem. A*, 101:6243–6251, 1997.

[210] J. Park and M. C. Lin. Direct determination of product branching for the NH_2 + NO reaction at temperatures between 302 and 1060 K. *J. Phys. Chem.*, 100:3317–3319, 1996.

[211] J. Park and M. C. Lin. Product branching ratios in the NH_2 + NO reaction: A re-evaluation. *J. Phys. Chem. A*, 103:8906–8907, 1999.

[212] P. Glarborg, P. G. Kristensen, K. Dam-Johansen, and J.A. Miller. The branching fraction of the NH_2+NO reaction between 1210 and 1370 K. *J. Phys. Chem. A*, 101:3741–3745, 1997.

[213] M. Votsmeier, S. Song, R. K. Hanson, and C. T. Bowman. A shock tube study of the product branching ratio for the reaction NH_2 + NO using frequency-modulation detection of NH_2. *J. Phys. Chem. A*, 103:1566–1571, 1999.

[214] V. P. Bulatov, A. A. Ioffe, V. A. Lozovsky, and O. M. Sarkisov. On the reaction of the NH_2 radical with NO_2 at 295-620 K. *Chem. Phys. Lett.*, 161:141–146, 1989.

[215] C. J. Howard. Kinetic study of the equilibrium HO_2+NO $\rightleftharpoons$ OH+NO_2 and the thermochemistry of HO_2. *J. Am. Chem. Soc.*, 102:6937–6941, 1980.

[216] N.K. Srinivasan, M.-C. Su, J.W. Sutherland, J.V. Michael, and B. Ruscic. Reflected shock tube studies of high-temperature rate constants for OH + NO_2 $\rightarrow$ HO_2 + NO and OH + HO_2 $\rightarrow$ H_2O + O_2. *J. Phys. Chem. A*, 110:6602–6607, 2006.

[217] W. Hack, H. Schacke, M. Schröter, and H. Gg. Wagner. Reaction rates of NH_2-radicals with NO, NO_2, C_2H_2, C_2H_4 and other hydrocarbons. *Symp. (Int.) Combust.*, 17:505–513, 1979.

[218] H. Kurasawa and R. Lesclaux. Kinetics of the reaction of NH_2 with NO_2. *Chem. Phys. Lett.*, 66:602–607, 1979.

[219] A. R. Whyte and L. F. Phillips. Rates of reactions of NH_2 with NO and NO_2. *Chem. Phys. Lett.*, 102:451–454, 1983.

[220] T. X. Xiang, L. M. Torres, and W. A. Guillory. State-selected reaction and relaxation of NH_2 radicals and NO_2. *J. Chem. Phys.*, 83:1623–1629, 1985.

[221] V. P. Bulatov, A. A. Ioffe, V. A. Lozovsky, and O. M. Sarkisov. On the reaction of the NH_2 radical with NO_2 at 295-620 K. *Chem. Phys. Lett.*, 159:171–174, 1989.

[222] P. Pagsberg, B. Sztuba, E. Ratajczak, and A. Sillesen. Spectrokinetic studies of the gas-phase reactions $NH_2 + NO_x$ initiated by pulse-radiolysis. *Acta Chem. Scand.*, 45:329–334, 1991.

[223] P. Glarborg, K. Dam-Johansen, and J.A. Miller. The reaction of ammonia with nitrogen dioxide in a flow reactor: Implications for the NH_2+NO_2 reaction. *Int. J. Chem. Kinet.*, 27:1207–1220, 1995.

[224] H. Meunier, P. Pagsberg, and A. Sillesen. Kinetics and branching ratios of the reactions $NH_2 + NO_2 \rightarrow N_2O + H_2O$ and $NH_2 + NO_2 \rightarrow H_2NO + NO$ studied by pulse radiolysis combined with time-resolved infrared diode laser spectroscopy. *Chem. Phys. Lett.*, 261:277–282, 1996.

[225] J. Park and M. C. Lin. A mass spectrometric study of the $NH_2 + NO_2$ reaction. *J. Phys. Chem. A*, 101:2643–2647, 1997.

[226] S. Song, D. M. Golden, R. K. Hanson, and C. T. Bowman. A shock tube study of the $NH_2 + NO_2$ reaction. *Proc. Combust. Inst.*, 29:2163–2170, 2002.

[227] J. Park and M. C. Lin. Mass-spectrometric determination of product branching probabilities for the $NH_2 + NO_2$ reaction at temperatures between 300 and 990 K. *Int. J. Chem. Kinet.*, 28:879–883, 1996.

[228] R. W. Quandt and J. F. Hershberger. Diode laser study of the product branching ratio of the NH_2 + NO_2 reaction. *J. Phys. Chem.*, 100:9407–9411, 1996.

[229] N. Lindholm and J. F. Hershberger. Product branching ratios of the NH_2 + NO_2 reaction. *J. Phys. Chem. A*, 101:4991–4995, 1997.

[230] M. Yumura and T. Asaba. Rate constants of chemical reactions in the high temperature pyrolysis of ammonia. *Symp. (Int.) Combust.*, 18:863–872, 1981.

[231] D.F. Davidson, K. Kohse-Hoinghaus, A.Y. Chang, and R.K. Hanson. A pyrolysis mechanism for ammonia. *Int. J. Chem. Kinet.*, 22:513–535, 1990.

[232] M. Rohrig and H.G. Wagner. The reactions of NH with the water gas components CO_2, H_2O, and H_2. *Symp. (Int.) Combust.*, 25:975–981, 1994.

[233] M.-K. Bahng and R.G. Macdonald. Determination of the rate constants for the radical-radical reactions NH_2 + NH and NH_2 + H_2 at 293 K. *J. Phys. Chem. A*, 113:2415–2423, 2009.

[234] P. Dransfeld, W. Hack, H. Kurzke, F. Temps, and H.G. Wagner. Direct studies of elementary reactions of NH_2-radicals in the gas phase. *Symp. (Int.) Combust.*, 20:655–663, 1972.

[235] J.D. Adamson, S.K. Farhat, C.L. Morter, G.P. Glass, R.F. Curl, and L.F. Phillips. The reaction of NH_2 with O. *J. Phys. Chem.*, 98:5665–5669, 1994.

[236] S. Inomata and N. Washida. Rate constants for the reactions of NH_2 and HNO with atomic oxygen at temperatures between 242 and 473 K. *J. Phys. Chem. A*, 103:5023–5031, 1999.

[237] Y. Song, H. Hashemi, J.M. Christensen, C. Zou, P. Marshall, and P. Glarborg. Ammonia oxidation at high pressure. *Fuel*, 181:358–365, 2016.

[238] C. P. Fenimore and G. W. Jones. Oxidation of ammonia in flames. *J. Phys. Chem.*, 65:298–303, 1961.

[239] D. I. MacLean and H. Gg. Wagner. The structure of the reaction zones of ammonia-oxygen and hydrazine decomposition flames. *Symp. (Int.) Combust.*, 11:871–878, 1967.

[240] R. J. Blint and C. J. Dasch. Formation of NO and N_2 from NH_3 in flames. *ACS Symp. Series*, 249:87–101, 1984.

[241] C. J. Dasch and R. J. Blint. A mechanistic and experimental study of ammonia in flames. *Combust. Sci. Technol.*, 41:223–244, 1984.

[242] A. M. Dean, M.-S. Chou, and D. Stern. Nitrogen chemistry in flames. Observations and detailed chemistry. *ACS Symp Series*, 249:71–86, 1984.

[243] A.M. Dean, M.-S. Chou, and D. Stern. Kinetics of rich ammonia flames. *Int. J. Chem. Kinet.*, 16:633–653, 1984.

[244] J. Bian, J. Vandooren, and P.J. van Tiggelen. Experimental study of the structure of an ammonia-oxygen flame. *Symp. (Int.) Combust.*, 21:953–963, 1986.

[245] C. Duynslaegher, H. Jeanmart, and J. Vandooren. Flame structure studies of premixed ammonia/hydrogen/oxygen/argon flames: Experimental and numerical investigation. *Proc. Combust. Inst.*, 32:1277–1284, 2009.

[246] T. Takeyama and H. Miyama. Kinetic studies of ammonia oxidation in shock waves II. The rate of ammonia consumption. *Bull. Chem. Soc. Japan*, 39:2352–2355, 1966.

[247] T. Takeyama and H. Miyama. A shock-tube study of the ammonia-oxygen reaction. *Symp. (Int.) Combust.*, 11:845–852, 1967.

[248] D. C. Bull. A shock tube study of the oxidation of ammonia. *Combust. Flame*, 12:603–610, 1968.

129

[249] H. Miyama. Kinetic studies of ammonia oxidation in ahock waves IV. Comparison of induction periods for the ignition of NH_3-O_2-N_2 with those for NH_3-O_2-Ar mixtures. *Bull Chem Soc Japan*, 41:1761–1765, 1968.

[250] H. Miyama. Ignition of ammonia-oxygen mixtures by shock waves. *J. Chem. Phys.*, 48:1421–1422, 1968.

[251] J.N. Bradley, R.N. Butlin, and D. Lewis. Oxidation of ammonia in shock waves. *Trans. Faraday Soc.*, 64:71–78, 1968.

[252] L. J. Drummond. High Temperature Oxidation of Ammonia. *Combust. Sci. Technol.*, 5:175–182, 1972.

[253] N. Fujii, H. Miyama, M. Koshi, and T. Asaba. Kinetics of ammonia oxidation in shock waves. *Symp. (Int.) Combust.*, 18:873–883, 1981.

[254] A. M. Dean, J. E. Hardy, and R. K. Lyon. Kinetics and mechanism of NH_3 oxidation. *Symp. (Int.) Combust.*, 19:97–105, 1982.

[255] T. Hasegawa and M. Sato. Study of ammonia removal from coal-gasified fuel. *Combust. Flame*, 114:246–258, 1998.

[256] E. Vilas and P. Glarborg. The selective non-catalytic reduction of NO with ammonia at high oxygen concentration. Technical Report CHEC R0410, DTU Chemical Engineering, 2004.

[257] R. K. Lyon and D. J. Benn. Kinetics of the NO-NH_3-O_2 reaction. *Symp. (Int.) Combust.*, 17:601–610, 1979.

[258] R.K. Lyon. NH_3-NO-O_2 reaction. *Int. J. Chem. Kinet.*, 8:315–318, 1976.

[259] R. K. Lyon and J. E. Hardy. Discovery and development of the thermal $DeNO_x$ process. *Ind. Eng. Chem. Fundam.*, 25:19–24, 1986.

[260] S. L. Chen, J. M. McCarthy, W. D. Clark, M. P. Heap, W. R. Seeker, and D. W. Pershing. Bench and pilot scale process evaluation of reburning for in-furnace NO_x reduction. *Symp. (Int.) Combust.*, 21:1159–1169, 1986.

130

[261] R. Mechenbier and H. Kremer. Brennstoffstufung kohlenstaub/methan zur minderung brennstoffbedingter NO_x-emissionen. *VDI-Ber.*, 645:87–98, 1987.

[262] P. Kilpinen, P. Glarborg, and M. Hupa. Reburning chemistry - A kinetic modeling study. *Ind. Eng. Chem. Res.*, 31:1477–1490, 1992.

[263] A. Kicherer, H. Spliethoff, H. Maier, and K. R. G. Hein. The effect of different reburning fuels on NO_x-reduction. *Fuel*, 73:1443–1446, 1994.

[264] R. Bilbao, A. Millera, and M. U. Alzueta. Influence of the temperature and oxygen concentration on NO_x reduction in the natural-gas reburning process. *Ind. Eng. Chem. Res.*, 33:2846–2852, 1994.

[265] R. Bilbao, M. U. Alzueta, and A. Millera. Experimental study of the influence of the operating variables on natural gas reburning efficiency. *Ind. Eng. Chem. Res.*, 34:4531–4539, 1995.

[266] R. Bilbao, A. Millera, M.U. Alzueta, and L. Prada. Evaluation of the use of different hydrocarbon fuels for gas reburning. *Fuel*, 76:1401–1407, 1997.

[267] M. U. Alzueta, P. Glarborg, and K. Dam-Johansen. Low temperature interactions between hydrocarbons and nitric oxide: An experimental study. *Combust. Flame*, 109:25–36, 1997.

[268] P. Dagaut, F. Lecomte, S. Chevailler, and M. Cathonnet. Experimental and detailed kinetic modeling of nitric oxide reduction by a natural gas blend in simulated reburning conditions. *Combust. Sci. Technol.*, 139:329–363, 1998.

[269] E.B. Ledesma, P.F. Nelson, and J.C. Mackie. An experimental and kinetic modeling study of the reduction of NO by coal volatiles in a flow reactor. *Proc. Combust. Inst.*, 28:2345–2351, 2000.

[270] P. Dagaut, J. Luche, and M. Cathonnet. The kinetics of C_1 to C_4 hydrocarbons/NO interactions in relation with reburning. *Proc. Combust. Inst.*, 28:2459–2465, 2000.

[271] P. Glarborg, P.G. Kristensen, K. Dam-Johansen, M.U. Alzueta, A. Millera, and R. Bilbao. Nitric oxide reduction by non-hydrocarbon fuels. *Energy Fuels*, 14:828–838, 2000.

[272] P. Dagaut and F. Lecomte. Experiments and kinetic modeling study of NO-reburning by gases from biomass pyrolysis in a JSR. *Energy Fuels*, 17:608–613, 2003.

[273] A. Frassoldati, T. Faravelli, and E. Ranzi. Kinetic modeling of the interactions between NO and hydrocarbons at high temperature. *Combust. Flame*, 135:97–112, 2003.

[274] S. L. Chen, J. C. Kramlich, W. R. Seeker, and D. W. Pershing. Advanced NO_x reduction processes using -NH and -CN compounds in conjunction with staged air addition. *J. Air Waste Manage. Assoc.*, 39:1375–1379, 1989.

[275] J. A. Miller, M. C. Branch, and R. J. Kee. A chemical kinetic model for the selective reduction of nitric oxide by ammonia. *Combust. Flame*, 43:81–98, 1981.

[276] R. Rota, D. Antos, E.F. Zanoelo, and S. Carra. Experimental study and kinetic modelling of nitric oxide reduction with ammonia. *Combust. Sci. Technol.*, 163:25–47, 2001.

[277] Z.-M. Lu and J.-D. Lu. Influences of O_2 concentration on NO reduction and N_2O formation in Thermal $DeNO_x$ process. *Combust. Flame*, 156:1303–1315, 2009.

[278] W. Duo. *Kinetic studies of the reactions involved in selective non-catalytic reduction of nitric oxide*. PhD thesis, DTU Chemical Engineering, Technical University of Denmark, 1990.

[279] J.W. Stephens, C.L. Morter, S.K. Farhat, G.P. Glass, and R.F. Curl. Branching ratio of the reaction amidogen + nitric oxide at elevated temperatures. *J. Phys. Chem.*, 97:8944–8951, 1993.

[280] F. Kasuya, P. Glarborg, and K. Dam-Johansen. The Thermal DeNO$_x$ process: Influence of partial pressures and temperature. *Chem. Eng. Sci.*, 50:1455–1466, 1995.

[281] M. U. Alzueta, H. Røjel, P.G. Kristensenand, P. Glarborg, and K. Dam-Johansen. Laboratory study of the CO/NH$_3$/NO/O$_2$ system: Implications for hybrid reburn/SNCR Strategies. *Energy Fuels*, 11:716–723, 1997.

[282] R.A. Perry amd D.L. Siebers. Rapid reduction of nitrogen oxides in exhaust gas streams. *Nature*, 324:657–658, 1986.

[283] D. L. Siebers and J. A. Caton. Removal of nitric oxide from exhaust gas with cyanuric acid. *Combust. Flame*, 79:31–46, 1990.

[284] B. Atakan and J. Wolfrum. Kinetic studies of the reactions of NCO radicals with NO and O$_2$ in the temperature range between 294 and 1260 K. *Chem. Phys. Lett.*, 178:157–162, 1991.

[285] J. D. Mertens, A.J. Dean, R. K. Hanson, and C. T. Bowman. A shock tube study of reactions of NCO with O and NO using NCO laser absorption. *Symp. (Int.) Combust.*, 24:701–710, 1992.

[286] L.J. Muzio, J.K. Arand, and D.P. Teixeira. Gas phase decomposition of nitric oxide in combustion products. *Symp. (Int.) Combust.*, 16:199–208, 1977.

[287] M.U. Alzueta, R. Bilbao, A. Millera, M. Oliva, and J. C. Ibanez. Interactions between nitic oxide and urea under flow reactor conditions. *Energy Fuels*, 12:1001–1007, 1998.

[288] S. Lee, K. Park, J.W. Park, and B.H. Kim. Characteristics of reducing NO using urea and alkaline additives. *Combust. Flame*, 141:200–203, 2005.

[289] R. Rota, D. Antos, E.F. Zanoelo, and M. Morbidello. Experimental and modeling analysis of the NO$_x$OUT process. *Chem. Eng. Sci.*, 57:27–38, 2002.

[290] R. Rota and E.F. Zanoelo. Influence of oxygenated additives on the NO_xOUT process efficiency. *Fuel*, 82:765–770, 2003.

[291] MU Alzueta, R Bilbao, A Millera, M Oliva, and JC Ibanez. Impact of new findings concerning urea thermal decomposition on the modeling of the urea-SNCR process. *Energy Fuels*, 14:509–510, 2000.

[292] H. Aoki, T. Fujiwara, Y. Morozumi, and T. Miura. Measurement of urea thermal decomposition reaction rate for NO selective non-catalytic reduction. *Fifth international conference on technologies and combustion for a clean environment*, 1:115–118, 1999.

[293] Wolfgang Brack, Barbara Heine, Felix Birkhold, Matthias Kruse, Gunter Schoch, and Olaf Deutschmann Steffen Tischer. Kinetic modeling of urea decomposition based on systematic thermogravimetric analyses of urea and its most important by-products. *Chem. Eng. Sci.*, 106:1–8, 2014.

[294] A.L. Myerson, F.R. Taylor, and B.G Faunce. Ignition limits and products of the multistage flames of propane-nitrogen dioxide mixtures. *Symp. (Int.) Combust.*, 6:154–163, 1957.

[295] J. O. L. Wendt, C. V. Sternling, and M. A. Matovich. Reduction of sulfur trioxide and nitrogen oxides by secondary fuel injection. *Symp. (Int.) Combust.*, 14:897–904, 1973.

[296] LD Smoot, SC Hill, and H Xu. NO_x control through reburning. *Prog. Energy Combust. Sci.*, 24:385–408, 1998.

[297] A.L. Myerson. The reduction of nitric oxide in simulated combustion effluents by hydrocarbon-oxygen mixtures. *Symp. (Int.) Combust.*, 15:1085–1092, 1975.

[298] J. Gimenez-Lopez, V. Aranda, A. Millera, R. Bilbao, and M. U. Alzueta. An experimental parametric study of gas reburning under conditions of interest for oxy-fuel combustion. *Fuel Process. Technol.*, 92:582–589, 2011.

[299] Thorne L.R., M.C. Branch, Chandler D.W., Kee R.J., and J.A. Miller. Hydrocarbon/nitric oxide interactions in low-pressure flames. *Proc. Combust. Inst.*, 21:965–977, 1986.

[300] A. Garo, C. Hilaire, and D. Puechberty. Experimental-study of methane oxygen flames doped with nitrogen oxide or ammonia - comparison with modeling. *Combust. Sci. Technol.*, 86:87–103, 1992.

[301] T. Etzkorn, S. Muris, J. Wolfrum, C. Dembny, H. Bockhorn, P. F. Nelson, A. Attia-Shahin, and J. Warnatz. Destruction and formation of NO in low pressure stoichiometric CH_4/O_2 flames. *Symp. (Int.) Combust.*, 24:925–932, 1992.

[302] B. A. Williams and J. W. Fleming. Comparative species concentrations in $CH_4/O_2/Ar$ flames doped with N_2O, NO, and NO_2. *Combust. Flame*, 93:98–106, 1994.

[303] W. Juchmann, H. Latzel, D. I. Shin, G. Peiter, T. Dreier, H. R. Volpp, J. Wolfrum, R. P. Lindstedt, and K. M. Leung. Absolute radical concentration measurements and modeling of low-pressure $CH_4/O_2/NO$ flames. *Symp. (Int.) Combust.*, 27:469–476, 1998.

[304] J. A. Miller, C. F. Melius, and P. Glarborg. The CH_3+NO rate coefficient at high temperatures: Theoretical analysis and comparison with experiment. *Int. J. Chem. Kinet.*, 30:223–228, 1998.

[305] B. Atakan, D. Kocis, J. Wolfrum, and P. Nelson. Direct investigations of the kinetics of the reactions of CN radicals with N atoms and $^3CH_2$ radicals with NO. *Symp. (Int.) Combust.*, 24:691–699, 1992.

[306] M. Fikri, S. Meyer, J. Roggenbuck, and F. Temps. An experimental and theoretical study of the product distribution of the reaction CH_2+NO. *Faraday Discuss.*, 119:223–242, 2001.

[307] D.L. Baulch, C.J. Cobos, R.A. Cox, P. Frank, G. Hayman, Th. Just, J.A. Kerr, T. Murrels, M.J. Pilling, J. Troe, R.W. Walker, and J. Warnatz.

Evaluated kinetic data for combustion modeling: Supplement I. *J. Phys. Chem. Ref. Data*, 23:847–1033, 1994.

[308] F. Stribel, L.E. Jusinski, A. Fahr, J.B. Halpern, S.J. Klippenstein, and C.A. Taatjes. Kinetics of the reaction of vinyl radicals with NO: Ab initio theory, master equation predictions, and laser absorption measurements. *Phys. Chem. Chem. Phys.*, 6:2216–2223, 2004.

[309] J. Peeters, H. van Look, and B. Ceursters. Absolute rate coefficients of the reactions of C2H with NO and H_2 between 295 and 440 K. *J. Phys. Chem.*, 100:15124–15129, 1996.

[310] W. Feng and J.F. Hershberger. Experimental and theoretical study of the product channels of the C_2H + NO reaction. *J. Phys. Chem. A*, 117:3585–3592, 2013.

[311] T. Kruse and P. Roth. High-temperature reaction of C_2 with NO including product channel measurements. *Int. J. Chem. Kinet.*, 31:11–21, 1999.

[312] S.A. Carl, Q. Sun, L. Vereecken, and J. Peeters. Absolute rate coefficient of the HCCO plus NO reaction over the range T=297-802 K. *J. Phys. Chem. A*, 106:12242–12247, 2002.

[313] W. Boullart, M.T. Nguyen, and J. Peeters. Experimental investigation of the reaction between nitric oxide and ketenyl radicals (HCCO+NO) - Rate coefficients at T=290-670 K and product distribution at 700 K. *J. Phys. Chem.*, 98:8036–8043, 1994.

[314] J.P. Meyer and J.F. Hershberger. Product channels of the HCCO + NO reaction. *J. Phys. Chem. B*, 109:8363–8366, 2005.

[315] W. D. Thweat, M.A. Erickson, and J. F. Hershberger. Kinetics of the CCO + NO and CCO + NO_2 reactions. *J. Phys. Chem. A*, 108:74–79, 2004.

[316] J. A. Miller, S. J. Klippenstein, and P. Glarborg. A kinetic issue in reburning: The fate of HCNO. *Combust. Flame*, 135:357–362, 2003.

[317] J. A. Miller, J.L. Durant, and P. Glarborg. Some chemical kinetics issues in reburning: The branching fraction of the HCCO+NO reaction. *Symp. (Int.) Combust.*, 27:235–243, 1998.

[318] W. H. Feng, J. P. Meyer, and J. F. Hershberger. Kinetics of the OH plus HCNO reaction. *J. Phys. Chem. A*, 110:4458–4464, 2006.

[319] M. Braun-Unkhoff, C. Naumann, K. Wintergest, and P. Frank. Untersuchung der reaktionen von NO und O_2 mit CH_3 bei hohen temperaturen. *VDI Ber.*, 1090:287–294, 1993.

[320] G. Hennig and H.Gg. Wagner. Investigation of the CH_3+NO reaction in shock-waves. *Ber. Bunsenges. Phys. Chem.*, 98:749–753, 1994.

[321] C. Vinckier and W. Debruyn. Temperature-dependence of the reactions of methylene with oxygen atoms, oxygen, and nitric oxide. *J. Phys. Chem.*, 83:2057–2062, 1979.

[322] V. Seidler, F. Temps, H.Gg. Wagner, and M. Wolf. Kinetics of the reactions of CH_2(X3B1) radicals with NO and NO_2. *J. Phys. Chem.*, 93:1070–1073, 1989.

[323] S. Bauerle, M. Klatt, and H.Gg. Wagner. Investigation of the reaction of CH_2 with NO at high temperatures. *Ber. Bunsenges. Phys. Chem.*, 99:97–104, 1995.

[324] H.G. Unfried, G.P. Glass, and R.F. Curl. Infrared flash kinetic spectroscopy of the ketenyl radical. *Chem. Phys. Lett.*, 177:33–38, 1991.

[325] F. Temps, H.Gg. Wagner, and M. Wolf. Some experiments concerning the reactions of HCCO with C_2H_2, O_2, NO, and NO_2. *Z. Phys. Chem.*, 176:27–39, 1992.

[326] U. Eickhoff and F. Temps. FTIR study of the products of the reaction between HCCO and NO. *Phys. Chem. Chem. Phys.*, 1:243–251, 1999.

[327] K.T. Rim and J.F. Hershberger. Product branching ratio of the HCCO plus NO reaction. *J. Phys. Chem. A*, 104:293–296, 2000.

[328] L. Vereecken, R. Sumathy, S.A. Carl, and J. Peeters. NO_x reduction by reburning: theoretical study of the branching ratio of the HCCO plus NO reaction. *Chem. Phys. Lett.*, 344:400–406, 2001.

[329] H. M. T. Nguyen and T. N. Nguyen. Calculations on the complex mechanism of the HCNO plus OH reaction. *Chem. Phys. Lett.*, 599:15–22, 2014.

[330] A.T. Chen and P.C. Malte. *paper WSS/CI 84–86 presented at the 1984 Fall Meeting of Western States Section, The Combustion Institute, October 22–23, Stanford, California*, 1984.

[331] C. N. Hinshelwood and R. E. Burk. The thermal decomposition of ammonia upon various surfaces. *J. Chem. Soc. Trans.*, 127:1105–1117, 1925.

[332] K. F. Roenigk and K. F. Jensen. Low-pressure CVD of silicon nitride. *J. Electrochem. Soc.*, 134:1777–1785, 1987.

[333] J. Suhlmann and G. Rotzoll. The influence of quartz glass surfaces on the reduction of NO with NH_3 at high-temperatures. *Chem.-Ing.-Tech.*, 64:580–581, 1992.

[334] B. Lewis and G. von Elbe. *Combustion and flames and explosions of gases*. Academic Press, second edition, 1987.

[335] M. Balat-Pichelin, J. M. Badie, R. Berjoan, and P. Boubert. Recombination coefficient of atomic oxygen on ceramic materials under earth re-entry conditions by optical emission spectroscopy. *Chem. Phys.*, 291:181–194, 2003.

[336] Y. C. Kim and M. Boudart. Recombination of O, N, and H-atoms on silica - kinetics and mechanism. *Langmuir*, 7:2999–3005, 1991.

[337] B. Gordiets, C. M. Ferreira, J. Nahorny, D. Pagnon, M. Touzeau, and M. Vialle. Surface kinetics of N and O atoms in N_2-O_2 discharges. *J. Phys. D Appl. Phys.*, 29:1021–1031, 1996.

[338] G. Cartry, L. Magne, and G. Cernogora. Atomic oxygen recombination on fused silica: experimental evidence of the surface state influence. *J. Phys. D Appl. Phys.*, 32:L53–56, 1999.

[339] P. Macko, P. Veis, and G. Cernogora. Study of oxygen atom recombination on a Pyrex surface at different wall temperatures by means of time-resolved actinometry in a double pulse discharge technique. *Plasma Sources Sci. Technol.*, 13:251–262, 2004.

[340] L. Bedra, M. Rutigliano, M. Balat-Pichelin, and M. Cacciatore. Atomic oxygen recombination on quartz at high temperature: Experiments and molecular dynamics simulation. *Langmuir*, 22:7208–7216, 2006.

[341] W.V. Smith. The surface recombination of H atoms and OH radicals. *J. Chem. Phys.*, 11:110–125, 1943.

[342] W. Hack, A. W. Preuss, F. Temps, and H. Gg. Wagner. Reaction O+HO_2 $\rightarrow$ OH+O_2 studied with a LMR-ESR spectrometer. *Ber. Bunsenges. Phys. Chem.*, 83:1275–1279, 1979.

[343] A. Garo, D. Puechberty, and M. Ledoux. Recombination kinetics of oh radicals on a quartz wall in a propane oxygen flame at 25 torr. *Combust. Flame*, 56:307–316, 1984.

[344] K. A. Sahetchian, A. Heiss, and R. Rigny. Evidence of the formation of hydrogen by the bimolecular recombination reaction of HO_2 radicals - low-temperature heterogeneous reaction of HO_2 radicals. *Can. J. Chem.*, 60:2896–2902, 1982.

[345] V. B. Rozhenshtein, Y.M. Gershenzon, S.D. Ilin, O. P. Kishkovich, and R.T. Malkhasyan. Study of reactions of HO_2 radicals by means of combined electron-spin-resonance LMR spectrometer - destruction on surface. *Kinet. Cat.*, 26:460–466, 1985.

[346] A. Zh. Arutyunyan, G. L. Grigoryan, and A. B. Nalbandyan. Electron-spin-resonance study of the heterogeneous radical decomposition of hydrogen-peroxide vapor on glass and silica. *Kinet. Cat.*, 26:678–682, 1985.

[347] C.A. Bank and E. A. Th. Verdurmen. On the catalytic reaction of carbon monoxide and oxygen at a quartz surface. *J. Phys. Chem.*, 67:2869–2871, 1963.

[348] V. Guerra. Theoretical investigation of the influence of the wall temperature on the probability for surface atomic recombination of a single species. *Jap. J. Appl. Phys.*, 45:8200–8203, 2006.

[349] A. A. Buchachenko, V. L. Kovalev, and A. A. Krupnov. Closed model of oxygen recombination on an Al_2O_3 surface. *Russ. J. Phys. Chem. B*, 32:86–94, 2013.

[350] P. G. Kristensen. *Nitrogen Burnout Chemistry*. PhD thesis, Department of Chemical Engineering and Technical University of Denmark, 1995.

[351] P. G. Kristensen, P. Glarborg, and K. Dam-Johansen. Verification of a quartz flow reactor system for homogeneous combustion chemistry. Technical Report CHEC Report 9511, DTU Chemical Engineering, 1995.

[352] A.W. Jasper, S.J. Klippenstein, L.B. Harding, and B. Ruscic. Kinetics of the reaction of methyl radical with hydroxyl radical and methanol decomposition. *J. Phys. Chem. A*, 111:3932–3950, 2007.

[353] C. Wilson and G.G. Balint-Kurti. New pathway for the CH_3+OH $\rightarrow$ CH_2+H_2O reaction on a triplet surface. *J. Phys. Chem. A*, 102:1625–1631, 1998.

[354] P.-F. Lee, H. Matsui, and N.-S. Wang. Study on the Reaction of CH_2 with H_2 at High Temperature. *J. Phys. Chem. A*, 116:1891–1896, 2012.

[355] J.M. Preses, C. Fockenberg, and G.W. Flynn. A measurement of the yield of carbon monoxide from the reaction of methyl radicals and oxygen atoms. *J. Phys. Chem. A*, 104:6758–6763, 2000.

[356] F. Hayes, W.D. Lawrance, W.S. Staker, and K.D. King. Temperature dependences of singlet methylene removal rates. *J. Phys. Chem.*, 100:11314–11318, 1996.

[357] A.W. Jasper, S.J. Klippenstein, and L.B. Harding. Secondary kinetics of methanol decomposition: Theoretical rate coefficients for $^3CH_2$ + OH, $^3CH_2$ + $^3CH_2$, and $^3CH_2$ + CH_3. *J. Phys. Chem. A*, 111:8699–8707, 2007.

[358] M. Rohrig, E.L. Petersen, D.F. Davidson, R.K. Hanson, and C.T. Bowman. Measurement of the rate coefficient of the reaction CH + O_2: products in the temperature range 2200 to 2600 K. *Int. J. Chem. Kinet.*, 29:781–789, 1997.

[359] P. Glarborg and L.L.B. Bentzen. Chemical effects of a high CO_2 concentration in oxy-fuel combustion of methane. *Energy Fuels*, 22:291–296, 2008.

[360] D. Husain and L.J. Kirsch. Reactions of atomic carbon C by kinetic absorption spectroscopy in vacuum ultra-violet. *Trans. Faraday Soc.*, 67:2025–2035, 1971.

[361] J. Grebe and K.H. Homann. Kinetics of the species OH and CH in the system C_2H_2-O-H. *Ber. Bunsenges. Phys. Chem.*, 86:581–587, 1982.

[362] T. Bohland and F. Temps. Direct determination of the rate-constant for the reaction CH_2 + H → CH + H_2. *Ber. Bunsenges. Phys. Chem.*, 88:459–461, 1984.

[363] T. Bohland, F. Temps, and H.Gg. Wagner. A direct study of the reactions of CH_2 radicals with H and D atoms. *J. Phys. Chem.*, 91:1205–1209, 1987.

[364] W. Boullart and J. Peeters. Product distributions of the C_2H_2+O and HCCO+H reactions - rate-constant of CH_2 + H. *J. Phys. Chem.*, 96:9810–9816, 1992.

[365] K. Devriendt, W. van Poppel, W. Boullart, and J. Peeters. Kinetic investigation of the $^3CH_2$ + H → CH + H_2 reaction in the temperature range 400 K < T < 1000 K. *J. Phys. Chem.*, 99:16953–16959, 1995.

[366] P. Frank, K.A. Bhaskaran, and Th. Just. High-temperature reactions of triplet methylene and ketene with radicals. *J. Phys. Chem.*, 90:2226–2231, 1986.

[367] J. Peeters and G. Mahnen. Reaction mechanisms and rate constants ofelementary steps in methane-oxygen flames. *Symp. (Int.) Combust.*, 14:133–146, 1973.

[368] J. Deppe and H. Gg. Wagner. Detection of $^1CH_2$ radicals in hydrocarbon pyrolysis behind shock waves using FM spectroscopy. *Z. Phys. Chem.*, 215:1501–1525, 2001.

[369] M.R. Berman and M.C. Lin. Kinetics and mechanisms of the reactions of CH and CD with H_2 and D_2. *J. Chem. Phys.*, 81:5743–5752, 1984.

[370] S. Zabarnick, J.W. Fleming, and M.C. Lin. Kinetic study of the reaction CH + H_2 = CH_2 + H in the temperature range 372 to 675 K. *J. Chem. Phys.*, 85:4373–4376, 1986.

[371] K.H. Becker, R. Kurtenbach, and P. Wiesen. Temperature and pressure-dependence of the reaction CH + H_2. *J. Phys. Chem.*, 95:2390–2394, 1991.

[372] R.A. Brownsword, A. Canosa, B.R. Rowe, I.R. Sims, I.W.M. Smith, D.W.A. Stewart, A.C. Symonds, and D. Travers. Kinetics over a wide

range of temperature (13-744 K): Rate constants for the reactions of CH(ν=0) with H_2 and D_2 and for the removal of CH(ν=1) by H_2 and D_2. *J. Chem. Phys.*, 106:7662–7677, 1997.

[373] A.J. Dean, D.F. Davidson, and R.K. Hanson. A shock tube study of reactions of C atoms with H, and O, using excimer photolysis of C_3O_2 and C atom atomic resonance absorption spectroscopy. *J. Phys. Chem.*, 95:183–191, 1991.

[374] R. van Harrevelt, M.C. van Hemert, and G.C. Schatz. The CH+H reaction studied with quantum-mechanical and classical trajectory calculations. *J. Chem. Phys.*, 116:6002–6011, 2002.

[375] J. Grebe and K. Homann. Blue-green chemiluminescence in the system C_2H_2-O-H - formation of the emitters CH, C_2 and C_2H. *Ber. Bunsenges. Phys. Chem.*, 86:587–597, 1982.

[376] K.H. Becker, B. Engelhardt, P. Wiesen, and K.D. Bayes. Rate constants for CH reactions at low total pressures. *Chem. Phys. Lett.*, 154:342–348, 1989.

[377] S. Zabarnick, J.W. Fleming, and M.C. Lin. CH Radical Reactions with H_2O and CH_2O. *Symp. (Int.) Combust.*, 21:713–719, 1986.

[378] M. A. Blitz, M. Pesa, M. J. Pilling, and P. W. Seakins. Reaction of CH with H_2O: Temperature dependence and isotope effect. *J. Phys. Chem. A*, 103:5699–5704, 1999.

[379] M. W. Bosnali and Perner D. Reaktionen von pulsradiolytisch erzeugtem CH mit methan und anderen substanzen. *Z. Naturforsh.*, 26:1768–1769, 1971.

[380] A. Bergeat, S. Moisan, R. Mereau, and J.-C. Loison. Kinetics and mechanisms of the reaction of CH with H_2O. *Chem. Phys. Lett.*, 480:21–25, 2009.

[381] Kevin M. Hickson, Philippe Caubet, and Jean-Christophe Loison. Unusual low-temperature reactivity of water: The CH + H_2O reaction as a source of interstellar formaldehyde? *J. Phys. Chem. Lett*, 4:2843–2846, 2013.

[382] J. E. Butler, J. W. Fleming, L. P. Goss, and M. C. Lin. Kinetics of CH radical reactions important to hydrocarbon combustion Systems. *Am. Chem. Soc. Symp. Ser.*, 134:397–401, 1980.

[383] M. R. Berman, J. W. Fleming, A. B. Harvey, and M. C. Lin. Temperature dependence of CH radical reactions with O_2, NO, CO and CO_2. *Symp. (Int.) Combust.*, 19:73–79, 1982.

[384] C. Mehlmann, M. J. Frost, D. E. Heard, B. J. Orr, and P. F. Nelson. Rate constants for removal of CH(D) (ν=0 and 1) by collisions with N_2, CO, O_2, NO and NO_2 at 298 K and with CO_2 at 296-873 K. *J. Chem. Soc. Faraday Trans.*, 92:2335–2341, 1996.

[385] M. W. Markus, P. Roth, and T. Just. A shock tube study of the reactions of CH with CO_2 and O_2. *Int. J. Chem. Kinet.*, 28:171–179, 1996.

[386] R.J. Hennessy, C. Robinson, and D.B. Smith. A comparative study of methane and ethane flame chemistry by experiment and detailed modeling. *Symp. (Int) Combust.*, 21:761–772, 1986.

[387] T. Etzkorn, J. Fitzer, S. Muris, and J. Wolfrum. Determination of absolute methyl radical and hydroxyl radical concentrations in a low-pressure methane oxygen flame. *Chem. Phys. Lett.*, 208:307–310, 1993.

[388] S. Cheskis, I. Derzy, V.A. Lozovsky, A. Kachanov, and F. Stoeckel. Intracavity laser absorption spectroscopy detection of singlet CH_2 radicals in hydrocarbon flames. *Chem. Phys. Lett.*, 277:423–429, 1997.

[389] V. A. Lozovsky, I. Derzy, and S. Cheskis. Radical concentration profiles in a low-pressure methane-air flame measured by intracavity laser absorption and cavity ring-down spectroscopy. *Symp. (Int.) Combust.*, 27:445–452, 1998.

[390] A. McIlroy. Direct measurement of $^1CH_2$ in flames by cavity ringdown laser absorption spectroscopy. *Chem. Phys. Lett.*, 296:151–158, 1998.

[391] I. Derzy and S. Cheskis V.A. Lozovsky. Absorption cross-section and absolute concentration of singlet methylene in methane/air flames. *Chem. Phys. Lett.*, 313:121–128, 1999.

[392] A. McIlroy. Laser studies of small radicals in rich methane flames: OH, HCO, and $^1CH_2$. *Israel J Chem*, 39:55–62, 1999.

[393] R. Evertsen, J. A. van Oijen, R. T. E. Hermanns, L. P. H. de Goey, and J. J. ter Meulen. Measurements of the absolute concentrations of HCO and $^1CH_2$ in a premixed atmospheric flat flame by cavity ring-down spectroscopy. *Combust. Flame*, 135:57–64, 2003.

[394] A. Fomin, T. Zavlev, V. A. Alekseev, I. Rahinov, S. Cheskis, and A. A. Konnov. Experimental and modelling study of $^1CH_2$ in premixed very rich methane flames. *Combust. Flame*, 171:198–210, 2016.

[395] D.E. Heard, J.B. Jeffries, G.P. Smith, and D.R. Crosley. LIF measurements in methane air flames of radicals important in prompt-NO formation. *Combust. Flame*, 88:137–148, 1992.

[396] J. Luque, G. P. Smith, and D. R. Crosley. Quantitative CH determinations in low-pressure flames. *Symp. (Int.) Combust.*, 26:959–966, 1996.

[397] D. R. Crosley, J. B. Jeffries, and G. P. Smith. Absolute concentration measurements of chemically-important flame radicals. *Israel J. Chem.*, 39:41–48, 1999.

[398] L. Gasnot, P. Desgroux, J. F. Pauwels, and L.R. Sochet. Detailed analysis of low-pressure premixed flames of $CH_4 + O_2 + N_2$: A study of prompt-NO. *Combust. Flame*, 117:291–306, 1999.

[399] I Derzy, VA Lozovsky, and S Cheskis. Absolute CH concentration in flames measured by cavity ring-down spectroscopy. *Chem. Phys. Lett.*, 306:319–324, 1999.

[400] R. Evertsen, R.L. Stolk, and J.J. Ter Meulen. Investigations of cavity ring down spectroscopy applied to the detection of CH in atmospheric flames. *Combust. Sci. Technol.*, 149:19–34, 1999.

[401] J. Luque, R.J.H. Klein-Douwel, J.B. Jeffries, P. Smith, and D.R. Crosley. Quantitative laser-induced fluorescence of CH in atmospheric pressure flames. *Appl. Phys. B - Lasers Optics*, 75:779–790, 2002.

[402] R. Evertsen, J. A. van Oijen, R. T. E. Hermanns, L. P. H. de Goey, and J. J. ter Meulen. Measurements of absolute concentrations of CH in a premixed atmospheric flat flame by cavity ring-down spectroscopy. *Combust. Flame*, 132:34–42, 2003.

[403] J. Luque, P.A. Berg, J.B. Jeffries, G.P. Smith, D.R. Crosley, and J.J. Scherer. Cavity ring-down absorption and laser-induced fluorescence for quantitative measurements of CH radicals in low-pressure flames. *Appl. Phys. B- Lasers Optics*, 78:93–102, 2004.

[404] L Pillier, A El Bakali, X Mercier, A Rida, JF Pauwels, and P Desgroux. Influence of C-2 and C-3 compounds of natural gas on NO formation: an experimental study based on LIF/CRDS coupling. *Proc. Combust. Inst.*, 30:1183–1191, 2005.

[405] P. Versailles, G. M. G. Watson, A. C. A. Lipardi, and J. M. Bergthorson. Quantitative CH measurements in atmospheric-pressure, premixed flames of C_1-C_4 alkanes. *Combust. Flame*, 165:109–124, 2016.

[406] R.G. Joklik, J.W. Daily, and W.J. Pitz. Measurements of ch radical concentrations in an acetylene/oxygen flame and comparisons to modeling calculations. *Symp. (Int.) Combust.*, 21:895–904, 1986.

[407] J. Luque and D. R. Crosley. Absolute CH concentrations in low-pressure flames measured with laser-induced fluorescence. *Appl. Phys. B - Lasers Optics*, 63:91–98, 1996.

Appendices

A: Surface reactions in quartz reactors.

A significant fraction of the experimental data on nitrogen chemistry in combustion is obtained in atmospheric pressure, laminar flow quartz reactors. While these data benefit from well-characterized experimental conditions, the potential impact of surface reactions on the reactor walls introduces an uncertainty in data interpretation. Heterogeneous reactions may involve decomposition of fuel components, promoting reaction, or loss of radicals, inhibiting reaction.

Some nitrogen species, in particular ammonia [186, 331, 332], are known to decompose on quartz surfaces. Dean et al. [254] observed that heterogeneous effects affected induction times for oxidation of ammonia. For Thermal $DeNO_x$, Lyon and Benn [257] found little impact of surfaces, consistent with the modeling study of Glarborg et al. [186] who concluded that surface decomposition of NH_3 was not important for SNCR in low S/V quartz reactors. However, Suhlmann and Rotzoll [333] reported that for high surface/volume ratios, presence of quartz surfaces widened the temperature window for the process.

Radical recombination on SiO_2 surfaces (quartz, Pyrex, etc.) has been studied extensively, due to its importance for reaction in reactors (e.g., explosion limits [334]) and on heat shields for space vehicles in earth reentry [335]. The radical recombination at the surface is usually described in terms of an apparent recombination efficiency γ. Data are available for H [336], O [335–340], OH [215, 341–343], HO_2 [215, 342, 344–346] and N [337].

It can be expected that the impact of the surface will depend on the concentration of water vapor in the system. In flow reactor experiments, the dominating radicals are O (dry conditions) or OH (moist conditions), provided the mixture is not too fuel-rich. In addition to controlling the main chain carrier, the pres-

ence of water vapor has been reported to alter the surface condition, for instance inhibiting oxidation of CO on a quartz surface [347].

In a dry system, where the silica surface may be more active, atomic oxygen is the dominating chain carrier under oxidizing conditions. The recombination probability for O on quartz is found to be a complex function of temperature [336], but in the 700-1430 K range results are consistent, indicating an activation energy for the apparent recombination efficiency of 4.2 kcal mol^{-1} [335, 336]. At these temperatures, it is likely that both Eley-Rideal and Langmuir-Hinshelwood recombination mechanisms contribute to the radical loss [340, 348, 349].

It is of interest whether a radical loss mechanism can explain the difference between measured and predicted temperatures for the onset of reaction in SNCR experiments conducted under dry conditions (see section 4.1.1 and Fig. 30). Figure 44 compares experimental results for the $NH_3/NO/O_2$ system obtained under dry conditions [278] with modeling predictions with and without heterogeneous removal of O. The sink of atomic oxygen on the quartz surface is represented in the mechanism by a pseudo-first-order reaction with an activation energy set to the value reported by Kim and Boudart [336] and the A-factor adjusted to predict the observed onset of reaction for the conditions of Fig. 44. Addition of this pseudo-reaction to the mechanism shifts the predicted window for the process towards higher temperature, providing a good agreement between modeling and experiments. However, results in literature on the impact of surface reactions on ammonia oxidation and Thermal DeNO$_x$ in dry systems indicate that heterogeneous radical loss is insignificant. Lyon and Benn [257] reported that reaction rates for the $NH_3/O_2/NO$ system was reproducible within 6% when varying the surface to volume ratio by a factor of two in a dry system. Furthermore, Dean et al. [254] varied the S/V ratio from 4 cm^{-1} to 20 cm^{-1} without observing significant changes in the post-induction time NH_3 oxidation rate.
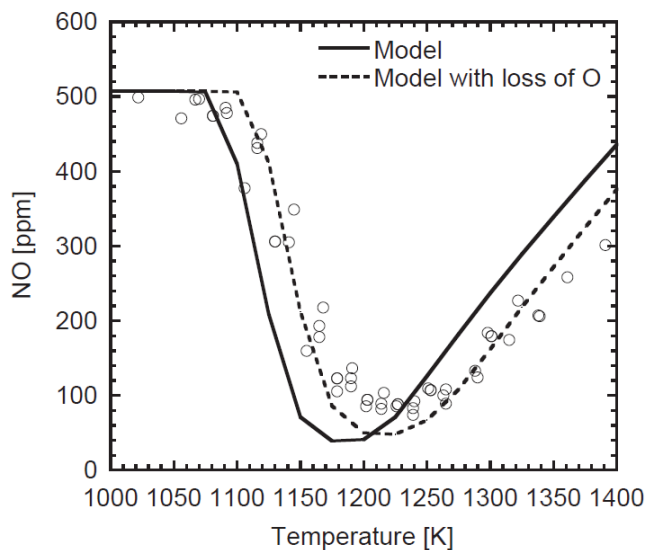
Figure 44: Comparison of experimental data [278] and modeling predictions for reduction of NO by NH_3 under dry conditions. Symbols denote experimental data, while lines denote modeling predictions. Inlet concentrations: $NH_3 = 832$ ppm, NO = 507 ppm, $O_2 = 4.0\%$, balance N_2. Residence time (s) = 92.7/T(K). The dashed line denotes modeling predictions conducted with surface loss of atomic O corresponding to a pseudo-first-order reaction with a rate constant $k_{O,surf} = 20 \cdot \frac{S}{V} \cdot T^{0.5} \exp(-2110/T)$ s^{-1}.

Loss of radicals on the surfaces of quartz flow reactors in moist systems was discussed by Kristensen and coworkers [350, 351]. Figure 45 shows their results for moist CO oxidation in quartz reactors of varying size. The moist CO oxidation experiments had good reproducibility, independent of time and among reactors of varying size. The results indicate that under moist conditions loss of radicals on the quartz surface of aged reactors is negligible. Modeling predictions conducted with loss of O atoms on the surface with the rate constant derived above (assuming it to be proportional to the surface/volume ratio of the reactor) shows an impact of reactor size not observed experimentally.

Based on this evidence, we conclude that surface loss of radicals in quartz reactors is generally insignificant at temperatures relevant to combustion. However, surface decomposition or oxidation of reactive species could conceivably play a
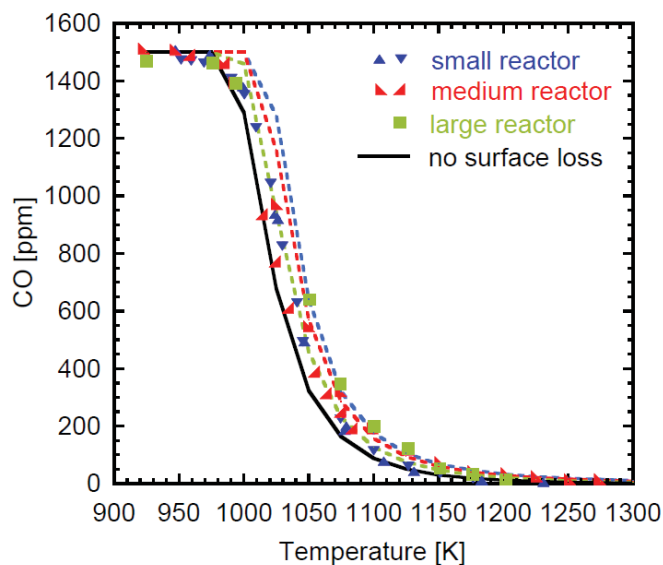
Figure 45: Comparison of experimental data [350] and modeling predictions for moist oxidation of CO in a flow reactor: effect of quartz reactor size. Symbols denote experimental data, while solid lines denote modeling predictions. Reactor surface to volume ratios are 10 cm^{-1} (small), 7.8 cm^{-1} (medium), and 4.4 cm^{-1} (large). Inlet concentrations: 1468-1520 (1500) ppm CO, 2.1% O$_2$, 2.0% H$_2$O, balance N$_2$. The residence times are 64/T[K] s (small or medium reactor) and 69/T[K] s (large reactor). Pressure is 1.05 atm. The modeling predictions are conducted with (dashed lines, color same as corresponding experimental data) and without (solid line) surface loss of atomic O corresponding to a pseudo-first-order reaction with a rate constant k$_{O,surf}$ = 20·$\frac{S}{V}$ · T$^{0.5}$exp(-2110/T) s^{-1}.

role, and data from flow reactor or batch reactor experiments on systems that react slowly (such as HNCO oxidation) or are sensitive to initiation (e.g, NH$_3$ oxidation) must be interpreted with caution.

B: Formation and consumption of hydrocarbon radicals.

Table 11 lists important reactions in the CH_n subset (n = 0-3). Formation of methylene in its triplet ($^3CH_2$) and singlet ($^1CH_2$) states from methyl occurs mainly by reactions involving H and OH. In the present mechanism, the rate constant for CH_3 + H to form $^3CH_2$ + H_2 (R99) is drawn from Klippenstein (unpublished work), while the channel to $^1CH_2$ + H_2 (R100b), represented by the reverse step, was adopted from the evaluation of Baulch et al. [26]. The rate constants for the CH_3 + OH reactions (R103, R104) were based on the theoretical work of Jasper et al. [352]. The calculated rate constant k_{103} for abstraction on the triplet surface is in good agreement with the measurement of Wilson and Balint-Kurti [353]. Singlet CH_2 formed in (R100b) and (R104) is mostly converted to its triplet state by the rapid collisionally induced inter-system crossing (R105).

The CH radical is formed from methylene by the reactions CH_2 + H $\rightarrow$ CH + H_2 (R106) and CH_2 + OH $\rightarrow$ CH + H_2O (R108). The rate constants for both of these steps have been in question. Low temperature data for reaction R106 [361–365] are in good agreement, indicating a fast reaction with a rate constant of around 10^{14} mol cm^{-3} s^{-1}. However, the extrapolation to high temperatures is uncertain. Early high-temperature data from shock tubes [366] and flames [367] indicated that the reaction is not faster than 10^{13} mol cm^{-3} s^{-1} at 2000 K, while more recent shock tube work of Rohrig et al. [358] and Deppe and Wagner [368] suggested a fast rate even at high temperature.

Measurements [369–372] of the rate constant of the reverse reaction, CH + H_2 $\rightarrow$ CH_2 + H (R106b), support the findings of Rohrig et al. and Deppe and Wagner that the CH_2 + H rate constant is largely independent of temperature. Figure 46 compares the available data for k_{106}, both from direct measurements of the forward reaction and from converting data for k_{106b} through the equilib-rium constant. Values of k_{106} derived from reaction R106b are generally larger,

		A	β	E	Source
99.	$CH_3 + H \rightleftarrows {}^3CH_2 + H_2$	1.2E06	2.43	11941	a
100.	${}^1CH_2 + H_2 \rightleftarrows CH_3 + H$	7.6E13	0.00	0	[354]
101.	$CH_3 + O \rightleftarrows CH_2O + H$	6.9E13	0.00	0	[26, 355]
102.	$CH_3 + O \rightleftarrows CO + H_2 + H$	1.5E13	0.00	0	[26, 355]
103.	$CH_3 + OH \rightleftarrows {}^3CH_2 + H_2O$	4.3E04	2.568	3997	[352]
104.	$CH_3 + OH \rightleftarrows {}^1CH_2 + H_2O$	2.2E14	-0.53832	-220	[352], 0.013 bar
		1.2E15	-0.72747	600	0.13 bar
		4.3E15	-0.85972	1888	1.3 bar
105.	${}^1CH_2 + M \rightleftarrows CH_2 + M$	1.3E13	0.00	400	[356] (N_2)
106.	${}^3CH_2 + H \rightleftarrows CH + H_2$	1.6E14	0.000	0	See text
107.	${}^3CH_2 + OH \rightleftarrows CH_2O + H$	2.9E13	0.1228	-162	[357]
108.	${}^3CH_2 + OH \rightleftarrows CH + H_2O$	8.6E05	2.019	6776	[357]
109.	${}^3CH_2 + O_2 \rightleftarrows CO_2 + H + H$	2.1E09	0.9929	-269	a
110.	${}^3CH_2 + O_2 \rightleftarrows CH_2O + O$	1.3E06	2.4202	1604	a
111.	$CH + H \rightleftarrows C + H_2$	1.2E14	0.000	0	[26]
112.	$CH + OH \rightleftarrows HCO + H$	3.0E13	0.000	0	[21]
113.	$CH + O_2 \rightleftarrows HCO + O$	9.7E13	0.000	0	[358]
114.	$CH + OH \rightleftarrows C + H_2O$	4.0E07	2.000	3000	[21]
115.	$CH + H_2O \rightleftarrows CH_2O + H$	8.5E08	1.144	-2051	a
116.	$CH + CO_2 \rightleftarrows HCO + CO$	8.8E06	1.750	-1040	[359]
117.	$C + OH \rightleftarrows CO + H$	5.0E13	0.000	0	est
118.	$C + O_2 \rightleftarrows CO + O$	2.0E13	0.000	0	[360]

a: Rate constant calculated by S.J. Klippenstein (unpublished work).

Table 11: Selected reactions involved in formation and consumption of hydro-carbon radicals. Parameters for use in the modified Arrhenius expression k = AT^{β} exp(-E/[RT]). Units are mol, cm, s, cal. In reactions R102 and R109 a significant fraction of the initial bimolecular products dissociate prior to their thermalization. In this instance, the proper phenomenological rate model for that directly dissociative fraction involves a description of the reactions as producing three separate molecular products.

perhaps due to interference from the competing step CH + H_2 (+M) $\longrightarrow$ CH_3 (+M). In the present work we have applied a rate constant of $1.6 \cdot 10^{14}$ cm^3 mol^{-1} s^{-1}, slightly faster than the recommendation of Baulch et al. [26]. However, there is significant scatter in the data and an accurate determination of k$_{106}$ over a wide temperature range is desirable.
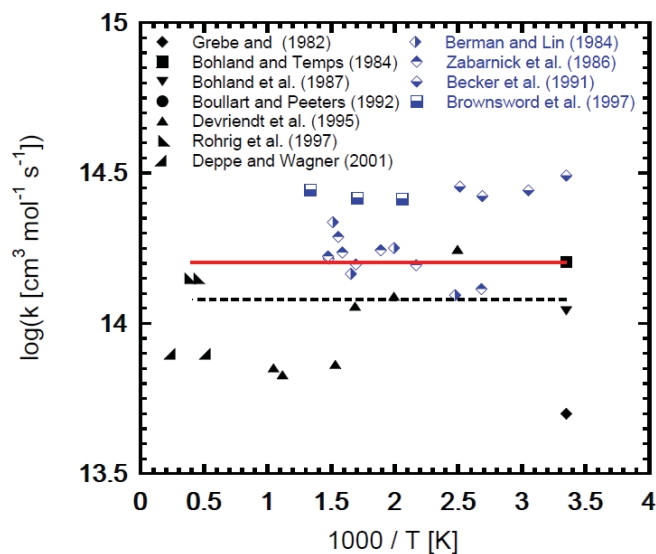
Figure 46: Arrhenius plot for the reaction $CH_2 + H \rightleftarrows CH + H_2$ (R106). The closed symbols denote measurements in the forward reaction while the open symbols denote data obtained from measurements of the reverse step, converted using the thermodynamic properties of the present work. Data for k_{106}: Grebe and Homann [361], Bohland and Temps [362], Bohland et al. [363], Boullart et al. [364], Devriendt et al. [365], Rohrig et al. [358] and Deppe and Wagner [368]. Data derived from measurements of k_{106b}: Berman and Lin [369], Zabarnick et al. [370], Becker et al. [371], Brownsword et al. [372]. The solid line shows the value used in the present model while the dashed line denotes the recommendation of Baulch et al. [26].

For the reaction of CH_2 with OH (R107, R108) we rely on the theoretical work of Jasper et al. [357]. Reactions R106 and R108 that form CH compete with steps involving O, OH, and O_2 that form oxygenated species and serve to diminish the CH_n radical pool.

The most important CH-consuming step under reducing conditions is the reaction with atomic hydrogen:

$$CH + H \rightleftarrows C + H_2 \qquad \qquad (R111)$$

Baulch et al. [26] recommend a value of k_{108} of $1.2 \cdot 10^{14}$ cm^3 mol^{-1} s^{-1}, based

153

on shock tube results for reaction R111b by Dean et al. [373]. The fast rate is supported by theory [374], but conflicts with measurements at room temperature [375, 376]. Reaction R111 competes with other consumption steps of CH, including reactions with O, OH, O_2, and H_2O. Even though they are much slower than the radical-radical reactions, reactions of CH with H_2O and CO_2 may become important under conditions with high concentrations of combustion products. The reaction between CH and H_2O yields formaldehyde,

$$CH + H_2O \rightleftarrows CH_2O + H \qquad (R115)$$

Figure 47 shows an Arrhenius plot for the reaction. Previous modeling studies have relied on the measurements of Zabarnick et al. [377] (298-669 K) and Blitz et al. [378] (291-673 K), which show a negative temperature dependence of reaction R115, making it comparatively slow under most combustion conditions. Recently, Klippenstein (unpublished work) studied the reaction at a high level of theory. He calculated a rate constant with a minimum at approximately 800 K and a slow increase with temperature above this value. His rate constant, which was adopted in the present model, results in a reaction which is more competitive at combustion temperatures and consequently a faster predicted consumption of CH.

The rate constant for the reaction between CH and CO_2 (R14) has been measured over a wider temperature range (298–3500 K) [382–385]. The data, which show a strong curvature in the Arrhenius expression, are well described by the rate constant proposed by Glarborg and Bentzen [359].

4.2.3 Modeling the CH_n radical pool in flames

Hydrocarbon radical concentrations reported from low-pressure, premixed methane flames include data for methyl [303, 386, 387], triplet methylene [386], and singlet methylene [388–394]. Most data are available for methylidyne (CH), which
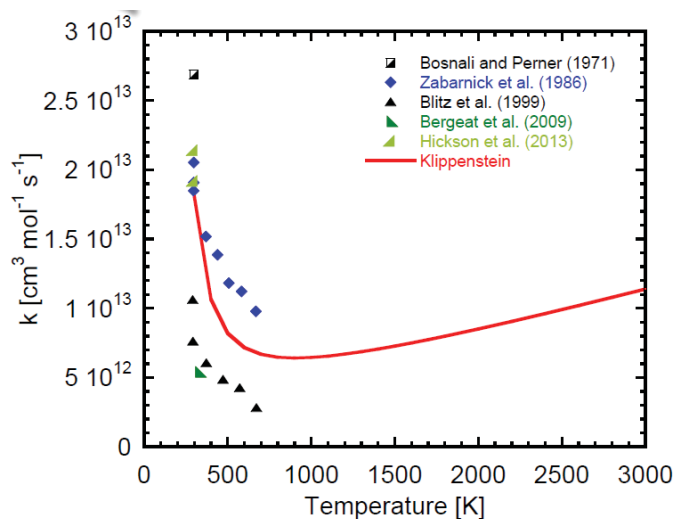
Figure 47: Arrhenius plot for the reaction CH + H$_2$O → CH$_2$O + H (R115). The symbols denote measurements while the solid line denotes a theoretical determination. Data were drawn from the following sources: Bosnali and Perner [379], Zabarnick et al. [377], Blitz et al. [378], Bergeat et al. [380], Hickson et al. [381], and Klippenstein (unpublished).

has been detected in methane flames [62, 70, 95, 97, 303, 395–405], as well as in flames of C$_2$H$_2$ [62, 97, 406], C$_2$H$_4$ [35], C$_2$H$_6$ [70, 405], C$_3$H$_6$ [66], and C$_3$H$_8$ [70, 396, 405, 407].

Figure 11 shown in section 3.2.3 compared the measured and calculated CH-profiles from two sets of low-pressure methane flames, obtained over a range of fuel-air equivalence ratios. Modeling predictions were generally in satisfactory agreement with measurements, capturing the CH concentration within a a factor of two under all conditions. Here we compare modeling predictions with measured profiles for a wider range of CH$_n$ radicals, obtained by molecular beam sampling and mass spectrometry.

In Fig. 48, modeling predictions are compared to data from Hennessy et al. [386] for a low-pressure, premixed methane/oxygen/argon flame. The structure of this flame is well predicted by the model; all major species (including CH$_4$

shown) are captured precisely. The peak concentrations of CH_3 and $^3CH_2$ are predicted within a factor of two, but the methylene peak is shifted by about 1.5 mm compared to the measured profile.
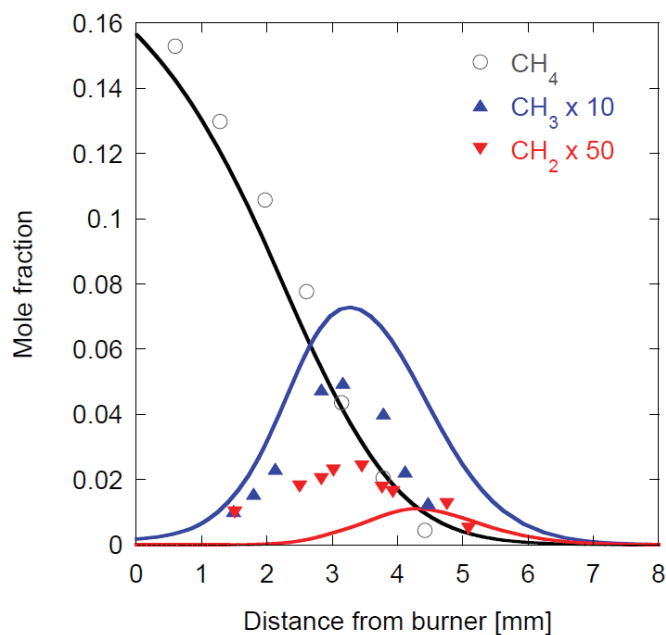

Figure 48: Comparison of measured [386] and predicted mole fractions of CH_4, CH_3, and $^3CH_2$ for a low-pressure premixed methane/air flame. The symbols denote experimental data, while the solid lines denote calculated values. Conditions: pressure of 20 torr, inlet composition 19% CH_4, 38% O_2; balance Ar. The maximum flame temperature was about 2300 K and the velocity of the unburnt gas mixture was 119 cm/s.

Figure 49 compares measured and predicted profiles of $^3CH_2$, CH, and C for the low-pressure, premixed ethylene/O_2/N_2 flame from Blauwens et al. [35]. The flame was operated under near-stoichiometric conditions. While CH is calculated quite accurately, the model overpredicts the $^3CH_2$ and C concentrations by factors of two and three, respectively.

The uncertainties in the measured radical concentrations in the flames of Hennesy et al. and Blauwens et al. were reported to be factors of three and two,
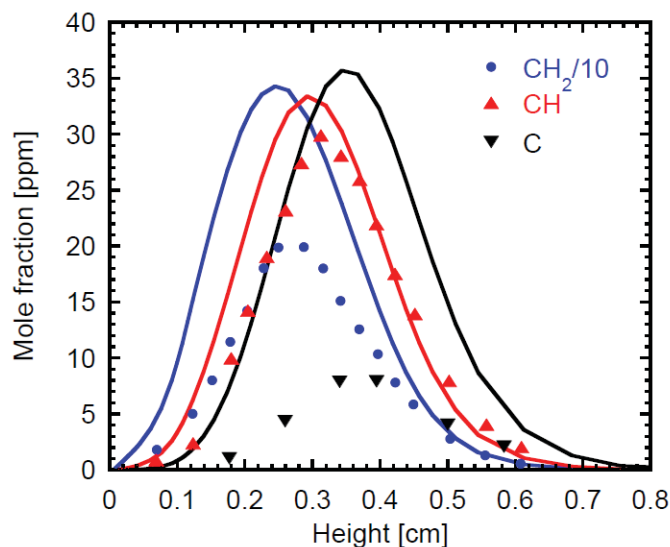
Figure 49: Comparison of measured [35] and predicted mole fractions of $^3CH_2$, CH, C, and NO for a low-pressure premixed ethylene/air flame. The symbols denote experimental data, while the solid lines denote calculated values. Conditions: pressure of 18.5 torr, fuel-air equivalence ratio of $\phi = 0.97$ (11.2% C_2H_4 in O_2/N_2 mixture) and a velocity of the unburnt gas mixture of 169 cm/s.

respectively. Lamoureux et al. [72] and Berg et al. [95] measured CH concentrations by laser diagnostics with an estimated accuracy of 20% (see section 3.2.3). We estimate that modeling predictions of the CH_n radical concentrations in combustion of small hydrocarbons are mostly accurate within a factor of two.

For larger hydrocarbons, formation and consumption of fuel-derived radicals are more complicated. Sutton et al. [70] compared modeling predictions to flame measurements for different fuels and stoichiometries and concluded that the tested mechanisms were not able to predict the CH concentration accurately over a wider range of fuels and conditions. Also, for more complex fuels larger hydrocarbon radicals, such as propargyl (C_3H_3), may become important in interacting with the nitrogen chemistry. More work is desirable in this area, but it is outside the scope of the present review.